DISSERTATION

THE FREQUENCY, MAGNITUDE AND CONNECTIVITY OF POST-WILDFIRE RAINFALL-RUNOFF AND SEDIMENT TRANSPORT

Submitted By

Codie R. Wilson

Department of Geosciences

In partial fulfillment of the requirements

For the Degree of Doctor of Philosophy

Colorado State University

Fort Collins, Colorado

Fall 2019

Doctoral Committee:

Advisor: Stephanie Kampf

Kelly Jones
Lee MacDonald
Sandra Ryan

ABSTRACT

THE FREQUENCY, MAGNITUDE AND CONNECTIVITY OF POST-WILDFIRE RAINFALL-RUNOFF AND SEDIMENT TRANSPORT

Wildfire increases the likelihood of runoff, erosion, and downstream sedimentation in many of the watersheds that supply water for communities across the western U.S. The goal of this research was to examine the complex interactions between fire, rainfall and landscape properties (e.g., burn severity, topography) across scales from hillslopes to watersheds. The research combines both regional data analysis and field monitoring to examine the frequency, magnitude and connectivity of post-fire rainfall-runoff events and associated sediment delivery.

In the first part of this study (chapter 2), the goal was to quantify rainfall thresholds that cause runoff and sediment delivery across multiple fires, years post-fire, spatial scales, and mulch treatments in the Colorado Front Range. Rain intensity thresholds were identified for plots, hillslopes, and watersheds across three Colorado Front Range fires. Thresholds did not significantly differ among fires for any year post-fire, but were significantly different between spatial scales and years post-fire. Thresholds increased with time since burn likely due to vegetation regrowth, litter accumulation and recovery of soil infiltration capacity. The frequency of storms exceeding thresholds for runoff and erosion was mapped across Colorado to provide a tool for identifying areas most vulnerable to post-fire runoff and sediment delivery and prioritizing post-fire treatments.

In chapter three, the goal was to improve understanding of the catch efficiency of sediment fences commonly used to measure post-fire hillslope erosion. During post-fire year two

(2014) of the 2012 High Park Fire four sediment fences were modified to collect and measure both the sediment deposited behind the fence and the amount of runoff and sediment that overtopped the fence. Sediment fence catch efficiency ranged from 28-100% for individual events and from 38-94% across the sampling season. Increasing rainfall intensities were correlated with greater runoff and total sediment loads and lower sediment fence catch efficiencies. Enrichment ratios indicate that the sediment behind the fence was significantly enriched in sand relative to the hillslope soil samples. These results indicate that sediment fences underestimate sediment yields and demonstrate how sediment particle sizes may be sorted en route to the stream network.

In chapter four, the goal was to examine connectivity between hillslopes and channel networks. Runoff and sediment from nested hillslopes (n = 31) and catchments (n = 12) were assessed for two rainfall events with different duration and intensity during post-fire year three (2015) of the High Park Fire to determine the factors affecting connectivity. The first event had a return interval of <1 year with low intensity rainfall over an average of 11 hours, whereas the second event had high intensity rainfall that lasted for an average of 1 hour with a maximum return interval of 10 years. The lower intensity event led to low hillslope sediment yields and widespread channel incision. The higher intensity event led to infiltration excess overland flow, high sediment yields and in-stream sediment deposition and fining. During both events, the percent of a catchment that burned at high severity was positively correlated with sediment delivery ratios and area-normalized absolute channel change.

Overall, this research demonstrated that the rainfall events and thresholds associated with the generation of post-fire runoff and sediment transport vary with spatial scale and time since burn. In addition, not every threshold-exceeding event will produce the same type of response

due to the complex and transient nature of post-fire responses from hillslope to watershed scale. Increasing our understanding of post-fire responses and connectivity will therefore require nested multi-scale monitoring over time to determine how sediment moves to and through channel networks.

ACKNOWLEDGEMENTS

Huge thanks to my advisor, Stephanie Kampf, for her patience and mentorship. For their support, I am also grateful to my committee members, Lee MacDonald, Kelly Jones and Sandra Ryan, as well as Ellen Wohl and Joe Wagenbrenner.

Many others brought me to CSU and kept me here: the National Science Foundation I-WATER Program, Jorge Ramirez, Neil Grigg, Scott Denning, LeRoy Poff, the Joint Fire Science Program, the Southern Rockies Fire Science Network, Gloria Edwards, Monique Rocca, Cameron Aldridge, Kimberly Melville-Smith, Nikki Foxley, Laurie Richards, The Colorado Water Center, the Nature Conservancy, Ben Gannon, Freddy Saavedra, the Natural Resource Conservation Service, Brett Bruyere and Kira Puntennay-Desmond.

Data collection would not have been possible without: Hunter Gleason, Mark Dixon, Junior Garza, Jill Oropeza, Jen Kovecses, Ray Ramos and family, Rick Fonken and family, Adam and Katie Johnson, Matt Kunze, Pete Robichaud, Mark Shaffer, Liz Grenard, the DeAngelis family, the Cities of Greeley and Fort Collins, the Coalition for the Poudre River Watershed, Cassidy Rosenkrance, Emily Chavez, Jason Gerlich, Chenchen Ma, Qichao Yao, Steven Filipelli, Ayla Lefsky, Matt Schiff, and many other volunteers from the CSU community.

I am especially grateful for my mom, who is an endless source of inspiration.

DEDICATION

To Clay and Killah, for our time in Colorado.

TABLE OF CONTENTS

LIST OF TABLES

LIST OF FIGURES

CHAPTER 1: INTRODUCTION

In the western U.S., most freshwater supplies begin as streamflow in forested watersheds (Brown et al. 2008) where abundant canopy and ground cover intercept precipitation, promote infiltration, and help maintain clean water supplies. Unfortunately, these same forests are increasingly susceptible to large wildfires (Westerling et al. 2006; Litschert et al. 2012) that combust organic cover, including tree canopy, understory, leaves, needles and duff. Fires burn at varying severity, with increasing severity related to the degree to which cover is removed (Parsons et al. 2010). For example, moderate to high burn severity removes most, if not all, surface and canopy cover leaving bare soils susceptible to rain drop impacts, soil surface sealing and reduced soil infiltration rates (Larsen et al. 2009). Compared to unburned conditions, overland flow initiates at much lower rainfall intensities (Moody and Martin 2001a; Schmeer 2014), and the area required to initiate concentrated flow decreases (Wohl 2013). Consequently both runoff and erosion increase by orders of magnitude (Benavides-Solorio and MacDonald, 2005; Noske et al. 2016; Wagenbrenner and Robichaud 2014; Moody and Martin 2001a,b; Moody et al. 2013). Across watersheds, interconnected areas of bare soil also increase connectivity of runoff and sediment from hillslopes to streams (Ortíz-Rodrígez et al. 2019), leading to channel erosion (or aggradation) when the sediment supplied is lower (higher) than in-stream transport capacity (Moody and Martin 2009; Kampf et al. 2016; Brogan et al. 2019).

Mulch treatments are often applied to areas burned at moderate to high severity to increase surface cover and reduce runoff, erosion and potential downstream impacts (BAER 2012), such as flooding and sediment delivery (Hohner et al. 2016; Martin 2016). Although mulch has been shown to reduce runoff and erosion from smaller spatial scales (<5.2 ha)

(Wagenbrenner et al. 2006; Robichaud et al. 2013a,b; Wainwright et al. 2000; Moreno-de las Heras et al. 2010; Inbar et al. 1998), these findings are not necessarily applicable to the larger areas of interest to managers (i.e., watersheds). Consequently, improved understanding of post-fire hydrological processes across watersheds is still needed (Smith et al. 2011; Hallema et al. 2017). This is challenging because of the heterogeneous nature of hillslopes and channel processes within watersheds. With increasing catchment area, variability of rainfall (Osborn and Laursen 1973), topography, surface cover (Moody et al. 2008b), and soil properties (Ebel and Martin 2017) affect locations of runoff generation and infiltration (Kutiel et al. 1995), and subsequent sediment detachment, remobilization and transport, or deposition (Moody et al. 2008a).

Not surprisingly, relationships between rainfall, runoff and erosion are often nonlinear and vary with spatial and temporal scale. For example, area-normalized peak discharge from ephemeral catchments within 19 burned basins across the western U.S. increased logarithmically with rainfall intensity only after sufficient rainfall (i.e., a threshold) was exceeded (Moody et al. 2013). After six wildfires across the western U.S., sediment yields from plots and catchments logarithmically increased with bare soil and rainfall intensity, and decreased with contributing area (20 m^2- 110 ha) (Wagenbrenner and Robichaud 2014). However, bare soil is difficult to quantify for large areas (Kampf et al. in review), making it difficult to extend these relationships to larger areas. Variability in processes with scale is also present in unburned semiarid catchments due to greater channel transmission losses with increasing catchment area and spatially variable thunderstorms (Sivalapan et al. 2002). The nonlinear production of runoff in semiarid areas has been attributed to scale-specific mechanisms (e.g., affected by soil properties,

vegetation distribution, variable source areas, and transmission losses) that increase rainfall thresholds from plot to watershed scale (Cammeraat 2004).

Obtaining reliable measurements over time before and after fire is another challenge for research on post-fire runoff and sediment production and delivery. For example, estimates of post-fire field-saturated hydraulic conductivity (K_{fs}; mm h^{-1}), which reflects a combination of soil properties (e.g., organic matter, bulk density, ground cover), were better from long-term repeat monitoring of the same sites over time than those from one-time sampling of different sites with time since burn (Ebel and Martin 2017). Further complexity arises with increasing spatial scale because the methods used to measure erosion vary (Stroosnijder 2005; Boardman 2006). For example, erosion rates measured at rainfall simulation plots may not be representative for hillslopes because of increased opportunities for infiltration (Cawson et al. 2016), and potential for the occurrence of rills and gullies, with increasing spatial scale. Uncertainty as to where and when wildfire will occur usually means a lack of pre-fire data. To get around this challenge, studies have used prescribed fire, but these usually do not have high burn severity (Cawson et al. 2016; Arkle and Pilliod 2010), which may unrealistically limit lateral (hillslope-channel) connectivity. Connectivity modeling is one potential method for linking measurements at the point and plot to larger spatial scales (Cawson et al. 2016), but hillslope to watershed-scale erosion and sediment transport is difficult to simulate accurately. Nested monitoring approaches may help to resolve some of these methodical discrepancies to increase understanding of how spatially variable patterns affect post-fire responses at larger spatial scales (Ferriera et al. 2008).

The goal of this research was to monitor runoff and sediment continuously from nested hillslopes and watersheds to determine the factors affecting connectivity. Very few previous studies of post-fire response have included nested measurements of both post-fire runoff and

erosion. Wagenbrenner and Robichaud (2014) compared erosion at nested plots (20-1000 m^2) and catchments (0.1-117 ha) within three wildfires in the western U.S. They found that sediment delivery ratios, defined as the sediment delivered to a catchment divided by that delivered to a nested plot, decreased as both the ratio of catchment length to plot length and catchment area to plot area increased. After a prescribed burn in Australia, upslope-downslope connectivity of sediment on planar unbounded plots ($\leq$0.2 ha) increased with rainfall intensity and high antecedent rainfall and decreased with the width of unburnt patches at the toe of the slope (Cawson et al. 2013). Nested monitoring of runoff and sediment has been conducted for unburned nested catchments (3-630 km^2), and demonstrates how longitudinal connectivity (upstream-downstream) of sediment increases with widespread rainfall and higher antecedent baseflow (Duvert et al. 2011). Although hydrologic complexity increases with spatial scale, and existing measurements are limited, recent post-fire reviews emphasize the importance of determining dominant drivers and patterns of post-fire landscape-scale responses (Nyman et al. 2013) and hillslope- to watershed-scale connectivity (Hallema et al. 2017; Leibowitz et al. 2018).

To these ends, this research includes both regional data analysis and field monitoring to estimate the frequency, magnitude and connectivity of post-fire rainfall-runoff events and associated sediment delivery. The first component of the dissertation (chapter 2) identifies rainfall thresholds for initiating post-fire runoff and erosion across plots, hillslopes and watersheds within three recent Colorado Front Range fires. This chapter addresses how the threshold for response varies with spatial scale, mulch treatments, and time since burn, and determines the frequency of threshold exceedance across the Colorado Front Range. The next two chapters are based on the field monitoring component of the research. The field monitoring was originally designed to compare runoff and sediment production between mulched and

unmulched hillslopes ($\leq$ 1.5 ha) and watersheds ($\leq$ 15 ha) within Colorado's 2012 High Park Fire. However, the focus evolved based on the relatively low mulch cover on the hillslopes and the type of responses that occurred during the time period of measurements (2014-2015). Chapter 3 focuses on runoff and sediment transport monitoring at the hillslope scale. Hillslope-scale erosion has traditionally been estimated from the sediment trapped behind sediment fences (Robichaud and Brown 2002). This technique was modified to include additional monitoring of runoff and suspended sediment; particle size analysis of the sediment trapped behind the fence and transported within the runoff indicates what types of materials may be transported from hillslopes to streams. Chapter 4 presents nested monitoring of runoff and sediment from hillslope through watershed scale during two rainfall events: one long duration with low intensity ($\leq$ 2 year return interval) and one high intensity ($\leq$ 10 year return interval). These data helped identify the sources of in-stream sediment and the factors affecting connectivity of runoff and sediment from hillslopes to channels and from upstream to downstream reaches. The final chapter summarizes and integrates important factors affecting post-fire runoff and sediment delivery across spatial scales and discusses how these findings can inform future post-fire research and land management.

CHAPTER 2: RAINFALL THRESHOLDS FOR POST-FIRE RUNOFF AND SEDIMENT DELIVERY FROM PLOT TO WATERSHED SCALES[1]

2.1. Introduction

In the western United States, higher temperatures and earlier spring snowmelt have increased the frequency and duration of large wildfires (Westerling et al. 2006; Litschert et al. 2012). After a wildfire, runoff and erosion can be up to several orders of magnitude higher than pre-fire conditions (e.g., Larsen et al. 2009; Noske et al. 2016; Wagenbrenner and Robichaud 2014); this can lead to difficulties for both emergency management and water treatment, such as flooding and delivery of sediment, ash and other constituents to streams (Hohner et al. 2016; Martin 2016).

In the Colorado Front Range, post-fire runoff and erosion are almost exclusively driven by summer thunderstorms and subsequent infiltration-excess (Hortonian) overland flow (Benavides-Solorio and MacDonald 2005; Moody et al. 2013; Wagenbrenner and Robichaud 2014). The generation of infiltration-excess overland flow exhibits threshold behavior, as high rainfall intensities are needed to exceed the infiltration capacities of soils and generate runoff on plots or hillslopes.

Rainfall thresholds for post-fire response (defined here as runoff or sediment delivery) vary with fire severity, time since burning and soil type (Benavides-Solorio and MacDonald 2005; Miller et al. 2011). The lowest thresholds are immediately after a high severity fire due to

[1] This chapter has been published as: Wilson, CR, Kampf, SK, Wagenbrenner, JW and LH MacDonald. 2018. Rainfall thresholds for post-fire runoff and sediment delivery from plot to watershed scale. Forest Ecology and Management (430): 346-356.

the loss of surface cover, decrease in soil organic matter, and exposure of the soils to raindrop impact and soil sealing (Moody and Martin 2001a; Larsen et al. 2009). Previous research on plots and hillslopes ($\leq$ 5.2 ha) has shown that post-fire mulch treatments and vegetation regrowth increase surface cover, surface roughness, and rainfall interception, thereby protecting soil from raindrop impact, slowing overland flow, and reducing runoff and erosion (Wagenbrenner et al. 2006; Robichaud et al. 2013a,b; Wainwright et al. 2000; Moreno-de las Heras et al. 2010; Inbar et al. 1998).

While the factors affecting post-fire runoff and erosion on plots and hillslopes are relatively well-documented, predicting post-fire runoff and sediment delivery for watersheds remains difficult due to high variability in rainfall, burn severity, soil properties and topography (Moody et al. 2008b; Kutiel et al. 1995). This increasing variability with larger drainage area generally causes thresholds to increase (Cammeraat 2002; Cammeraat 2004) due to longer flow paths (Wagenbrenner and Robichaud 2014) that allow more opportunities for water infiltration and storage.

After a fire, the production of infiltration-excess overland flow reduces over time and typically only the most extreme storms generate overland flow by three to four years after burning (Ebel and Martin 2017; Moody and Martin 2001a; Wagenbrenner et al. 2015). As recovery conditions and rates may vary among fire locations and responses of interest (e.g., runoff or sediment delivery), modeling specific complex hydrological processes remains difficult, particularly across spatial scales. However, approaches that simplify interactions between fire, rainfall and landscape properties may be more important than the exact hydrologic transfer processes that occur in a recovering landscape (Nyman et al. 2013).

Rainfall thresholds can be used to integrate complex processes into a single comparable metric for predicting the frequency of post-fire runoff and sediment delivery without having to rely on more complex process-based models. Comparing thresholds between spatial scales, fires, and post-fire treatments is useful for interpreting the hydrologic processes and scale-effects that emerge with post-fire mulch treatments and recovery. Therefore, the goal of this study is to provide information on post-fire thresholds for runoff and sediment delivery across multiple fires, years post-fire, spatial scales, and mulch treatments in the Colorado Front Range. Specific objectives are to:

1. Identify rainfall intensity thresholds for a post-fire runoff or sediment delivery response at plots ($\leq$0.06 ha), hillslopes (0.07-5.2 ha) and watersheds (100-1500 ha) after three Colorado Front Range wildfires for up to four years post-fire;
2. Determine how rainfall thresholds varied by fire location, year post-fire, spatial scale, and mulch treatments;
3. Use long-term rainfall data to map the likely frequency of rainfall events above these intensity thresholds as an indicator of risk for post-fire runoff or sediment delivery from future high severity fires in Colorado.

2.2. Materials and methods

2.2.1. Site descriptions and sample sizes

Post-fire rainfall, runoff and sediment delivery data were compiled for three Colorado Front Range wildfires: the 2000 Bobcat fire (Wagenbrenner et al. 2006; Wagenbrenner and Robichaud 2014; Kunze and Stednick 2006), the 2002 Hayman fire (Robichaud et al. 2013a,b; Robichaud et al. 2008; Wagenbrenner and Robichaud 2014), and the 2012 High Park fire (This study; Schmeer 2014; S. Ryan, USFS, unpublished data; Figure 2.1). These fires were selected

because they each had relatively detailed rainfall data linked with either runoff or sediment delivery data for at least three years post-fire and two or more spatial scales.

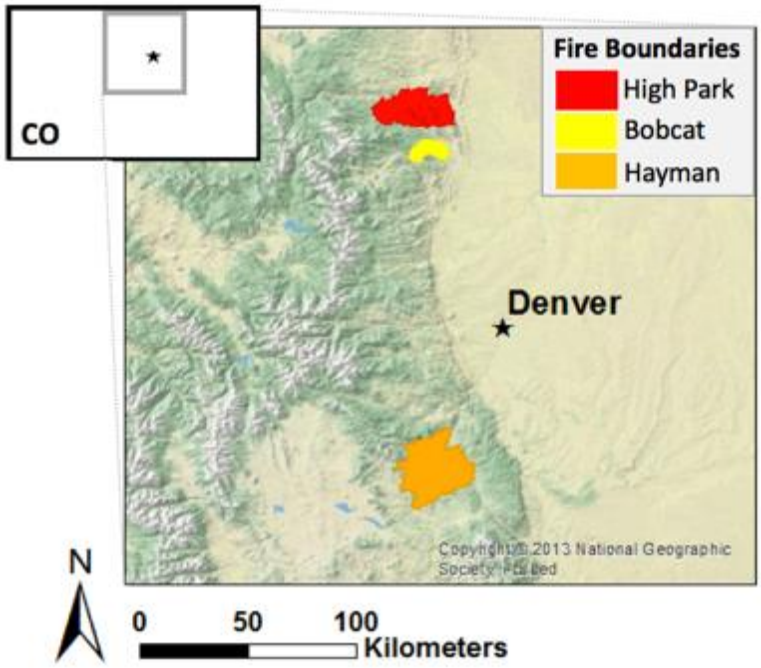

Figure 2.1. Location of the three Colorado Front Range fires used in this analysis; from north to south, they are the 2012 High Park fire, the 2000 Bobcat fire, and the 2002 Hayman fire. Imagery from ESRI (2013). Maps produced using GCS WGS 1984.

Elevations of the study sites within these fires ranged from 1700 to 2700 m. Climate within the study area is semiarid and monsoonal with 60-75% of the annual 400-600 mm of precipitation occurring as rain during the spring and summer months (April - September; PRISM Climate Group 2018). The primary pre-fire vegetation was ponderosa pine (*Pinus ponderosa*) at lower elevations and denser mixed conifer forests at higher elevations, with grasses and shrubs on drier south-facing slopes (BAER 2012; Robichaud 2013b; Kunze and Stednick 2006; Schmeer et al. 2018). Soils are derived from granitic (Robichaud et al. 2013b; Schmeer et al. 2018) and metasedimentary parent materials (Braddock et al. 1970). The dominant soil type in

the Bobcat and High Park fires is sandy loam, whereas soil in the Hayman fire is gravelly coarse sand (Robichaud et al. 2013a; Wagenbrenner and Robichaud 2014; BAER 2012).

We classified each monitoring site as a plot, hillslope or watershed. Plots were typically on planar slopes with an area of $\leq$0.06 ha in which sediment fences were used to measure sediment delivery (cf. Robichaud and Brown 2002). Data were available for eleven plots within the Bobcat fire and 32 plots within the Hayman fire (Table 2.1). The Bobcat, Hayman and High Park fires each had 23-32 hillslopes, defined here as ephemeral, convergent swales or headwater channels with contributing areas of 0.07-5.2 ha. Sediment fences or larger sediment traps were used to measure hillslope sediment delivery. In both plots and hillslopes, sediment fences were cleaned out after major storms to measure deposited sediment mass. At the watershed scale of 100-1500 ha, runoff responses were measured at two watersheds within the Bobcat fire and six watersheds within the High Park fire (Table 2.1).

Site characteristics and treatments to mitigate post-fire responses varied by spatial scale. Plots and hillslopes were generally placed in locations burned at high severity, whereas watersheds covered larger areas and therefore had combinations of moderate and high severity. Average slopes by spatial scale were 17° for planar plots, 15° for the convergent hillslopes, and 17° for watersheds. Treatments included straw mulch, contour felling, straw wattles, and aerial seeding in the Bobcat fire; straw mulch, hydromulch, wood mulch, contour felling, and aerial seeding in the Hayman fire; and straw and wood-shred mulch in the High Park fire. Aerial seeding in parts of the Bobcat and Hayman fires did not significantly affect vegetation regrowth or post-fire sediment delivery rates (Wagenbrenner et al. 2006; Rough 2007). Contour felled logs at two plots in the Bobcat fire and one hillslope in the Hayman fire also did not significantly reduce sediment yields (Wagenbrenner et al. 2006; Robichaud et al. 2008). Because mulch was

the most common treatment used across all fires, we chose to consider only the effects of mulch treatments on thresholds. We stratified sites by the presence or absence of mulch rather than the extent of mulch cover because the extent and type of mulch varied widely, and not all locations had data on the amount of mulch cover over time. One Bobcat plot and 16 Hayman plots were mulched. For hillslopes, 6 Bobcat, 11 Hayman, and 9 High Park fire sites were mulched (Table 2.1). Mulch was applied to 0-16% ($\bar{x}$ = 8%) of the watershed areas in the Bobcat fire (Kunze and Stednick 2006) and 1-77% ($\bar{x}$ = 22%) of the watershed areas in the High Park fire. We chose not to consider the effects of mulch at the watershed scale because the areas mulched were generally small fractions of the watershed areas.

Table 2.1. Spatial scale, contributing area, total number of sites (with number mulched in parentheses), years monitored post-fire, and references for the data from each of the three fires used in this study.

Fire, Year	Spatial scale	Area (ha)	No. of sites (no. mulched)	Years post-fire	Reference
Bobcat, 2000	Plot	≤ 0.06	11 (1)	0-3	Wagenbrenner et al. 2006
	Hillslope	0.07-5.2	23 (6)	0-3	Wagenbrenner and Robichaud 2014
	Watershed	100-1500	2	0-2	Kunze and Stednick 2006
Hayman, 2002	Plot	≤ 0.06	32 (16)	1-4	Robichaud et al. 2013a
	Hillslope	0.07-5.2	32 (11)	0-4	Robichaud et al. 2008, Wagenbrenner & Robichaud 2014; Robichaud et al. 2013b
High Park, 2012	Hillslope	0.07-5.2	31 (9)	0-3	This study; Schmeer 2014
	Watershed	100-1500	6	2-4	This study; S. Ryan, US Forest Service, unpublished data

2.2.2. Observations of rainfall, runoff or sediment delivery

We included observations of rainfall, runoff or sediment delivery from the summer thunderstorm season of June-September because this is when nearly all post-fire sediment delivery from plots and hillslopes occurs in this region (e.g., Benavides-Solorio and MacDonald

2005). Post-fire summers and years were numbered consecutively, with 0 representing the year of the fire. Most plot and hillslope data extended from year 0 through at least post-fire year 3. Watershed data were collected for post-fire years 0-2 in the Bobcat fire and post-fire years 2-4 in the High Park fire (Table 2.1).

Tipping bucket rain gauges were located within or relatively near (100 - 2500 m) each plot, hillslope and watershed. Rainfall events recorded by the gauges were identified using the USDA Rainfall Intensity Summarization Tool (RIST; ARS 2013). Rain storms were separated by a period of at least 6 h with <1 mm of rain (Renard et al. 1997). The following rainfall metrics were calculated for each rain storm: depth (mm); maximum intensity (mm h^{-1}) over 5-, 15-, 30-, and 60-minute intervals (MI_5, MI_{15}, MI_{30} and MI_{60}); and erosivity (EI_{30}).

To determine which rainfall metric to use in the threshold analysis, the ability of different rainfall metrics to predict runoff or sediment delivery was tested using a nominal logistic model. MI_{15}, EI_{30} and MI_{60} were the best rainfall metrics to predict a response ($p<0.0001$). We chose to identify thresholds with MI_{60} because hourly rainfall data are more commonly available than finer time step data.

Runoff at plots and hillslopes was ephemeral, only occurring during and immediately after rain storms. The time intervals for inspecting and cleaning out the sediment fences varied, but all sites were visited multiple times each summer. For two hillslopes in the Hayman fire and four hillslopes in the High Park fire runoff was continuously monitored using sediment traps with stage recorders (Robichaud et al. 2013b); these concurrent measurements of runoff and sediment delivery showed that sediment only accumulated in the sediment fences during storms that generated runoff. For locations without continuous runoff monitoring we could therefore assume that the presence of sediment in the fence indicated that runoff had occurred. All

watersheds had perennial flow, and in most cases stream stage was continuously monitored with either capacitance rods (TruTrack WT-HR 1000 mm, Auckland, NZ) or pressure transducers (Model PDCR 1230 Druck) and data loggers (CR10X Campbell Scientific Inc., Logan, UT); indirect estimates based on high water marks were used for Bobcat watersheds in year 0 (Kunze and Stednick 2006). Stage-discharge relationships were developed for each site using manual velocity measurements; runoff responses to rain events were identified as rises in streamflow above baseflow following Kunze and Stednick (2006).

For each rain storm, we determined if there had been a response of either runoff or sediment delivery. If multiple rain storms occurred between site visits or if multiple rain gauges were associated with a site, the rain storm or gauge with the highest EI_{30} was linked to the observed response (e.g., Benavides-Solorio and MacDonald 2005). Rainfall events with no observed response, including multiple rainfall events between site visits, were designated as no response. The varying intervals between site visits for the plots and hillslopes causes some uncertainty about which rainfall event generated a given response. We evaluated the extent to which our procedure biased the results using Spearman's rank correlation coefficient (r) between EI_{30} and the magnitude of runoff or sediment yields (Mg ha^{-1}) for sites with continuous monitoring (watersheds in Bobcat and High Park fires and select hillslopes within Hayman and High Park). The magnitudes of runoff and sediment yields were positively related to EI_{30} (Spearman's r = 0. 57 and 0.54; $p < 0.0001$; n = 132 and 64, respectively), indicating that selecting the event with the highest EI_{30} between site visits is a reasonable approach for determining which rain storm to associate with each response.

2.2.3. Threshold identification and assessment

All rain storms with their associated presence or absence of a response were compiled into sample groups by fire (n=3), year post-fire (n≤5), spatial scale (n≤3) and presence or absence of mulch treatments. We did not stratify by slope because prior research on these fires showed that slope did not significantly affect sediment yields (Wagenbrenner et al. 2006; Wagenbrenner and Robichaud 2014; Schmeer et al. 2018). Altogether this resulted in 48 distinct sample groups (Table 2.2).

For each sample group, we identified thresholds as the MI_{60} value(s) that maximized the fraction (*F*) of rainfall events for which a response was correctly predicted using:

$$F = \frac{TP+TN}{P} \quad (2.1)$$

where *TP* was the number of true positives, defined as rainfall events with MI_{60} greater than or equal to the identified threshold with an observed response; *TN* was the number of true negatives, defined as rain storms with MI_{60} less than the identified threshold with no observed response, and *P* was the total number of rainfall events for that sample group. In most cases, more than one MI_{60} value produced the maximum *F* value; for these, we identified the minimum MI_{60} value (T_{min}) and the maximum MI_{60} value (T_{max}). Threshold prediction errors were either false positives (*FP*) or false negatives (*FN*). *FP* were storms without an observed response but with an MI_{60} greater than T_{min}, and *FN* were storms with an observed response but with an MI_{60} less than T_{min}.

Table 2.2. Number of summer rain storms and percent with runoff or sediment delivery (Y) for unmulched and mulched (N/Y) plots, hillslopes and watersheds by year post-fire, fire (BC=Bobcat; HM=Hayman; HP=High Park), and spatial scale. Blank cells indicate no data.

	Spatial scale:		Plot		Hillslope		Watershed	
Year	Fire	Mulch	No. of rain storms	Y (%)	No. of rain storms	Y (%)	No. of rain storms	Y (%)
0	BC	N	80	10	78	24	22	18
		Y	2	100	35	14		
	HM	N			1232	6		
		Y			143	3		
	HP	N			94	24		
		Y			22	23		
1	BC	N	210	14	384	21	50	40
		Y	25	16	135	11		
	HM	N	268	18	368	27		
		Y	268	12	298	13		
	HP	N			387	22		
		Y			178	9		
2	BC	N	110	22	223	12	28	7
		Y	15	13	70	6		
	HM	N	534	13	957	10		
		Y	528	11	365	12		
	HP	N			598	11	155	8
		Y			221	11		
3	BC	N	150	2	255	2		
		Y	15	0	90	0		
	HM	N	442	4	37	3		
		Y	442	4	26	4		
	HP	N			486	5	253	11
		Y			178	9		
4	HM	N	438	16	40	3		
		Y	438	15	37	3		
	HP	N					112	13

The agreement between predicted and observed responses was evaluated by Cohen's kappa statistic (κ):

$$\kappa = \frac{F - p_e}{1 - p_e} \tag{2.2}$$

where F was defined in equation 2.1 and p_e was the hypothetical probability of chance agreement computed as:

$$p_e = p_{o,Y} * p_{t,Y} + p_{o,N} * p_{t,N} \quad (2.3)$$

where p_o is the fraction of observed responses and p_t is the fraction of responses predicted by T_{min}. The Y subscript indicates a response, while N indicates no response. κ can range from -1 to 1 with values of 0.41-0.60 indicating moderate agreement, 0.61-0.80 indicating substantial agreement, and 0.81-0.99 indicating almost perfect agreement (Viera and Garrett 2005). We use κ values ≥ 0.61 to indicate high-confidence in a given threshold.

2.2.4. Effects of fire location, year post-fire, spatial scale, and mulch treatments on thresholds

Comparisons among sample groups were used to evaluate whether fire location, year post-fire, spatial scale or mulch treatment affected the threshold values. We first computed four separate ANOVAs because a single ANOVA applied to the full dataset simultaneously had insufficient degrees of freedom. For the first two ANOVAs, we assessed the effects of mulch treatments on T_{min} for (1) plots and (2) hillslopes with fire location, year post-fire, and mulch presence/absence as fixed effects (JMP Version 12.0.1); only plots and hillslopes were included in the first two ANOVAs because we did not stratify watersheds by mulch presence/absence. The first two ANOVAs indicated that mulch was not a significant fixed effect, so we conducted a third ANOVA for all spatial scales assessing fire location, year post-fire and spatial scale as fixed effects on T_{min}. Fire location was an insignificant fixed effect in each of the first three ANOVAs, so we conducted a final ANOVA assessing year post-fire, spatial scale and interactions between year and spatial scale as fixed effects on $T_{min.}$ Pairwise differences among significant fixed effects for all models were further examined using Tukey's HSD (JMP Version 12.0.1).

We also examined differences in T_{min} between sample groups to assess the effects of fire location, year post-fire, spatial scale and mulch treatments; these comparisons did not involve statistical tests. For fire location, we compared T_{min} for unmulched hillslopes in post-fire years 0-3 among each of the three fires. We used the unmulched hillslopes for this comparison because this was the most extensive dataset common to all three fires. To examine the effect of year post-fire, we compared T_{min} for each year post-fire stratifying by fire, spatial scale and the presence or absence of mulch. The effect of spatial scale was evaluated by comparing T_{min} for each year and fire across the spatial scales for which data were available (Table 2.1). Finally, the effect of mulch was evaluated for plots and hillslopes by comparing thresholds for sites with and without mulch when stratified by fire, year post-fire, and spatial scale.

The effect of antecedent precipitation on thresholds was also assessed for watersheds with perennial flow, continuous monitoring, and high-confidence thresholds. For this, we used High Park fire watershed scale data for post-fire years 2-4 (n = 520); watershed scale data from the Bobcat fire for years 0-2 (n = 99) were excluded because continuous monitoring was not available in post-fire year 0 (Kunze and Stednick 2006), and kappa was low in post-fire years 1-2. We calculated the daily antecedent precipitation index (I_a) as:

$$I_a = I_o k + I \tag{2.4}$$

where I_o was the initial value of I_a, I was the rainfall on a given day, and k the recession factor set to 0.9 (Dingman 2002). We compared differences in I between rain storms with and without runoff responses across all six watersheds using ANOVA. Our significance level for all analyses and results was 0.05.

2.2.5. Threshold frequency maps

The frequencies of rain storms in Colorado with intensities equal to or greater than the MI_{60} thresholds were computed using data from the 47 NOAA stations with 25-39 years of 15-minute rainfall data (Perica et al. 2013). We used data from the summer thunderstorm season (June-September) and excluded summers missing more than 14 days of data to minimize underestimation of event frequencies. Rain storms with MI_{60} less than 3 mm h^{-1} were also excluded because these values were below the precision of most NOAA rain gauges. The remaining rainfall events for each station were ranked over the period of record by MI_{60}, and the frequency of occurrence for each rain storm was computed by:

$$Frequency = \frac{rank}{(n+1)} \tag{2.5}$$

where *rank* is an integer and *n* is the number of summers with rainfall data.

The calculated MI_{60} frequencies allowed us to determine the average number of times that the MI_{60} from summer rain storms would equal or exceed a given MI_{60} threshold. For each NOAA station, a polynomial was fit to MI_{60} values plotted against calculated MI_{60} frequencies (equation 2.5) for rain storms of 4-12 mm h^{-1}. We chose this range because most higher intensities are already mapped in the NOAA Atlas. Rain storm frequencies were spatially interpolated in 1 mm h^{-1} increments from 4-12 mm h^{-1} over the state of Colorado by co-kriging the calculated frequencies from the 47 stations with the mean June-September rainfall as estimated for 1981-2010 using Parameter-elevation Relationships on Independent Slopes Model (PRISM) data (PRISM Climate Group 2017). The inclusion of PRISM rainfall helped to smooth edges and fill in spatial gaps among the 47 stations.

The density of NOAA stations used in this analysis was lower in northwestern Colorado than in central and eastern Colorado. To limit uncertainty, we focused the frequency analysis on

the fire-prone eastern slope of the Colorado Front Range (Veblen et al. 2000), where our study fires occurred. For this region, we determined how the frequency of events in the range of 4-12 mm h^{-1} varied with elevation.

2.3. Results

2.3.1. Number and magnitude of rainfall events

The total number of site-rain events was 11,522, but the sample size varied greatly by spatial scale and fire (Table 2.2). Overall, more than 94% of the rain storms in the dataset were for plot and hillslope scales (Figure 2.2). The Hayman fire accounted for 85% of the rain storms at the plot scale and 50% of the storms at the hillslope scale. Slightly less than 6% of the rain storms were recorded at the watershed scale, and 84% of these were from the High Park fire (Figure 2.2). In a given year, the percent of rain storms that produced a response ranged from 0-100% for plots ($\bar{x}$ across years = 17%), 0-24% for hillslopes ($\bar{x}$ = 11%), and 7-40% for watersheds ($\bar{x}$ = 16%; Table 2.2). MI_{60} values for most rain storms were very low (Figure 2.2), with median values generally from 2 to 5 mm h^{-1} for a given fire, year post-fire and spatial scale. The maximum MI_{60} values for the different sample groups ranged from 5 to 31 mm h^{-1}, with most values ranging from 10 to 23 mm h^{-1}.

2.3.2. Effects of fire location, year post-fire spatial scale, and mulch treatments on thresholds

Overall, thresholds ranged from 2-31 mm h^{-1}, and prediction accuracy (*F*) for minimum thresholds (T_{min}) was high, averaging 0.92 (Table 2.3, Figure 2.3). Agreement between predictions and observations was not as strong; κ for T_{min} ranged from -0.51 to 1 with an average of 0.54. The percent of summer storms resulting in threshold prediction errors ranged from 0-50% ($\bar{x}$ = 4%), with more false positives ($\bar{x}$ = 5%) than false negatives ($\bar{x}$ = 2%) (Table C1). For

post-fire years 0-2, high-confidence T_{min} values ($\kappa \geq 0.61$) were 4-8 mm h^{-1} across all spatial scales ($\bar{x}$ = 7 mm h^{-1}). Thresholds increased to a range of 7-22 mm h^{-1} in post-fire year 3 ($\bar{x}$ = 10 mm h^{-1}). High-confidence thresholds in post-fire year 4 were 5-6 mm h^{-1}, but these only represent plots in the Hayman fire and watersheds in the High Park fire.

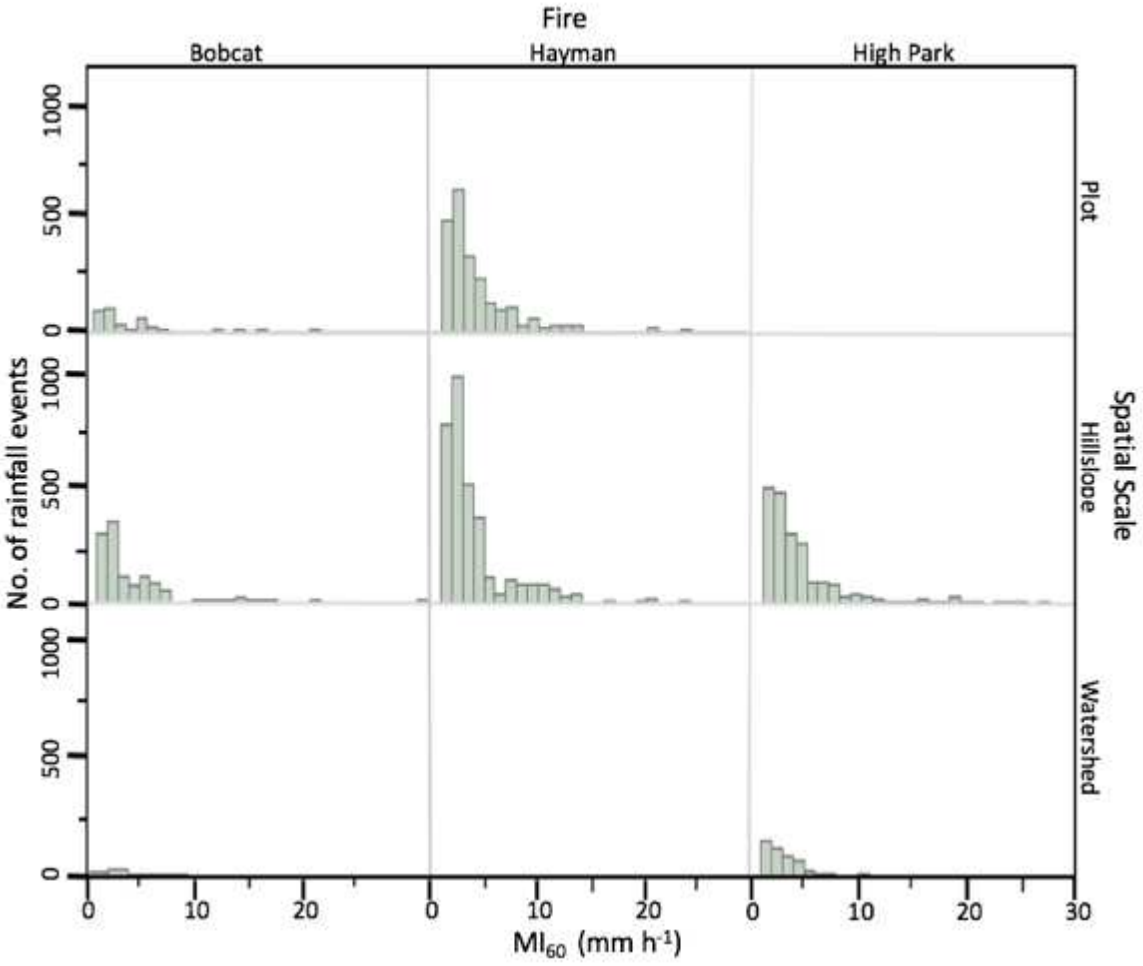

Figure 2.2. Histograms of MI_{60} rainfall events in increments of 2 mm h^{-1} by fire and spatial scale. Blank cells indicate no data.

The first two ANOVAs with fire location, year post-fire and mulch presence/absence as fixed effects on T_{min} revealed nearly significant (p = 0.06) and significant effects (p = 0.02) of year post-fire for plots and hillslopes, respectively (Table 2.4). Fire location and mulch treatments were not significant fixed effects. Subsequent pairwise comparisons (Tukey's HSD)

of year post-fire for the hillslope model revealed significant differences between: (1) years 0 and 4, and (2) years 1 and 4 (p=0.01 and 0.05, respectively) (Table C2). The third ANOVA with fire location, year post-fire, and spatial scale as fixed effects on T_{min} showed significant effects of year post-fire (p = 0.01) and spatial scale (p = 0.01) (Table 2.4). Pairwise comparisons for the third model indicated that T_{min} across all fires and spatial scales was significantly greater for post-fire year 3 than year 0. The final ANOVA with year post-fire, spatial scale, and interactions of year post-fire and spatial scale as fixed effects on T_{min} identified only spatial scale as significant (p=0.01).

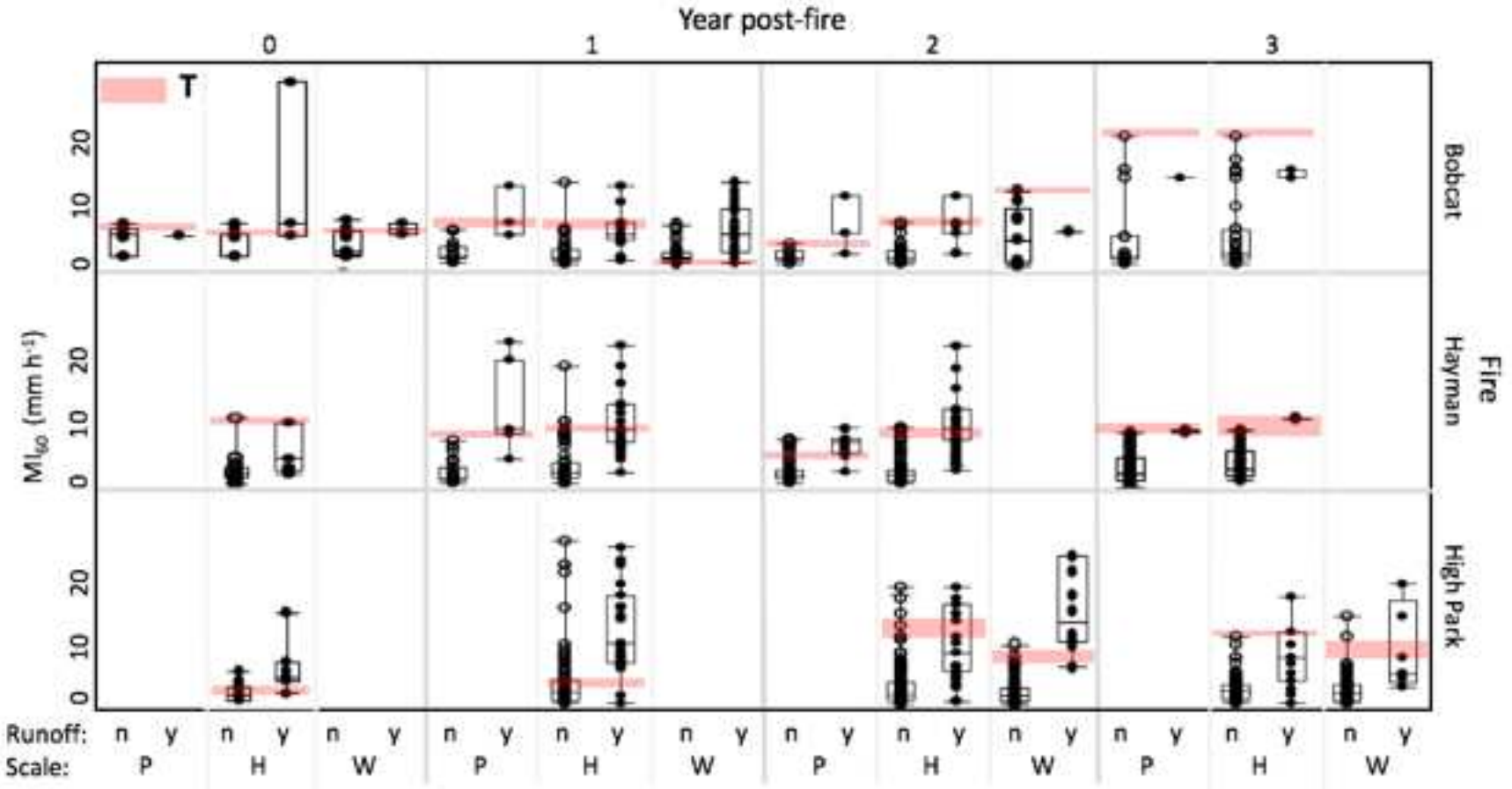

Figure 2.3. MI_{60} rainfall and thresholds (T) for unmulched sites by year post-fire, fire location, spatial scale, and response absence (n; open circles) or presence (y; filled circles). Spatial scale abbreviations are plots (P), hillslopes (H) and watersheds (W). Box plots include: median (horizontal line), 25% and 75% quantiles (box), and observations (circles). Shaded areas are the range of MI_{60} thresholds (T) that maximized the prediction accuracy (*F*) for each dataset.

Table 2.3. MI_{60} rainfall thresholds (T_{min} and T_{max}; mm h^{-1}) for unmulched and mulched (N/Y) plots, hillslopes and watersheds by year post-fire, fire (BC=Bobcat; HM=Hayman; HP=High Park), and spatial scale with the fraction (*F*) of rain storms that correctly predicted a response of runoff or sediment delivery, and corresponding kappa statistic (κ). Blank cells indicate no data.

Spatial scale:			Plot				Hillslope				Watershed			
Year	Fire	Mulch	T_{min}	T_{max}	*F*	κ	T_{min}	T_{max}	*F*	κ	T_{min}	T_{max}	*F*	κ
0	BC	N	7.6	7.6	0.9	0	6.8	7.5	0.88	0.67	6.8 [b]	7.5	0.86	0.58
		Y	5.4[a]	31.3	0.5	0	7.6	31.2	0.89	-0.51				
	HM	N					10.9	11.1	0.96	0.57				
		Y					11.2	11.2	0.97	0				
	HP	N					4.1	4.3	0.88	0.69				
		Y					3.5	4	0.95	0.88				
1	BC	N	6.6	7.7	0.95	0.77	6.6	6.7	0.87	0.82	2	3.3	0.6	0.22
		Y	6.8[b]	7.4	0.88	0.5	11.1	13.5	0.92	0.55				
	HM	N	8.1	9.1	0.99	0.97	9.3	9.7	0.85	0.58				
		Y	8.1	9.1	1	1	11	11.1	0.9	0.5				
	HP	N					6.9	7.3	0.88	0.7				
		Y					16.6	18.5	0.93	0.51				
2	BC	N	4.4	6.1	0.96	0.89	7.3	7.7	0.93	0.76	12 [b]	12	0.93	0
		Y	7.3[b]	7.7	0.93	0.63	12	12	0.94	-0.43				
	HM	N	5.4	5.6	0.95	0.8	7.9	9.5	0.94	0.69				
		Y	5.4	5.6	0.95	0.8	8	8.2	0.93	0.7				
	HP	N					12	15.6	0.92	0.45	8.4	10.4	0.98	0.86
		Y					17.1	18	0.92	0.43				
3	BC	N	21.5	21.5	0.98	0	21.5	21.5	0.98	0.61				
		Y	17.8 [b]	17.8	1	[c]	21.5	21.5	1	[c]				
	HM	N	7.7	7.7	1	1	7.9	9.5	1	1				
		Y	7.7	7.7	1	1	7.7 [b]	7.9	0.96	0.65				
	HP	N					12	12.6	0.97	0.52	7.4	10.1	0.96	0.74
		Y					10.2	10.6	0.94	0.64				
4	HM	N	6.2	6.3	0.92	0.75	20.6	20.6[c]	0.98	0				
		Y	6.2	6.3	0.92	0.73	20.6	20.6[c]	0.97	0				
	HP	N									5	5.7	0.92	0.68

[a] sample size ≤10; [b] sample size ≤30; [c] κ could not be calculated because all events predicted to have no flow

Table 2.4. ANOVA results for T_{min} using four models: (1) plots, (2) hillslopes, (3) all spatial scales, and (4) all spatial scales with interactions. Data are degrees of freedom (DF) and p-values for T_{min}. Bold text indicates $p \leq 0.05$.

Model	Fixed effects	DF	p-value
Plot	Fire	1	0.11
	Year	4	0.06
	Mulch	1	0.85
Hillslopes	Fire	2	0.52
	Year	4	**0.02**
	Mulch	1	0.29
All Spatial scales	Fire	2	0.13
	Year	4	**0.01**
	Spatial scale	2	**0.01**
Year*Spatial scale	Year	4	0.18
	Spatial scale	2	**0.01**
	Year*Spatial scale	8	0.09

The comparison of threshold ranges between sample groups helps illustrate why the ANOVA models did or did not show significant differences in thresholds. First, mulch was not found to be a statistically significant effect on threshold values for the plot and hillslope models (Table 2.4), which may be because the effects of mulch varied by fire, spatial scale and year post-fire (Figure 2.4). Within the Bobcat fire, confidence in threshold predictions for plots in years 0 and 3 was low, and T_{min} was similar for both mulched and unmulched plots (Table 2.3). For Bobcat hillslopes, confidence in both the mulched and unmulched thresholds was high only in post-fire year 1, when the T_{min} was 7 mm h^{-1} for unmulched and 11 mm h^{-1} for mulched hillslopes (Table 2.3). In post-fire year 3, both the unmulched and mulched hillslopes in the Bobcat fire had T_{min} values of 22 mm h^{-1} (Table 2.3). In the Hayman fire, thresholds were similar for mulched and unmulched plots and hillslopes (Table 2.3). In the High Park fire, during post-fire year 1, the mulched hillslopes had a T_{min} of 17 mm h^{-1}, more than twice the value of the unmulched hillslopes, but differences between the mulched and unmulched hillslope thresholds

decreased in post-fire year 2 and became negligible in year 3 (Table 2.3). In summary, mulch treatments did increase the T_{min} values in a few cases, but in most comparisons by fire and year post-fire, T_{min} values were similar for mulched and unmulched sites.

Fire location also did not emerge as a significant fixed effect in the ANOVA analyses. This is probably because no fire had consistently higher or lower thresholds than the others (Table 2.3). For example, at unmulched hillslopes during years 0-1 Hayman T_{min} values were highest (9-11 mm h^{-1}), whereas during year 2 High Park T_{min} was highest (16 mm h^{-1}), and in year 3 Bobcat was highest (22 mm h^{-1}).

Year post-fire was a significant fixed effect in the first three ANOVA models (Table 2.4). For unmulched hillslopes, T_{min} in Bobcat fire was 7 mm h^{-1} for years 0-2 then increased to 22 mm h^{-1} in year 3. T_{min} at unmulched hillslopes in the Hayman fire was 8-11 mm h^{-1} for years 0-3 then increased to 21 mm h^{-1} in year 4. For unmulched hillslopes in the High Park fire, T_{min} increased from 4 mm h^{-1} in year 0 to 7 mm h^{-1} in year 1 and 12 mm h^{-1} in years 2-3. Overall, each of the fires exhibited increases in thresholds over time, but the timing of this increase varied between fires.

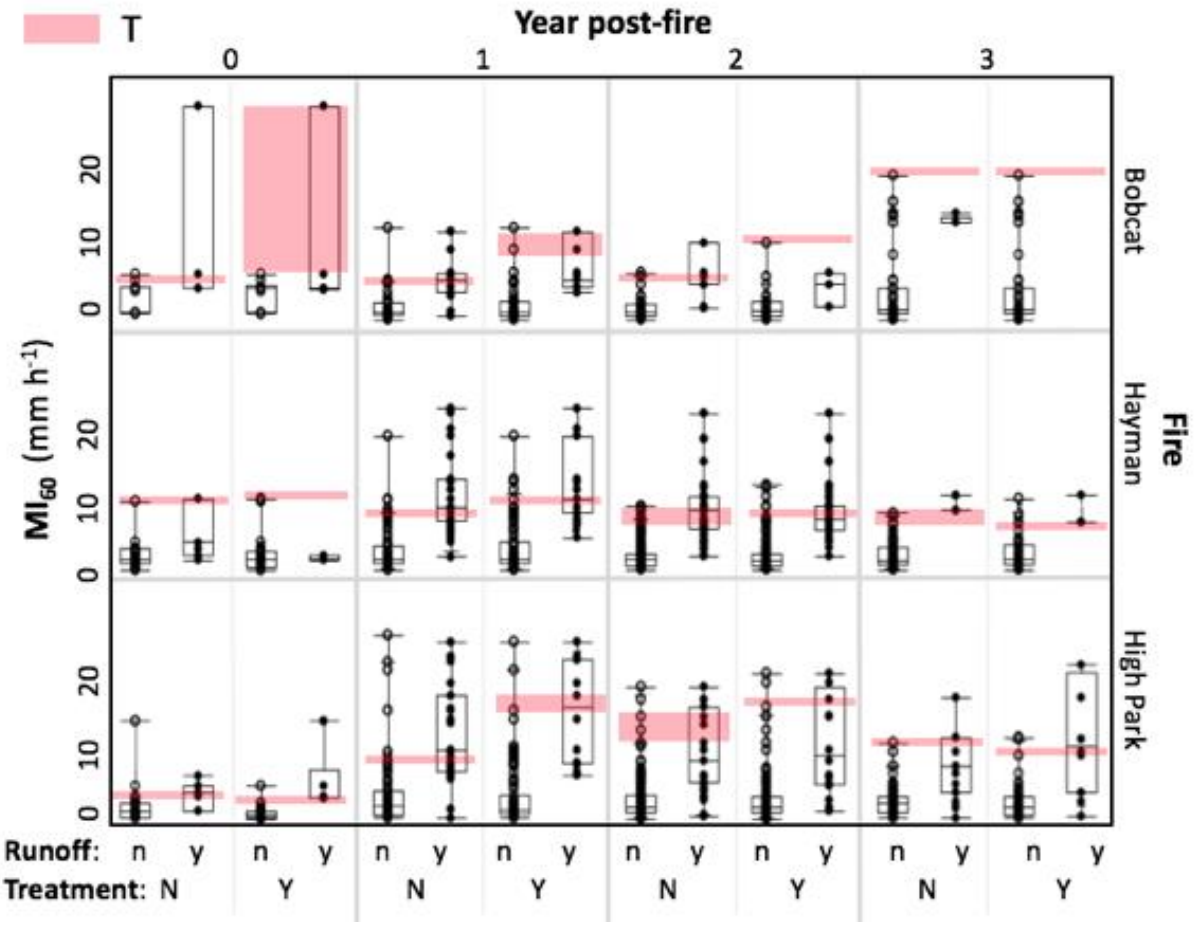

Figure 2.4. MI_{60} rainfall and thresholds (T) for hillslopes by mulch treatment (N/Y), year post-fire, fire and response absence (n; open circles) or presence (y; filled circles). Box plots include the median (horizontal line), 25% and 75% quantiles (box), and observations (circles). Shaded areas are the range of MI_{60} values that maximized the prediction accuracy (*F*) for each dataset.

Spatial scale was also a significant fixed effect in the third and fourth ANOVAs (Table 2.4). The ANOVA models with subsequent multiple comparisons using Tukey's HSD indicate that T_{min} was significantly higher for hillslopes than either plots or watersheds, but this result may be misleading because half of the thresholds at watershed scale were low-confidence (Tables 2.3 and A2). In the Bobcat fire, T_{min} values were the same for plots and hillslopes (7 mm h^{-1}) in year 1, but increased from plot to hillslope scale (4-7 mm h^{-1}) in year 2; other years did not have high-confidence thresholds across multiple spatial scales. In the Hayman fire, for the

years where T_{min} could be compared between scales, values increased from plot to hillslope scale (5-8 mm h^{-1}) in year 2 and stayed the same for plot and hillslope scale in year 3 (8 mm h^{-1}). In the High Park fire, the years with threshold predictions for both hillslopes and watersheds (years 2-3) did not have high confidence thresholds at the hillslope scale. Lower thresholds for watersheds than plots or hillslopes may have been the result of antecedent precipitation, which was significantly higher (ANOVA; $p<0.0001$) for rain storms with responses in runoff ($\bar{x}$ = 32 mm) as compared to those without ($\bar{x}$ = 22 mm).

2.3.3. Frequency of threshold exceedance

For the frequency analysis of threshold-exceeding MI_{60} summer rain storms, we focused on post-fire years 0-2 because thresholds tended to increase significantly after post-fire year 2 (Tables 2.3 and 2.4). Frequencies of threshold exceedance for a given summer were generally higher on the drier eastern slopes of the Front Range and lower for the forests in the western mountainous portion of Colorado (Figure 2.5).

For the eastern slope of Colorado's Front Range, the frequency of threshold exceedance increased with increasing elevation from 1500-2100 m, decreased with increasing elevation from 2100-2300 m, and was relatively consistent above 2300 m (Figure 2.6). Summer rain storms exceeding MI_{60} of 4 mm h^{-1}, the lower bound of high-confidence post-fire response thresholds for years 0-2, were estimated to occur from five to eleven times per typical summer (Figure 2.5). Storms with an MI_{60} threshold of 8 mm h^{-1} were estimated to occur between two to five times per summer, and rainfall events with an MI_{60} threshold of 12 mm h^{-1} were estimated to occur between one to three times per summer (Figure 2.5). The highest frequency for each threshold

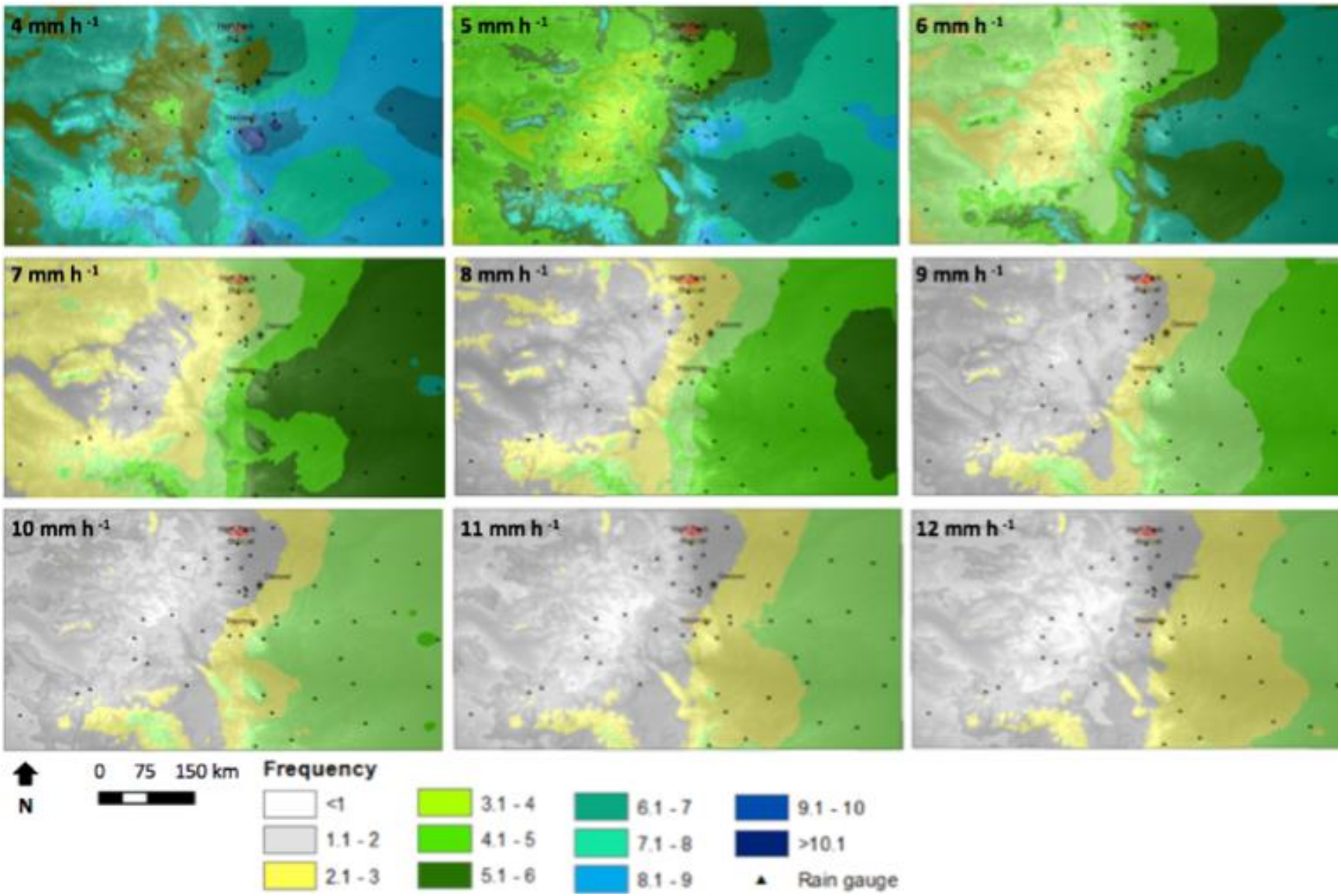

Figure 2.5. Annual average June-September threshold exceedance frequencies for MI_{60} values of 4-12 mm h^{-1} across Colorado. The black triangles are the NOAA rain gauges with at least 25 years of 15-minute data (Perica et al. 2013). Maps produced GCS WGS 1984.

generally occurred just southeast of the Hayman fire (Figure 2.5). Frequencies higher than 8 mm h^{-1} are greater than the range of high-confidence thresholds we identified for post-fire years 0-2 (4-8 mm h^{-1}), but we include them here to illustrate how frequencies change with increasing intensities.

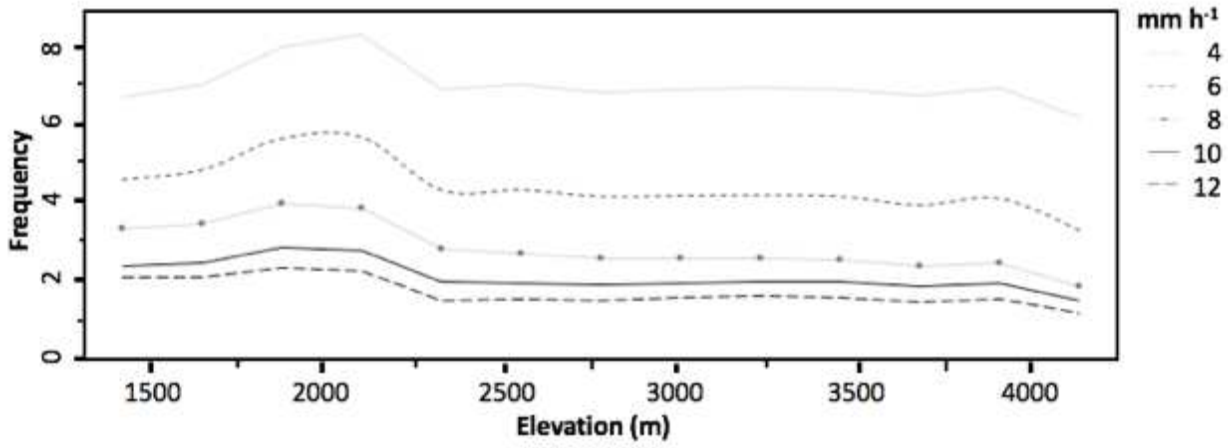

Figure 2.6. Annual average June-September threshold exceedance frequencies by elevation for rainfall with MI_{60} values of 4 to 12 mm h^{-1} on the eastern slope of Colorado's Front Range.

2.4. Discussion

2.4.1. Relationship to other research

Rainfall thresholds for post-fire runoff and sediment delivery have been mentioned in previous research, but this is the first paper to rigorously identify and compare post-fire runoff and sediment delivery thresholds across multiple fires, years post-fire, spatial scales, and the presence or absence of mulch treatments. Most previous studies have reported thresholds as maximum 30-minute rainfall intensity (MI_{30}) values. We related our MI_{30} values to MI_{60} values from the same storms, and found that these were strongly correlated (equation 2.6; n = 1296; Spearman's r = 0.97). The following linear fit equation allows us to compare our thresholds to those in the literature:

$$MI_{60} = 0.57\, MI_{30} + 0.13 \quad (2.6)$$

where all units are mm h^{-1}.

The conversion of published MI_{30} thresholds to MI_{60} values using equation 2.6 results in MI_{60} values that are very similar to our MI_{60} thresholds. Estimated MI_{60} thresholds for post-fire runoff in 220 to 2200 ha basins across the western US were 5 mm h^{-1} for post-fire years 0-1 and 6 mm h^{-1} for post-fire year 2 (Moody 2002). The MI_{60} thresholds were 3-5 mm h^{-1} for post-fire years 1 and 2 in Spring Creek (260 ha) following the Buffalo Creek fire (Moody 2002). In New Mexico's 2000 Cerro Grande fire runoff was not generated in seven sub-watersheds (24 to 85 ha) until MI_{60} was at least 5 mm h^{-1} (Moody et al. 2008b). After the 2010 Fourmile Canyon fire, hydrologic responses were primarily driven by MI_{60} >6 mm h^{-1} (Murphy et al. 2016). These thresholds mostly fall within the 4-8 mm h^{-1} range of high-confidence MI_{60} thresholds that we identified for plots, hillslopes and watersheds of the Bobcat, Hayman and High Park fires in post-fire years 0-2.

We can also compare the increase in our MI_{60} thresholds over time with other studies. In our study the unmulched hillslope data showed a progressive increase in thresholds from year 0 to year 2 in the High Park fire, a large increase in year 3 in the Bobcat fire, and a large increase in year 4 in the Hayman fire. The slower recovery in the Hayman fire has been noted previously and attributed to the very coarse granitic soils with low water holding capacity and poor nutrient status (e.g., Robichaud et al. 2013a,b; Wagenbrenner et al. 2015). The Buffalo Creek fire also has very coarse-textured granitic soils, and hillslope runoff and sediment delivery rates only dropped after 3-4 years post-fire (Moody and Martin 2001a,b). Other Front Range fire studies have documented substantial recovery in terms of hillslope sediment production by the third summer after burning (Benavides-Solorio and MacDonald 2005; Wagenbrenner et al. 2006). In

other Rocky Mountain study areas, post-fire recovery of vegetation and ground cover occurred within 1-6 years after burning, while the recovery of infiltration capacity occurred 2-3 years after burning (Ebel and Martin 2017). This corresponds to the time needed for sufficient vegetation regrowth and litter accumulation to allow infiltration capacities of soils to exceed summer rainfall intensities.

2.4.2. Factors affecting thresholds

Our analyses highlighted similarities in thresholds across fires, increases in thresholds with year post fire, and potential changes in thresholds with spatial scale. There are several important limitations to note in interpreting these results. First, post-fire infiltration rates and thresholds for post-fire surface runoff and sediment delivery are affected by high spatial and temporal variability in site characteristics. Previous studies have found that surface cover and soil sealing (Wainwright et al. 2000; Larsen et al. 2009; Moreno-de las Heras et al. 2010; Inbar et al. 1998), spatial scale (Cammeraat 2002), flow path length (Wagenbrenner and Robichaud 2014), soil type (Miller et al. 2011) and soil water repellency (Benavides-Solario and MacDonald 2001; Woods et al. 2007) are all important for post-fire response, but we did not have data on all of these factors for all study sites. Consequently, there may have been important factors affecting thresholds that we did not consider in the analyses. Second, given the differences in sample size across fires, years, and scales, our dataset was imbalanced, which made it difficult to isolate the effects of individual factors. Third, rainfall data contributed additional uncertainty to the analyses. Relating a specific storm to a response in runoff or sediment delivery is inherently uncertain if there are multiple storms between field visits to empty sediment fences. When multiple storms occurred between site visits, we attributed the response to the storm with the maximum EI_{30}. This potentially led to higher than expected

thresholds if multiple storms produced sediment, and at least one of those storms was less intense than the one that was attributed to the observed response. In addition, some plots and hillslopes were more than a kilometer away from the nearest rain gauge. Summer convective storms can generate highly variable rainfall intensities with maximum rainfall depths occurring within 2500 m of the storm center (Osborn and Laursen 1973). If higher rainfall intensities occurred at a given site compared to its nearest rain gauge, these sites would have an unrealistically low threshold response. The opposite problem, where a site had lower intensity rain than recorded by the nearest rain gauge, could lead to false positives. Finally, for each rain storm, the threshold analysis assigned binary responses of runoff or sediment delivery (i.e., presence or absence), excluding information on the magnitude of responses. For hillslopes, smaller sediment yields (<0.05 Mg ha^{-1}) accounted for 70% of responses (Figure A1), and higher thresholds would likely be needed to predict larger production events.

Despite these limitations, our analysis draws on a large dataset to reveal which factors influence post-fire response thresholds, providing important insights about how fire affects runoff and sediment delivery. The factor that most consistently emerged as an important influence on thresholds was year post-fire. Scale was also a significant effect, but these results are not as straightforward to interpret. The data were easier to compare among plots and hillslopes because these inherently have less spatial variability than watersheds, and the plot and hillslope scales are also more easily replicated. The MI_{60} thresholds at the plot and hillslope scales were generally quite similar across all fires, likely because processes of overland flow generation and downslope connectivity are similar among plot and hillslope scales in areas of high burn severity. Watershed thresholds are more difficult to compare to one another because watersheds typically have much more spatial variability in burn severity, and a given

thunderstorm will probably not be evenly distributed across a watershed (Kampf et al. 2016; Brogan et al. 2017). For our study, there was also very little temporal overlap in the years with watershed data or low confidence thresholds otherwise, so we could not rigorously compare watershed scale thresholds across fires. We found a lower MI_{60} for generating a response at the watershed scale than hillslope scale in the High Park fire (Table 2.3), but this was only in post-fire years 2-3 when threshold confidence was low for hillslopes. During these years, only 50% of the rain storms that caused a response at hillslopes also caused a watershed response. On the other hand, for nearly 20% of the rain storms, a runoff response was observed at watersheds when there was no response in sediment delivery at the monitored hillslopes. This may have been caused by storms with limited spatial extent or differences in antecedent precipitation. Antecedent precipitation was higher for rain storms with runoff than those without at watersheds within the High Park fire, potentially leading to increased water storage within the channel and riparian zones and lower MI_{60} thresholds to initiate a runoff response in watersheds. Concurrent monitoring of runoff across different spatial scales is needed for understanding when and how hillslope runoff connects to downstream areas.

We also aimed to examine the effects of mulching on thresholds, but this proved challenging because of differences in treatments and sample sizes between fires and scales. Mulch did not emerge as a significant source of differences for plot or hillslope scale thresholds in the ANOVA analyses, possibly because of limited sample sizes of mulched and unmulched sites across multiple fires and years. The biggest effect of mulching was to increase T_{min} at the hillslope scale, especially in the Bobcat and High Park fires in post-fire years 1 and 2 (Table 2.3). Mulching had little or no effect on the response thresholds at either the hillslope or plot scales in post-fire years 3 and 4. Previous studies have shown that mulching is most effective in reducing

percent bare soil and sediment delivery compared to relatively bare unmulched sites; vegetation regrowth at both mulched and unmulched sites causes a progressively smaller effect of mulch over time (Wagenbrenner et al. 2006; Rough 2007). It is surprising that mulch did not have much of an effect on the MI_{60} thresholds in the Hayman fire because mulch did cause a large reduction in erosion at the plot and hillslope scales in other studies (Rough 2007; Robichaud et al. 2013b).

2.4.3. Frequency of threshold exceedance

The rainfall thresholds and frequency maps identified the likelihood of post-fire runoff and sediment delivery at plot, hillslope and watershed scales. Our results showed that Colorado's Front Range is likely to experience several (2-11) rain storms that exceed thresholds for generating post-fire responses each summer. The frequency maps were most reliable in areas with high NOAA Atlas station density, such as central and eastern Colorado, and least reliable in areas with fewer stations such as northwestern Colorado. On the eastern slope of the Colorado Front Range, the peak frequency of high intensity storms was at an elevation near 2100 m. This indicates that burned areas near this elevation—like the three study fires—are also most susceptible to high intensity storms. Further analyses are needed to determine if the elevation dependence of the <1 year recurrence interval storms we mapped is similar to spatial patterns of less frequent, more intense storms.

The frequency maps can be used by burned area emergency response (BAER) teams or emergency management organizations and water utilities to rapidly estimate the number of post-fire runoff or sediment delivery events that might occur in a typical summer. This information can be useful for land management, flood mitigation, and water treatment decisions. Our thresholds are relatively conservative in that not all threshold-exceeding events will generate a large response (Figure A1). Additional monitoring is needed to determine how the responses at

hillslope or small watershed scales relate to downstream impacts in larger rivers. The thresholds and frequencies we identified should also be adjusted as needed for specific site conditions, as some sites may have a slower revegetation rate, and therefore lower MI_{60} thresholds may persist over a longer time period.

2.4.4. Future work

A more robust threshold analysis would be possible with some changes and improvements in future post-fire data collection efforts. In particular, rain gauges must be carefully maintained and closely spaced (e.g., Osborn et al. 1972), especially in areas where convective storms are the main cause of post-fire runoff and erosion. At least annual measurements of post-fire ground cover should also be made to help explain the variability in response thresholds over time. Obtaining watershed scale ground cover data is difficult, so intensively monitored plots and hillslopes should be nested within monitored watersheds, with other sampling points added as needed to characterize ground cover at the watershed scale. Ground cover measurements could also be designed to inform remote sensing image classification for mapping cover across larger areas. These measurements would be particularly useful to evaluate the amount and persistence of mulch cover and effect on thresholds at the watershed scale. The applicability of our results also can be improved by collecting data across a wider range of climates and soils.

The rainfall thresholds identified here are related to the effective hydraulic conductivity of the domains sampled and could help calibrate and evaluate models that are currently being used to estimate post-fire runoff and erosion, such as disturbed WEPP (Elliot 2004) and ERMiT (Robichaud et al. 2007). Our methods for determining thresholds and mapping frequencies of threshold exceeding rainfall events could be applied to other regions using region-specific data.

Thresholds could also be adjusted to account for projected changes in the frequency and magnitude of rainfall intensities in future climate conditions.

2.5. Conclusions

This study identified rainfall intensity thresholds for post-fire runoff and sediment delivery at the plot, hillslope and watershed scales for three fires in the Colorado Front Range. The analysis focused on the summer thunderstorms that generate almost all of the post-fire responses at plots and hillslopes and the largest responses at watersheds. Considering all years post-fire, thresholds varied significantly among spatial scales and years post-fire, but insignificantly among fire locations and with mulch treatment. For the first three summers after burning (post-fire years 0-2), we have high confidence that runoff or sediment delivery were observed when maximum 60-minute rainfall intensities exceeded 4 to 8 mm h^{-1}. On the eastern slope of the Colorado Front Range, storms at or exceeding this range of intensities will likely occur between two to eleven times in a typical summer. Areas most likely to generate post-fire runoff and erosion can be identified with the threshold exceedance frequency maps, which can aid rapid assessment of potential post-fire impacts to downstream residents, infrastructure and water supplies.

CHAPTER 3: CATCH EFFICIENCY OF SEDIMENT FENCES FOR MONITORING POST-FIRE HILLSLOPE SCALE SEDIMENT PRODUCTION[2]

3.1. Introduction

Land surface disturbances such as wildfire, agriculture or construction can lead to increased erosion and sediment delivery to streams. In the case of wildfire, organic surface cover is consumed thereby increasing bare soil and depositing ash on the soil surface (Keeley 2009). While ash may temporarily protect the soil (Woods & Balfour, 2010), raindrop impacts lead to soil sealing (Larsen et al. 2009) and higher magnitudes of runoff and erosion compared to pre-fire conditions (Wagenbrenner & Robichaud, 2014). Following fires, increased overland flow can result in extensive rilling, gullying, and headwater channel extension (Wohl & Scott, 2017). Associated increases in sediment transport capacities and sediment yields (Pietrasek 2006; Moody & Martin, 2001; Moreno-de las Heras et al., 2010; Prosser &Williams, 1998; Parsons et al., 2006; Wainwright et al., 2000) can result in increased sediment delivery to streams.

Detachment and transport of sediment typically increases with increasing rainfall intensity (Farmer, 1973; Wan & El-Swaify, 1998), rainfall erosivity and overland flow (Bagnold, 1977; Shi et al., 2012). Rainsplash can detach a wide range of soil particle sizes, but the smaller particles are more readily entrained and transported from hillslopes by sheetflow (Sutherland, 1991; Wan & El-Swaify, 1998). Once flow concentrates into rills in topographically convergent areas, the deeper and faster flow can both detach and transport coarser particles (Shi et al., 2012;

[2] This chapter submitted for publication as: Wilson, CR, Kampf, SK, Wagenbrenner, JW, MacDonald, LH and H Gleason. In review. Catch efficiency of sediment fences for monitoring post-fire hillslope scale sediment production. Earth Surface Processes and Landforms.

Wan & El-Swaify, 1998). Along a hillslope, coarser particles tend to be deposited in areas with lower slopes, while organic matter and finer particles are more readily transported downslope (Parsons et al., 2006), where they are more likely to enter streams, affect water quality and pose problems for water treatment and supplies and aquatic organisms. The capacity of burned hillslopes to retain runoff and sediment increases with vegetation regrowth, litter accumulation, and mulch treatments that increase cover, intercept rainfall and slow overland flow (Wagenbrenner et al., 2006; Robichaud et al., 2013a,b; Wainwright et al., 2000; Moreno-de las Heras et al., 2010; Inbar et al., 1998; Yanosek et al., 2006).

Sediment fences are a commonly used low-cost method to measure post-fire erosion on planar and convergent hillslopes and small ephemeral catchments (Wagenbrenner & Robichaud, 2014; Robichaud et al., 2013b; Schmeer et al., 2018). Where drainage areas are small (<0.01 ha), these fences may have catch efficiencies >90% (Robichaud et al., 2001). However, sediment fences have been used to quantify erosion for sites with larger contributing areas (Pietraszek, 2006; Olsen, 2016; Wagenbrenner et al., 2006; Schmeer, 2014; Robichaud et al., 2019; Wagenbrenner et al., 2015; Benavides-Solorio & MacDonald, 2005; James & Krumland, 2018). Increases in both drainage area and bare soil lead to higher runoff and erosion (Johansen et al., 2001; Pannkuk & Robichaud, 2003; Larsen et al., 2009; Prosser & Williams, 1998; Parsons et al., 2006; Wainwright et al., 2000). When runoff is high, it can overtop the fence and reduce catch efficiency by carrying suspended sediment. In more extreme cases the fence can completely fill with sediment, so all subsequent sediment is simply washed over the top, resulting in a potentially very large underestimate of the sediment yield. These problems have been addressed in some cases by installing sequential or larger sediment fences (e.g., Wagenbrenner et al., 2006; Robichaud et al., 2019; Olsen, 2016; James & Krumland, 2018), but

usually the quantity of sediment under-catch is unknown in cases when the full amount of runoff and sediment are not stored within the fence(s).

The goal of this study was to improve understanding of the catch efficiency of sediment fences used to measure erosion rates from highly erodible soils in recently burned areas. Specific objectives were to: (1) determine the catch efficiency and particle size sorting of sediment fences measuring post-fire hillslope erosion and (2) evaluate how catch efficiency and particle size sorting related to rainfall, erosion and runoff event characteristics.

3.2. Methods

3.2.1. Study Sites

In June 2012, the High Park Fire burned 330 km^2 of primarily coniferous forest in the northern Colorado Front Range west of Fort Collins (Figure 3.1). This fire was of particular concern because the burned area drains into the Cache la Poudre or the Big Thompson Rivers, which supply drinking water for Fort Collins, Greeley, Loveland, and other municipalities. Mulch treatments to mitigate post-fire runoff and sediment delivery were applied to some areas of the High Park Fire with moderate to high severity burn and steep slopes (BAER, 2012; Figure 3.1). In this study, precipitation, surface cover, runoff and sediment yields were monitored from July through early October 2014 on four severely burned convergent hillslopes nested within the headwater catchments of two larger watersheds in the High Park Fire.

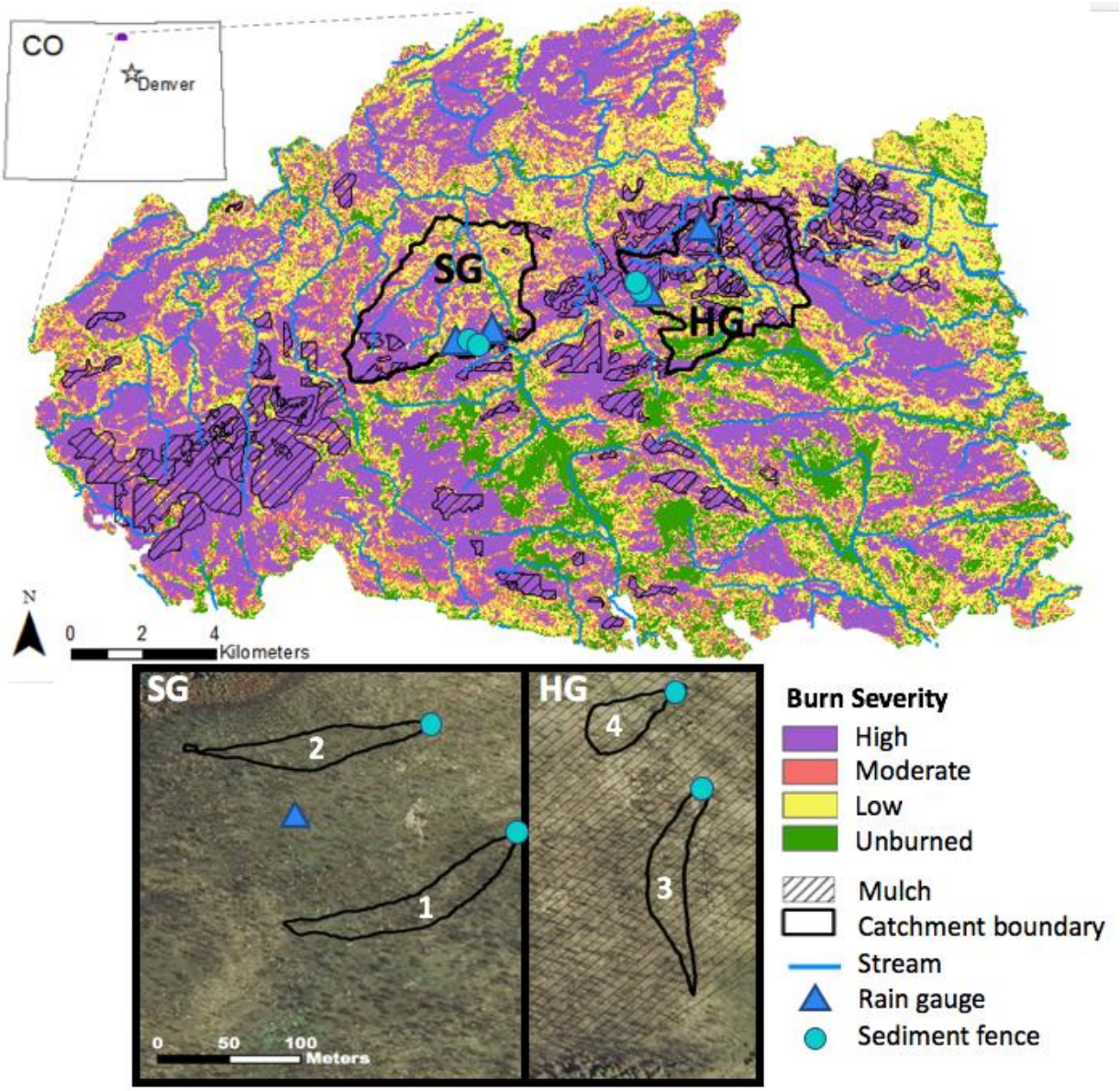

Figure 3.1. Upper: High Park Fire burn severity (Stone 2015), mulch treatments, study watersheds (Skin and Hill Gulch; SG and HG, respectively), streams, rain gauges, and sediment fences; Lower: monitoring sites with sediment fences and co-located rain gauges in SG and HG. Refer to upper panel for the location of additional rain gauges, which are approximately 1-2 km from study sites (Imagery: USDA 2013).

Geology of the High Park Fire area is Precambrian metasedimentary and metaigneous schists, gneisses, and plutonic igneous rocks (Abott, 1970); soils are predominantly Redfeather sandy loam (BAER, 2012). The climate of this region is semiarid and monsoonal with 60–75%

of precipitation occurring as rain during spring and summer (April – September) and the remainder primarily as snow. Peak streamflows in the Colorado Front Range are typically rainfall dominated where mean watershed elevation is below 2000 m and snowmelt dominated where mean watershed elevation is above 3100 m (Kampf & Lefsky, 2016). The elevation of our study sites ranges from 2280-2490 m (Table 3.1), so streamflow is driven by a mix of snowmelt and rainfall. Post-fire runoff and erosion at the hillslope-scale is predominantly generated by summer thunderstorms (Benavides-Solario & MacDonald, 2005). For our study sites, average summer (June-Sept.) precipitation from 1981-2010 averaged 200 mm (PRISM Climate Group, 2018).

In June 2014 four convergent hillslopes (0.19-0.43 ha) were identified for this study, with two adjacent drainages in Skin Gulch and two in Hill Gulch (Figure 3.1). Average slope at these sites ranged from 17-19 degrees with predominant aspects of either N, E or NE. Width length ratios calculated as hillslope width divided by main axis length were similar at the two sites in Skin Gulch and HG3 (0.1), but was higher at HG4 (0.3; Table 3.1). The Hill Gulch sites were scheduled to receive 2-3 Mg ha^{-1} of wood strand mulch in October-November 2012 and 14 Mg ha^{-1} of straw mulch in June 2013. However, the actual application rates varied, and much of the straw applied to the Hill Gulch sites was removed by wind and overland flow (Figures 3.1 & 3.2, Table 3.1). Sediment fences were installed at SG1 and SG2 on July 1st and July 10th, 2014, respectively; the runoff and suspended sediment collection barrels were installed on July 23rd (Table 3.2; Figure 3.3 and 3.2). Sediment fences in Hill Gulch were installed in 2012, and runoff collection equipment was installed on July 7th, 2014. Sites were monitored from the date of equipment installation through the beginning of October 2014.

Table 3.1. Characteristics of the hillslope runoff and sediment collection sites within Skin Gulch (SG) and Hill Gulch (HG).

	SG1	SG2	HG3	HG4
Area (ha)	0.43	0.32	0.32	0.19
Elevation (m)	2420-2480	2430-2490	2300-2370	2280-2300
Average slope (°)†	17	19	19	19
Aspect (predominant)†	NE	E	N	NE
Width-length ratio‡	0.1	0.1	0.1	0.3
Mulch (%)§	0	0	100	100
Mulch (%)¶	0 (0)	0 (0)	10 (7)	27 (10)

† Slope and aspect determined from a 2m DEM in ArcGIS 10.3 (ESRI 2013).
‡ Width calculated as hillslope area (m^2) divided by length of the main axis length (m); ratio calculated as width divided by main axis length.
§Percent mulch based on GIS polygons of the areas targeted to receive mulch treatments (Fig.1).
¶Percent mulch based on field measurements of basal (and canopy) cover.

3.2.2. Precipitation, soil texture, and surface cover

Tipping bucket rain gauges (Rainwise Inc., Trenton, Maine, USA) with a resolution of 0.25 mm were installed within 0.2-1.0 km of the hillslopes in Skin Gulch and 0.4-2.4 km of the hillslopes in Hill Gulch (Figures 1, 2). The distance to the closest operating rain gauge for each site varied throughout the season. From June 1st to August 9th, the closest gauge in Skin Gulch was 1 km east of the sites; on August 9th, an additional gauge was installed 0.1 km from the sites (Figure 3.1). In Hill Gulch, the closest operable rain gauge was 0.4 km east of the sites from June 1st to September 11th, and then, due to malfunctioning of the nearby gauge, 2.4 km northeast from September 11th through the end of the season (Figure 3.1).

Rainfall data were processed using the USDA Rainfall Intensity Summarization Tool (ARS, 2013) with events separated by at least 6 h with <1 mm of rain (Renard et al., 1997). The following rainfall metrics were calculated for each event: rainfall depth (mm), duration (h), maximum intensity (mm h^{-1}) over 5-, 15-, 30-, and 60-minute intervals (MI_5, MI_{15}, MI_{30} and MI_{60}), and 30-minute erosivity (EI_{30}), where EI_{30} is defined as the product of event rainfall

kinetic energy and maximum 30-minute intensity (Brown & Foster, 1987). The depths of rainfall exceeding a specific MI_5 threshold were also calculated for MI_5 values between 10 and 20 mm h^{-1} in intervals of 5 mm h^{-1} (i.e., P>10, P>15 and P>20; Kampf et al., 2016). Site visits were conducted after each rain storm to the extent possible. If multiple rain storms occurred between site visits or if multiple gauges were associated with a site, the rain storm with the highest EI_{30} was assigned to the runoff and sediment producing event (Benavides-Solario & MacDonald, 2005).

Soil texture was determined for each hillslope from three aggregated soil samples (60-100 g) collected at a depth of 0-5 cm below the ground surface during the summer each fence was installed. The percent of sand, silt, clay and gravel were determined using either sieving and the hydrometer method (Gee & Or, 2002; Schmeer, 2014) or wet sieving and filtration (ASTM D3977-97 Test Method C; ASTM, 2013a).

Surface cover was systematically quantified for each hillslope in mid-August 2014 using transects of at least 100 points per site. For each point, ground and canopy cover were each classified as bare soil, bedrock, live vegetation, litter, rock (> 1 cm diameter), wood (> 1 cm diameter), tree, straw mulch, or wood mulch. As defined here, canopy cover was observed as the first surface a raindrop would encounter from < 1 m above the ground surface, and ground cover was observed at the ground surface.

3.2.3. Runoff and sediment yields

To measure runoff and sediment yields, each hillslope was instrumented with a sediment fence (Robichaud & Brown, 2002); fences were modified to include a 90° V-notch weir and an enclosed gutter to direct the V-notch overflow into a series of three 250-liter barrels (Bonilla et al., 2006; Figure 3.2). For the purpose of this paper, we defined sediment load as either bedload

or suspended load; the sum of these was the total load. Bedload is the sediment trapped behind the fence (Figure 3.2a), and suspended load is the sediment that is carried by the runoff over the sediment fence. While some suspended sediment settles out and is trapped behind the sediment fence, this functional separation of eroded sediment into bedload and suspended load allows us to compute the catch efficiency of sediment fences and the total sediment load.

Bedload was collected from the fence in 20-L buckets, and the mass was measured in the field to the closest 0.5 kg using a hanging scale. For each event, a representative grab sample of bedload (approximately 0.5 kg) was collected and stored in a sealed 0.65 L plastic bag until gravimetric water content could be determined (ASTM D2974-13 Test Method A; ASTM, 2013b). Water content was used to adjust the field-wet mass of sediment to a dry mass. For each event, dry mass was normalized by contributing area to give bedload per unit area (Mg ha^{-1}).

If sufficient runoff was produced to overtop the fence, water and suspended sediment were routed through the weir and into a series of three 250 L barrels (Figure 3.2b). The first and second barrels were fitted with 15-way flow splitters (Bonilla et al., 2006) (Figure 3.2b), with $1/15^{th}$ of the flow being directed to the subsequent downstream barrel. Sample proportions were 1/1 in barrel 1, 1/15 in barrel 2, and 1/225 in barrel 3. These samples were used to determine total runoff (Q) volume (equation 3.1):

$$Q = B1_v + (15\ x\ B2_v) + (225\ x\ B3_v) \quad (3.1)$$

where $B1_v$, $B2_v$, and $B3_v$ were the volumes of Q collected in barrels 1-3, respectively. The volume collected in each barrel was determined using a stage-volume relationship, and the total runoff volume as calculated with equation 3.1 was normalized by contributing area and reported as depth in mm. The runoff ratio was calculated as the depth of Q (mm) divided by the depth of rainfall (mm) for the rain storm associated with the runoff response.

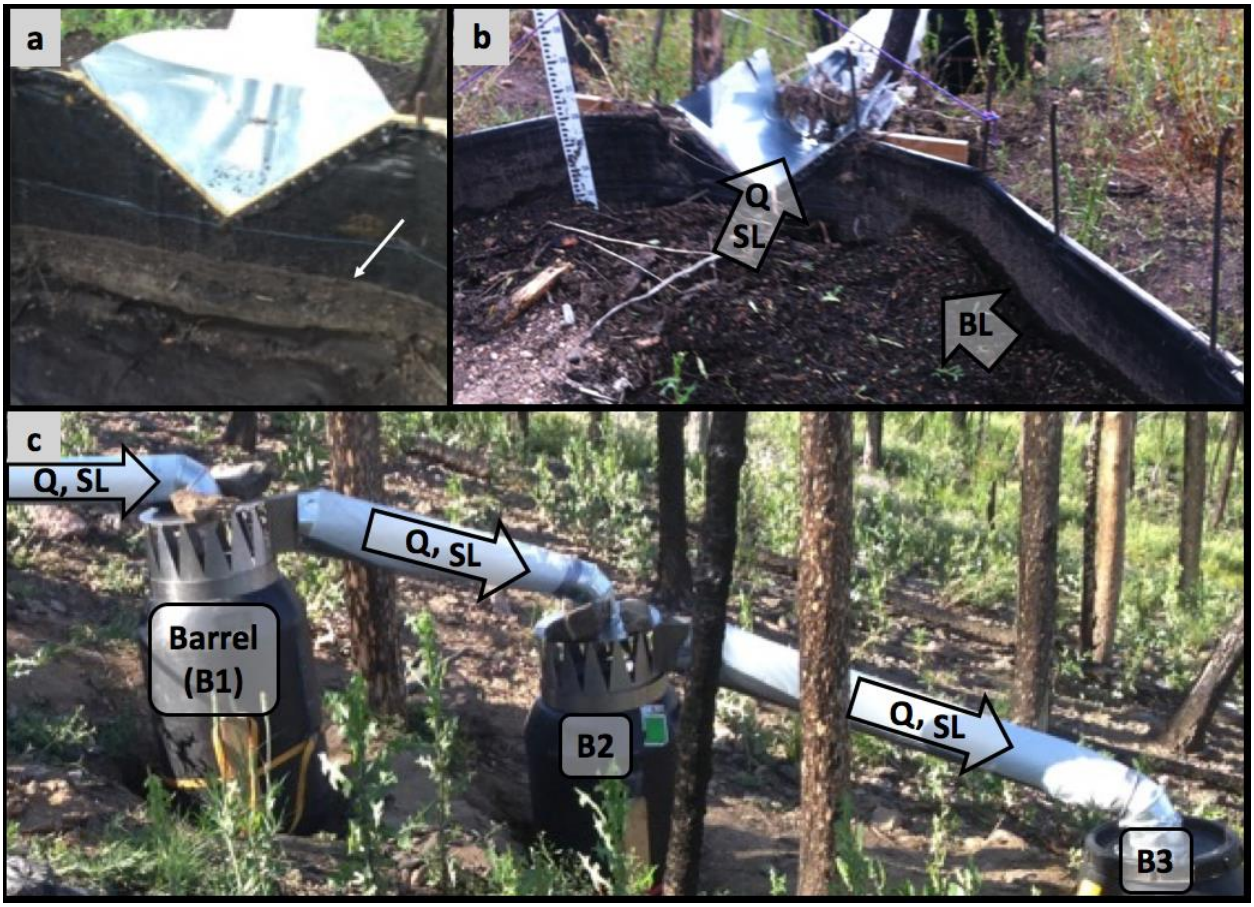

Figure 3.2. Hillslope runoff and sediment collection site showing: (a) downslope view of a sediment fence containing bedload sediment produced by an event that did not result in runoff or suspended load samples in downstream barrels (HG4, July 7th); the white arrow points to the high water mark below the V-notch weir; (b) downslope view of sediment fence in the foreground with captured bedload (BL); the 90° V-notch weir routed runoff (Q) and suspended sediment (SL) into a series of three collection barrels; and (c) side view of the barrel collection system: the first two barrels (B1 and B2) were equipped with flow splitters that each sent 1/15th of the runoff into the next barrel downslope.

The suspended sediment concentration (SSC; mg L^{-1}) of the collected Q for each barrel was determined by stirring and sampling approximately 500 mL of runoff per barrel using either grab samples or a DH-48 depth-integrating suspended sampler mounted to a 0.9 m wading rod. The sediment mass within each sample was determined through wet sieving and filtration (ASTM D3977-97 Test Method C; ASTM, 2013a), and the event suspended sediment load (mg) was determined by

$$Suspended\ Load = \sum_{B=1}^{3} SSC_B x Q_B \quad (2)$$

where SSC_B and Q_B are the suspended sediment concentration (mg L^{-1}) and volume of Q (L) of each barrel (B). Suspended loads were normalized by the contributing area and reported as Mg ha^{-1}.

For both bedload and suspended load by barrel, the fraction of mineral mass and organic matter was determined by wet sieving and filtration (ASTM D3977-97 Test Method C; ASTM, 2013a) and subsequent analysis of ash content (ASTM D2974-13 Test Method C; ASTM, 2013b). Particle size fractions were categorized as either: (i) sand (i.e., coarse mineral sediment; >53µm in diameter); (ii) silt/clay (i.e., fine mineral sediment; <53µm in diameter); (iii) total mineral sediment (sand + silt/clay); (iv) coarse organic matter (>53µm in diameter); (v) fine organic matter (<53µm in diameter); or (vi) total OM.

3.2.4. Analyses

For each rain storm with Q, bedload, and/or suspended load ("site-event"), the total load (Mg ha^{-1}) was calculated as the sum of bedload and suspended load. If Q from one or more rain storms did not overtop the sediment fence, the sediment deposited behind the fence was equal to the total load. Catch efficiencies were calculated for each site as the ratio of bedload to total load for each rain storm individually and for the total sediment produced over the entire season; values were computed for minerals and organic matter (total-catch efficiency) and for minerals only (mineral-catch efficiency). When there was no flow over the fence, the catch efficiency equaled 1, and when flow overtopped the fence, catch efficiency was less than 1. For each site-event, the total sediment concentration was calculated as the total load (minerals and organic matter; g) divided by total Q (L).

Enrichment ratios (ER) indicate how the collected sediment compares to hillslope soil texture and how sediment particles are sorted between the hillslope and collection system. ER values were calculated for each site-event with bedload and suspended load samples to determine whether preferential erosion and transport occurred. ER was calculated as the fraction of coarse (sand) or fine (silt/clay) particles within the bedload and suspended load divided by the corresponding coarse or fine fraction of the surface soil in the contributing area for each site (Wan & El-Swaify, 1998). An ER > 1 indicates enrichment of the particle type in the sediment collection system relative to the hillslope soils, while an ER <1 indicates depletion (Wan & El-Swaify, 1998).

To examine which variables may have affected catch efficiency (CE) and enrichment ratios (ERs), we computed Pearson correlations between CE and ERs and: rainfall metrics, sample location (bedload and barrels 1-3), day of the year, and production variables (Q, suspended load, bedload, total load, runoff ratio, and total sediment concentration). Each variable was assessed to determine whether it was normally distributed, and data were transformed to natural logarithms to normalize distributions when needed. We also used ANOVA to test for differences in: (i) production variables and rainfall metrics for Skin and Hill Gulch; and (ii) ER by sample type (bedload or suspended load). Our significance level for all analyses was 0.05.

3.3. Results

3.3.1. Hillslope and rainfall-runoff event characteristics

Over all sites, bare soil was significantly higher for measurements made at the ground surface than for those observed from the canopy (ANOVA; $p < 0.05$). Bare soil at the ground surface was lowest for HG4 at 29%, and was similar for HG3 (47%) and the Skin Gulch sites (50-56%); these differences were likely due to mulch applications, which represented 10-27% of

ground and 7-9% of the cover observed from the canopy in Hill Gulch (Figure A2). Bare soil observed from the canopy was only 10-14% across all sites. From our soil texture analysis, hillslope soils were either loamy sand or sandy loam.

The number of rain storms and total rainfall (mm) in June-October 2014 were similar between Skin and Hill Gulch, with 34 storms in Skin Gulch totaling 302 mm of rain and 36 storms in Hill Gulch totaling 290 mm of rain (Figure 3.3). Four rain storms generated runoff and erosion at both hillslopes in Skin Gulch, although the first of these storms occurred before installation of the barrels to collect runoff and suspended sediment (Table 3.2; Figure 3.2 and 3.3). HG3 had five rain storms with runoff and erosion ("site-events") while HG4 had only three; of the latter, one site-event did not generate enough runoff to overtop the sediment fence (Table 3.2; Figure 3.2 and 3.3).

Q ranged from 0.1 to 2.4 mm in Skin Gulch ($\bar{x}$ = 1.1) and 0.1 to 6.7 mm in Hill Gulch ($\bar{x}$ = 2.1) with suspended loads of 0.003 to 1 Mg ha^{-1} in Skin Gulch ($\bar{x}$ = 0.3) and from 0.001 to 0.4 Mg ha^{-1} in Hill Gulch ($\bar{x}$ = 0.1). Bedload ranged from 0.01 to 0.59 Mg ha^{-1} in Skin Gulch ($\bar{x}$ = 0.21) and from 0.004 to 0.64 Mg ha^{-1} in Hill Gulch ($\bar{x}$ = 0.18). SG1 and SG2 had simultaneous and similar magnitude site-events, whereas HG3 responded with greater magnitude to more rain storms than HG4 (Table 3.2; Figure 3.3). Runoff ratios were more similar and less variable within Skin Gulch sites (0.01 to 0.07) than Hill Gulch; HG3 ranged from 0.03 to 0.24 while HG4 was much lower from 0.004 to 0.005 (Table 3.2; Figure 3.3). Total sediment concentrations ranged from 7 to 73 mg L^{-1} in Skin Gulch ($\bar{x}$ = 31) and from 4 to 79 mg L^{-1} in Hill Gulch ($\bar{x}$ = 24). Runoff and sediment variables (Q, bedload, suspended load, total load, runoff ratio, and total sediment concentration) were not significantly different between Skin and Hill Gulches (ANOVA; Table 3.2).

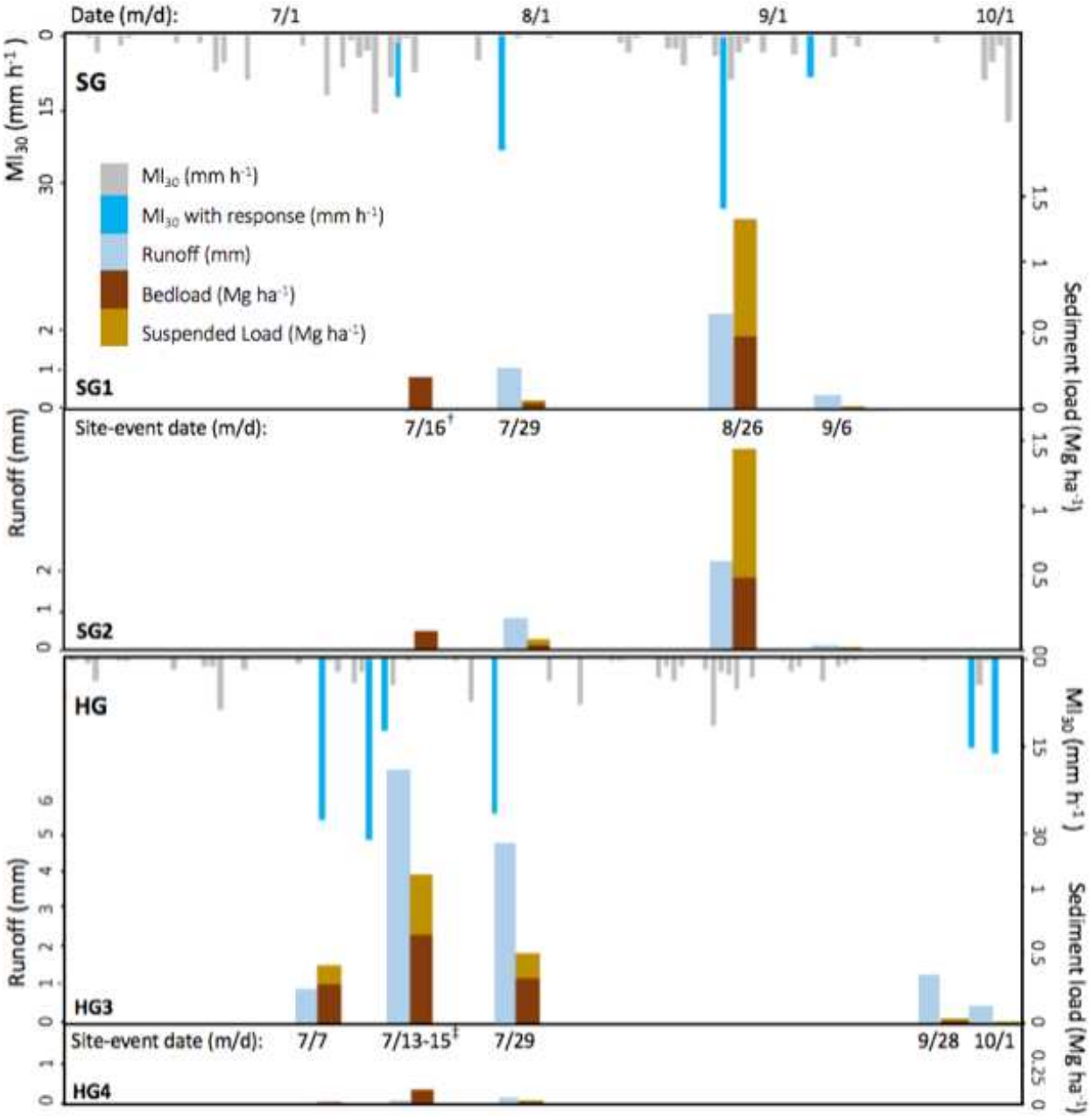

Figure 3.3. June-Oct. 2014 rainfall intensity (MI_{30}; mm h^{-1}) and site-event production within Skin (SG; upper) and Hill Gulch (HG; lower); rainfall is shown as a single value per watershed while runoff (mm), bedload and suspended load (Mg ha^{-1}) are shown for each site (from top to bottom: SG1, SG2, HG3, and HG4). Note the differences in rainfall and site-event timing in the two watersheds. † Site-events occurred before runoff collection equipment was installed. ‡ Site-events represent two rainfall events.

3.3.2. Particle sorting and catch efficiency

Over all sites and sample types, enrichment ratios ranged from 0.2 to 1.0 for sand ($\bar{x}$ = 0.7) and 0.3 to 3.5 for silt/clay ($\bar{x}$ = 1.2), indicating that the eroded sediment was on average depleted in sand and enriched in silt/clay relative to the hillslope soil samples. Enrichment ratios for sand were significantly higher in bedload than in suspended load (ANOVA; p = 0.0004), while enrichment ratios for silt/clay were significantly higher in suspended load than in bedload (ANOVA; p = 0.01). There were no clear temporal trends in enrichment ratios over the monitoring period (r = 0.02-0.20).

The sediment demonstrated significant particle sorting with sample location along the collection system (i.e., sediment fence through collection barrels 1-3). Percent sand was highest in bedload samples, ranging from 45 to 83%. Both percent sand and total minerals significantly decreased from the fence through the collection barrels (r = -0.51 and -0.33, respectively; Figure B1) while silt/clay, total and fine organic matter fractions significantly increased at each subsequent sampling point in the collection system (r = 0.33 to 0.49; Figure B1).

By site-event, catch efficiency ranges were similar between sites. Total catch efficiency of both minerals and organic matter ranged from 36-75% in Skin Gulch ($\bar{x}$ = 56%) and from 28-67% at HG3 ($\bar{x}$ = 53%) and from 86-100% at HG4 ($\bar{x}$ = 95%; Table 3.2). Mineral catch efficiencies were slightly higher, ranging from 39-77% in Skin Gulch ($\bar{x}$ = 58%) and from 48-100% in Hill Gulch ($\bar{x}$ = 65%; Table 3.2). Total-catch efficiency and mineral-catch efficiency were significantly higher at HG4 as compared to all other sites (ANOVA; p = 0.001 and 0.002, respectively). When integrated over the entire season, total catch efficiencies were lower in Skin Gulch (38-40%) as compared to Hill Gulch (62-94%).

Table 3.2. Summer 2014 site-events with date, runoff (Q), bedload (BL), suspended load (SL), total load (TL), runoff ratios (RR), total sediment concentration (TSC), total catch efficiency (CE; %), mineral catch efficiency (M-CE; %), and enrichment ratios (ER) for sand and silt/clay for bedload and suspended load (in parentheses). Blank cells indicate no data.

Site	Date (m/d)	Q (mm)	BL (Mg ha^{-1})	SL (Mg ha^{-1})	TL (Mg ha^{-1})	RR (Q/P)	TSC (g L^{-1})	CE (%)	M-CE (%)	ER sand	ER silt/clay
SG1	7/16		0.24		0.24						
	7/29	0.92	0.05	0.02	0.07	0.01	7	74	76	0.61 (0.27)	1.42 (2.07)
	8/26	2.44	0.59	0.96	1.55	0.07	64	38	42	1.13 (0.84)	0.51 (1.00)
	9/6	0.31	0.02	0.01	0.03	0.06	11	57	59	0.91 (0.36)	1.00 (2.51)
SG2	7/16		0.15		0.15						
	7/29	0.71	0.05	0.04	0.09	0.01	12	58	56	0.70 (0.20)	1.32 (3.52)
	8/26	2.05	0.54	0.95	1.49	0.06	73	36	39	1.07 (0.79)	0.62 (1.23)
	9/6	0.08	0.01	0.003	0.013	0.02	17	75	77	0.87 (0.21)	1.33 (3.37)
HG3	7/7	0.95	0.28	0.14	0.42	0.05	44	67	68	0.84 (0.66)	0.77 (0.81)
	7/13-15	6.71	0.64	0.42	1.06	0.24	16	60	63	1.04 (0.76)	0.47 (0.85)
	7/29	5.14	0.32	0.18	0.5	0.06	10	64	66	1.04 (0.69)	0.42 (1.15)
	9/28	1.16	0.02	0.03	0.05	0.12	4	44	48	0.83 (0.49)	0.77 (1.61)
	10/1	0.38	0.004	0.01	0.01	0.03	4	28	26	0.90 (1.08)	0.55 (0.29)
HG4	7/7		0.02		0.02			100	100		
	7/13-15	0.13	0.1	0.001	0.1	0.005	79	99	99	0.97 (0.60)	0.64 (0.81)
	7/29	0.32	0.03	0.01	0.04	0.004	11	86	87	0.96 (0.30)	0.62 (2.23)

3.3.3. Correlations

Log-transformed Q increased for events with higher rainfall intensity and depth (Figure 3.4; Table 3.3), but correlations were not consistently strong across all rainfall metrics (Table 3.3). Two site-events at HG3 (July 13-15th and 29th) had significantly higher Q (ANOVA; $p < 0.0001$) (Figure 3.4), but rainfall depth and intensity (MI_{30}) were not significantly higher for these events (ANOVA; $p = 0.41$ and 0.32, respectively).

Sediment production was more clearly linked to rainfall intensity than depth, with log-transformed suspended and bedload increasing with intensity for the rain storms with the highest MI_{30} ($r = 0.57$-0.60, respectively; Table 3.3), specifically for site-events on August 26th in Skin Gulch and July 13-15th at HG3 (Figure 3.3). However, bedload was more strongly correlated with the shortest bursts of high intensity rainfall (MI_5) ($r = 0.73$; Table 3.3). Both suspended load and bedload increased with Q ($r = 0.87$ and 0.73, respectively; Table 3.3); for site-events on August 26th in Skin Gulch and July 13-15th at HG3, high suspended and bedloads are likely also due to the high intensity rainfall during these site-events (Figure 3.3). The log-transformed total sediment concentration of events also increased with rainfall intensity and log-transformed bed and total loads (Table 3.3; Figure 3.4). Log-transformed Q and sediment loads increased with the depth of rainfall exceeding an MI_5 threshold of 10 mm h^{-1} (i.e., P>10; $r = 0.54$ - 0.71; Table 3.3); sediment loads and total sediment concentrations also increased with the depth of rainfall exceeding MI_5 thresholds of 15 to 20 mm h^{-1} (i.e., P>15 and P>20; $r = 0.61$ - 0.85; Table 3.3).

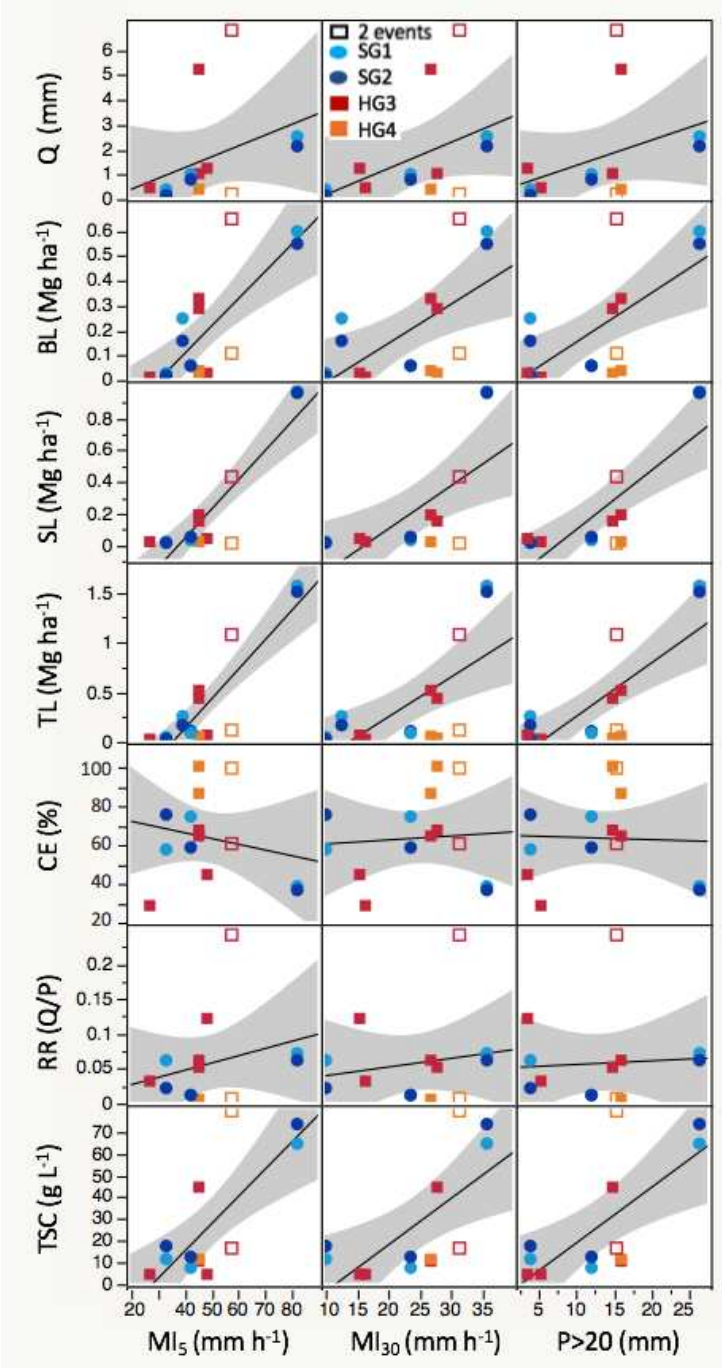

Figure 3.4. Runoff (Q; mm), bedload (BL; Mg ha^{-1}), suspended load (SL; Mg ha^{-1}), total load (TL; Mg ha^{-1}), total-CE (%), runoff ratio (RR; Q/P) and total sediment concentration (TSC; g L^{-1}) vs. rainfall intensity (MI_5 and MI_{30}; mm h^{-1}) and P>20 (mm); open symbols for HG3 and HG4 indicate that these samples represent two rainfall events (July 13-15th). The shaded area represents the 95% confidence interval for each fitted line.

Table 3.3. Pearson correlation coefficients relating event rainfall or cover metrics to runoff (Q), bedload (BL), suspended load (SL), total load (TL), runoff ratio (RR), total sediment concentration (TSC) and total-catch efficiency (CE). Lower portion of table shows cross correlations of these response variables. Sample size is 16 for bedload and 13 for all other variables. The natural logarithm (Log) was used to transform all response data except CE to achieve normality. Bold text indicates significance at the 0.05 level.

	Log [Q (mm)]	Log [BL (Mg ha^{-1})]	Log [SL (Mg ha^{-1})]	Log [TL (Mg ha^{-1})]	Log [RR]	Log [TSC (g L^{-1})]	CE
Depth (mm)	0.30	0.17	0.09	0.16	-0.40	-0.12	0.28
Duration (h)	0.15	0.00	-0.07	-0.08	-0.46	-0.33	0.29
MI_5 (mm h^{-1})	0.51	**0.72**	**0.61**	**0.83**	0.28	**0.72**	-0.13
MI_{15} (mm h^{-1})	0.47	**0.66**	0.53	**0.82**	0.19	**0.75**	-0.03
MI_{30} (mm h^{-1})	**0.56**	**0.60**	**0.57**	**0.85**	0.09	**0.67**	0.00
MI_{60} (mm h^{-1})	0.53	0.33	0.41	**0.59**	-0.14	0.29	0.14
EI_{30} (MJ mm ha^{-1} h^{-1})	0.48	0.42	0.43	0.54	-0.19	0.27	0.06
P>10 (mm)	**0.56**	**0.54**	**0.58**	**0.71**	0.02	0.46	-0.08
P>15 (mm)	0.54	**0.61**	**0.65**	**0.82**	0.09	**0.65**	-0.13
P>20 (mm)	0.53	**0.62**	**0.65**	**0.85**	0.11	**0.73**	-0.12
Log [BL (Mg ha^{-1})]	**0.73**						
Log [SL (Mg ha^{-1})]	**0.87**	**0.77**					
Log [TL (Mg ha^{-1})]	**0.79**	**0.97**	**0.86**				
Log [RR]	**0.71**	0.44	**0.74**	0.54			
Log [TSC (g L^{-1})]	0.03	**0.67**	0.30	**0.63**	-0.02		
CE	-0.44	0.00	**-0.62**	-0.24	**-0.62**	0.17	

Enrichment ratios were also correlated with rainfall intensity, with higher intensity rain events producing sediment more enriched in sand (r = 0.56; Table 3.4; Figure 3.5). The depth of rainfall for events exceeding MI_5 thresholds of 15 and 20 mm h^{-} (i.e., P>15 and P>20) was also related to increased enrichment ratios for sand within bedload (r = 0.56). For bedload samples, enrichment ratios for sand also increased when total sediment loads increased (Table 3.4; Figure 3.5; r = 0.56). For suspended load samples, samples were depleted in sand with higher CE (Table 3.4; Figure 3.5; r = -0.61).

Catch efficiency had no significant relationships to rain event metrics, but it did decrease with higher suspended loads and runoff ratios (r = -0.62; Table 3.3). Although our sample size was small, catch efficiency appears to decrease with increasing drainage area between 0.19 and

0.43 ha, particularly for events with high runoff ratios. Catch efficiency also appeared to decrease with higher bare soil at the ground surface, and was highest for the site with the smallest area and highest width-length ratio (HG4; Figure 3.1).

Table 3.4. Pearson correlation coefficients relating enrichment ratios (ER) for sand and silt/clay within bedload (BL) and suspended load (SL) to event rainfall metrics, runoff (Q), bedload (BL), suspended load (SL), total load (TL), runoff ratio (RR), total sediment concentration (TSC) and total-catch efficiency (CE). The natural logarithm (Log) was used to transform some data to achieve normality. Bold text indicates significance at the 0.05 level.

	ER - BL		ER – SL	
	Sand	Silt/clay	Sand	Silt/clay
Rainfall metrics				
Depth (mm)	-0.21	0.08	-0.30	0.21
Duration (h)	-0.39	0.26	-0.46	0.39
MI_5 (mm h^{-1})	**0.58**	-0.45	0.34	-0.37
MI_{15} (mm h^{-1})	0.44	-0.40	0.39	-0.46
MI_{30} (mm h^{-1})	0.48	-0.52	0.42	-0.50
MI_{60} (mm h^{-1})	0.13	-0.36	0.18	-0.32
EI_{30} (MJ mm ha^{-1} h^{-1})	0.19	-0.20	-0.01	-0.02
P>10 (mm)	0.48	-0.48	0.26	-0.28
P>15 (mm)	**0.56**	-0.47	0.33	-0.32
P>20 (mm)	**0.56**	-0.46	0.37	-0.37
Q (mm)	0.49	-0.52	0.40	-0.38
Log [BL (Mg ha^{-1})]	0.51	-0.45	0.32	-0.39
Log [SL (Mg ha^{-1})]	0.44	-0.39	0.47	-0.32
Log [TL (Mg ha^{-1})]	**0.56**	-0.50	0.45	-0.45
Log [RR]	0.42	-0.41	0.51	-0.39
Log [TSC (g L^{-1})]	0.48	-0.21	0.18	-0.20
CE	-0.23	0.27	**-0.61**	0.30

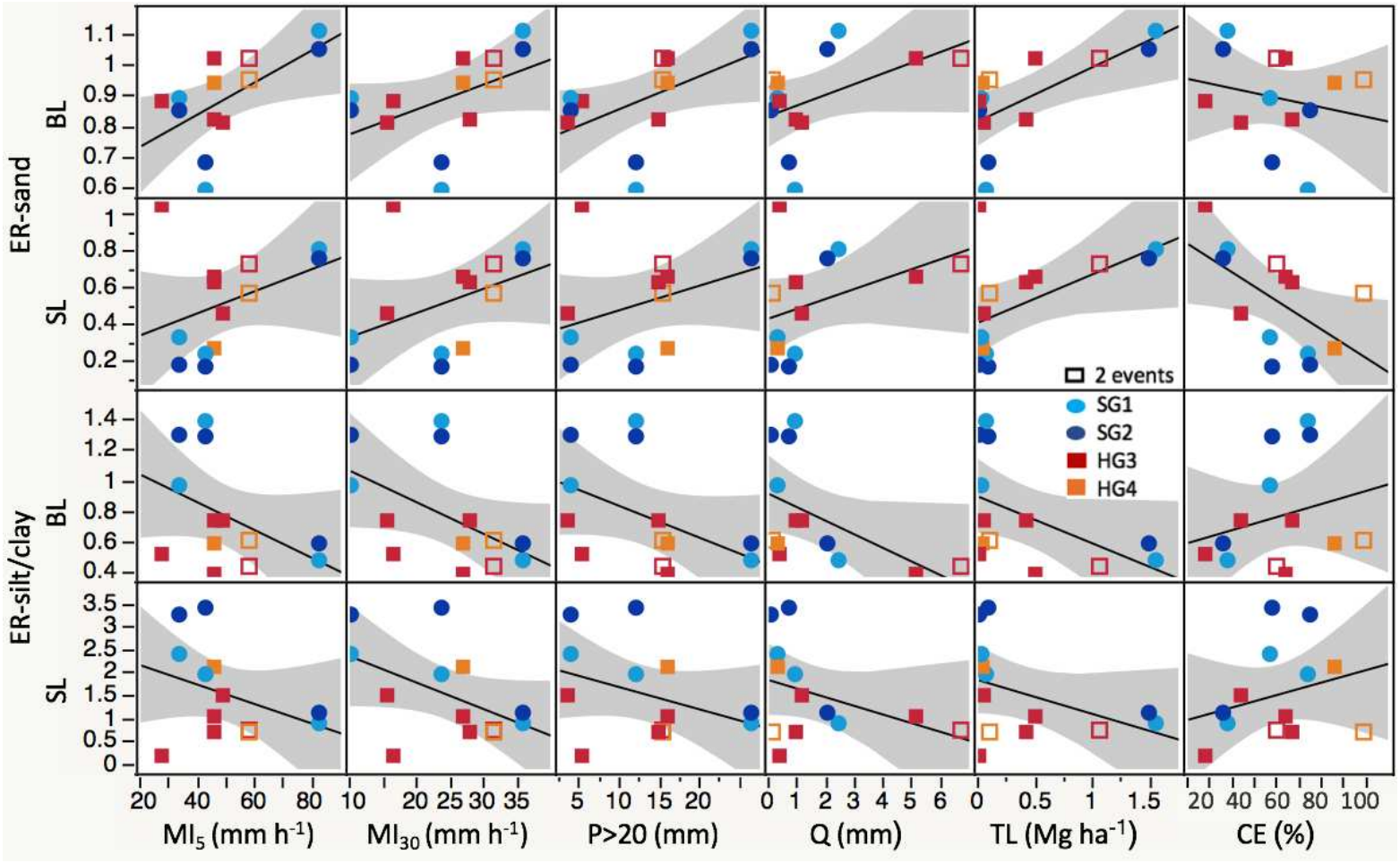

Figure 3.5. Enrichment ratios (ER) of sand and silt/clay for bedload (BL) and suspended load (SL) samples by site for rainfall intensity (MI_5 and MI_{30}; mm h^{-1}) and P>20 (mm), runoff (Q; mm), total load (TL; Mg ha^{-1}) and total-catch efficiency (CE; %); open symbols for HG3 and HG4 indicate that these samples represent two events. The shaded area represents the 95% confidence interval for each fitted line.

3.4. Discussion

3.4.1. Factors affecting runoff, sediment production, and particle sorting

Similar to the findings of other post-fire studies in the region, our results highlight the importance of rainfall intensity for producing runoff and sediment (Moody and Martin 2001b; Robichaud et al., 2013b; Benavides-Solario & MacDonald, 2005; Wagenbrenner et al., 2006; Schmeer et al., 2018). Here, higher rainfall intensities, particularly $MI_{30,}$ were significantly related to increased runoff production ($r = 0.56$; Table 3.3), which can transport more sediment (Prosser & Williams, 1998; Parsons et al., 2006; Wainwright et al., 2000). This was supported by the significant relationships between Q and sediment production (i.e., bedload, suspended load, and total load; $r = 0.71$-0.87; Table 3.3). Although higher Q led to significantly higher sediment loads at all sites (Table 3.3), erosion rates were greater in Skin Gulch than Hill Gulch, possibly due to differences in erodibility and/or ground cover (Figure 3.3). For events with relatively similar MI_{30}, total sediment concentration (TSC) in Skin Gulch (Aug. 26th; $MI_{30} = 36$ mm h^{-1}; TSC = 73 g L^{-1}) was up to seven times higher than that of Hill Gulch (July 29th; $MI_{30} = 27$ mm h^{-1}; TSC = 11 g L^{-1}).

During hillslope erosion, larger particles may be retained in the soil profile or settle out of transport while smaller particles are preferentially transported downslope (Parsons et al. 2006); once flow concentrates into rills, coarser particles are more easily detached and transported (Wan & El-Swaify, 1998). While we did not measure the occurrence or extent of interrill or rill erosion, we found that higher intensity rainfall increased enrichment ratios for sand in bedload samples (Table 3.4). This is consistent with other studies that found rainfall intensity increased the size of particles detached and subsequently available for transport (Farmer, 1973; Wan & El-Swaify, 1998). Higher rainfall intensities have also been found to produce more infiltration

excess overland flow and higher runoff depths that increase transport capacity (Bagnold, 1977; Shi et al., 2012). Overall, the variability in sediment size distributions among events reflects differences in transport capacity or detachment power of raindrops rather than source limitation, as enrichment ratios did not change with day of year. While shallow overland flow may initially protect soil particles from rain drop impact, smaller particles may be preferentially transported during this flow condition as larger particles may be retained in the soil profile or settle out of transport (Shi et al., 2012; Wan & El-Swaify, 1998). Enrichment ratios were on average higher for silt/clay ($\bar{x}$ = 1.2) than sand ($\bar{x}$ = 0.7) across all sites and sample types, which indicates rainsplash and sheetwash may have predominated (Sutherland, 1991; Wan & El-Swaify, 1998).

Additionally, the particle sorting observed along our collection system highlights how particle size distributions of sediment change during transport. Bedload samples were more enriched in sand, which was less likely to be suspended and transported downstream of the sediment fences. The suspended sediment loads were more enriched in finer mineral particles and organic matter, and once delivered to the stream network, these components have greater implications for aquatic organisms (Jones et al., 2012) and municipal water treatment (Emelko et al., 2011) than the larger particles.

The separation of sediment into bedload and suspended load applied here is consistent with the pragmatic, functional distinction made in sediment transport studies that attempt to measure both bedload and suspended load (e.g., Edwards & Glysson, 1988). However, as the sediment collection system caused water to pond where it would otherwise flow downhill, the natural transport regime was modified, and the “bedload” and “suspended load” values given here are specific to the collection system and not directly analogous to bedload and suspended loads that would reach streams. In the future, other methods such as detailed surface topographic

surveys may allow us to infer the amount of sediment transport without modifying the flow regime, but such methods cannot yet resolve the depth of splash or interrill erosion or deposition (DeLong et al., 2018).

3.4.3. Catch efficiency

Our findings indicate that the sediment fence method for monitoring post-fire erosion may lead to underestimates of sediment production, as total- and mineral-catch efficiencies at our sites averaged only 56-65%, respectively. Although reported catch efficiencies for sediment fences are as high as 90% for hillslope areas <0.01 ha (Robichaud et al., 2001), post-fire erosion has been monitored with sediment fences for sites up to 1.5 ha (Pietraszek, 2006; Schmeer, 2014) with the average size of monitored hillslopes within the Bobcat, Hayman and High Park fires ranging from 0.2 to 0.3 ha (Wilson et al., 2018). At our sites, catch efficiency decreased with increasing drainage area between 0.19 and 0.43 ha. The decrease with increasing drainage area was significant for events with high runoff ratios, indicating that the undercatch of sediment may be more severe for sediment fences on hillslopes that generate high runoff volumes. The lack of observed relationships between catch efficiency and rainfall metrics may be due to differences in Q generation among the sites, leading to variability in bedload and suspended loads for a given event. Catch efficiency decreased with increasing runoff ratios which suggests higher runoff ratios result in greater velocity of flow overtopping the sediment fence, leading to more suspended sediment transport. For rainfall events with greater capacity to transport sand the catch efficiency may initially be higher (Table 3.4) but will decrease as more sand and other material is deposited behind the fence thereby reducing storage capacity.

Sediment catch efficiency for a given fence is highly dynamic, and depends on the rate of incoming flow, volume of material already stored in the fence, the concentration and particle size

distribution of the sediment in the runoff, and the rate of flow overtopping the fence. Water backed up upslope of the fence has lower velocity, allowing coarser particles to settle. As the sediment settles, the storage capacity in the fence declines. In this study, the sediment fences never came close to filling with sediment, so storage capacity did not substantially decline during runoff events. Consequently, the rate of inflow was likely the dominant influence on whether the fence overtopped with water, and once overtopped the amount of outflow was nearly the same as the amount of inflow. During conditions with higher erosion rates such as those in the first two years after fire, sediment fences in this area often filled (Schmeer et al., 2018), so storage capacity would have been more limiting. Consequently, it is likely that catch efficiencies were even lower in the first two years post-fire.

3.4.4. Future work

Sediment fence modifications such as those shown here can allow for more accurate estimation of hillslope sediment loads. Where Q and suspended load measurements are not feasible, lower cost alternatives would be to construct larger sediment fences or include additional fences downslope. The total fence storage capacity should be large enough to accommodate peak volumes of Q without water overtopping the total fence storage capacity, as overtopping causes underestimation of suspended loads. This may not be realistic for large hillslopes, so an alternate option would be using multiple fences in sequence to expand storage capacity. Researchers can estimate the necessary sediment fence volume by taking the depth of an extreme storm, multiplying by the contributing area and a runoff coefficient. For example, most sediment fences have a storage capacity <5 m^3: assuming a hillslope drainage area of 0.5 ha, in the range of those observed here, a storm with 5 mm of rainfall and a runoff ratio of 0.2

would produce enough runoff (5,000 L) to fill the sediment fence and increase Q estimates by 1 mm. For the site-events measured here this corresponds to 10-90% more runoff ($\bar{x}$ = 50%).

Field visits to measure sediment and empty sediment fences should occur as soon as possible after rainfall events, as this will reduce the likelihood that runoff and suspended loads exceed the storage capacity of collection equipment. Continuous monitoring of runoff at sediment fences would also enable more detailed analysis of how runoff patterns affect erosion, and this information could be used to refine values of rainfall thresholds that cause erosion (Wilson et al., 2018). Telemetered runoff monitoring, in addition to higher capacity sediment fences, may further decrease the likelihood of overtopping. Our results demonstrate that suspended sediment is a larger portion of the total sediment delivered from hillslopes than previously recognized. Additional observations are needed to fully understand the contribution of suspended sediment to post-fire sediment delivery across different burn severities, rainfall regimes, and through post-fire recovery periods.

3.5. Conclusions

We modified hillslope sediment fences to measure runoff volume and suspended load from four severely burned hillslopes during the 2014 summer thunderstorm season, two years after the High Park Fire. We found that high intensity rainfall increased runoff, sediment loads, and the transport of coarser particles, consistent with other studies. Higher intensity rain storms and runoff volumes decreased the proportion of silt/clay that was captured in sediment fences, as these particles were more readily carried over the sediment fence as suspended load. Overall, we observed progressively smaller proportions of coarse particles through the collection system, indicating that these would be less likely to be delivered for long distances through the stream network. Total- and mineral-sediment fence catch efficiency averaged 56-65%, respectively,

which means that in some cases nearly as much sediment was transported as suspended load as was trapped behind the sediment fences. This indicates that sediment load measurements with sediment fences often underestimate erosion. To represent hillslope erosion more accurately, future monitoring with sediment fences should maximize the storage capacity, and ideally incorporate runoff measurements and suspended sediment collection systems.

CHAPTER 4: LATERAL AND LONGITUDINAL CONNECTIVITY OF POST-FIRE RUNOFF AND SEDIMENT FROM HILLSLOPE TO WATERSHED SCALE[3]

4.1. Introduction

High severity wildfire increases the potential for connectivity of runoff and sediment both laterally (hillslope-channel) and longitudinally (upstream-downstream). Hydrologic connectivity has been defined as the water-mediated transfer of materials such as sediment (Pringle 2001). The transfer of sediment via hydrologic connectivity is affected by hydro-geomorphic factors (Heckman et al. 2018) such as spatial variability in site characteristics (e.g., topography, burn severity) and hydroclimatic variables (e.g., rainfall-runoff) (Lexartaz-Artza and Wainwright 2009; Wainwright 2011). Indices of connectivity can be computed with static variables like topographic and soils data, but connectivity is also affected by dynamic processes such as remobilization of stored sediments stored during rainfall-runoff events (Duvert et al. 2011). Post-fire landscapes are particularly sensitive to this balance of how static features of watersheds interact with time-varying runoff and sediment transport processes, as less rainfall is needed to produce a response in runoff and erosion than for unburned conditions (Wilson et al. 2018; chapter 2). Post-fire, lateral connectivity is further promoted by interconnected areas of bare soil (Ortíz-Rodrígez et al. 2019).

Wildfire combusts organic surface cover and leaves soil exposed to raindrop impacts and soil sealing (Larsen et al. 2009). On hillslopes, surface runoff and erosion increase after fire

[3] This chapter is being prepared for publication as: Wilson, CR, Kampf, SK, Ryan, S and T Covino. Lateral and longitudinal connectivity of post-fire runoff and sediment from hillslope to watershed scale. Geomorphology.

(Benavides-Solorio and MacDonald, 2005; Wagenbrenner and Robichaud, 2014), and the area required to initiate channelized flow decreases (Wohl 2013) by orders of magnitude compared to pre-fire conditions. In Colorado's Front Range, post-fire hillslope responses, specifically runoff and sediment delivery, are predominantly produced by infiltration-excess overland flow during spatially variable convective rainfall events (Moody and Martin 2001a,b; Moody et al. 2013) in which the highest intensities of rainfall may be concentrated in areas <10 km^2 (Osborn and Laursen 1973). These high rainfall intensities cause increases in peak streamflow and sediment transport rates within channels (Moody and Martin 2001a,b). However, due to the limited spatial extent of convective rainstorms, upstream-downstream connectivity of runoff may be greater for storms with greater spatial extent and/or those and following high antecedent rainfall (Moody and Martin 2001a,b; Murphy et al. 2018; Wilson et al. 2018; chapter 2).

In a comparison of post-fire measurements across the western US, Moody and Martin (2009) found that hillslopes produced higher area-normalized runoff than channels on average, whereas channels produce higher area-normalized sediment yields than hillslopes. However, well-established methods for measuring hillslope erosion may underestimate sediment yields due to the suspended sediment that is transported away from hillslopes within runoff (Wilson et al., in review). Organic matter and finer particles are more readily transported downslope (Parsons et al., 2006; Wilson et al. in review; chapter 3); once sediment enters a channel it can remain stored for centuries (Moody and Martin 2001a) or be exported if post-fire storms produce high enough streamflow. In many cases sediment storage and therefore dis-connectivity of sediment within channels increases with time since burn and in lower gradient reaches as the frequency of flows capable of sediment transport decreases (Smith et al. 2011; Moody and Martin 2001a). Depending on the magnitude and sequence of post-fire events, higher hillslope runoff can erode

channel banks and beds where there is a lack of previously stored sediments available for transport, or cause aggradation in lower gradient channels when there is insufficient sediment entrainment and transport capacity (Moody and Martin 2009; Kampf et al. 2016; Brogan et al. 2019).

Connectivity of runoff and sediment after wildfire generally decreases over time as vegetation returns. Post-fire mulch treatments can also increase surface cover and associated opportunities for rainfall interception and storage of runoff and sediment (Wagenbrenner et al. 2006; Robichaud et al., 2013a,b; Wagenbrenner and Robichaud 2014; Wainwright et al., 2000; Moreno-de las Heras et al., 2010; Inbar et al., 1998; Parsons et al. 2006; Woods et al. 2007). By three to four years post-fire, typically only the most extreme storms (e.g., > 1 year return interval) produce a runoff and erosion response on hillslopes (Ebel and Martin 2017; Moody and Martin 2001a; Wagenbrenner et al. 2015; Wilson et al. 2018; chapter 2). By four years post-fire, the drainage areas required for concentrated flow increase, comparable to unburned conditions (Wohl and Scott 2017).

Though post-fire responses are well-documented for plot, hillslope, or watershed scales independently, studies linking responses across these scales are needed (Smith et al. 2011). Post-fire runoff and sediment create difficulties for emergency management and water treatment (Emelko et al. 2011; Hohner et al. 2016; Martin 2016). Many communities depend on forested watersheds for water supplies, and these areas are vulnerable to wildfire (Brown et al. 2008; Westerling et al. 2006; Robinne et al. 2018). Concurrent information on connectivity of runoff and sediment from hillslopes through watershed channel networks can further our understanding of connectivity and inform catchment management (Lexartaz-Artza and Wainwright 2009). This research uses nested hillslope and stream channel observations post-fire to (i) identify sources

and quantify magnitudes of runoff and sediment transport during two rain events: one long duration with low intensity (≤ 2 year return interval) and one high intensity (≤ 10 year return interval); and (ii) determine the factors affecting connectivity of runoff and sediment for these rain storms.

4.2. Methods

4.2.1. Site description

In June 2012, the High Park Fire burned 330 km^2 of Colorado Front Range forest draining into the Cache la Poudre or Big Thompson Rivers. Approximately 50% of the High Park Fire burned at moderate or high severity (BAER 2012). As these watersheds supply drinking water to the cities of Fort Collins, Greeley, Loveland, and other municipalities, mulch treatments to reduce erosion and sedimentation of water supplies were targeted for areas with moderate to high burn severity and steep slopes (BAER 2012; Figure 4.1).

Geology of the High Park Fire area is Precambrian metasedimentary and metaigneous schists, gneisses and plutonic igneous rocks (Abott 1970). Soils are predominantly sandy loam (BAER 2012) with moderately high to high saturated hydraulic conductivity and drainage ranging from well drained to somewhat excessively drained (Soil Survey Staff, NRCS, USDA 2019). The primary pre-fire vegetation was ponderosa pine (*Pinus ponderosa*) at lower elevations and denser mixed conifer forests at higher elevations, with grasses and shrubs on drier south-facing slopes (BAER 2012; Schmeer et al. 2018).

Peak annual streamflow in the Colorado Front Range is rainfall dominated below 2000 m, snowmelt dominated above 3100 m, with mixed sources in-between (Kampf and Lefsky 2015). Elevation for our study sites ranges from 1740-2680 m, and runoff during our sampling season (June 1 to Oct. 1) is primarily caused by infiltration excess overland flow driven by

convective rain storms. From 2013-2015 the average sampling season rainfall was 270 mm at tipping bucket gauges (n = 8) within the High Park Fire (Figure 4.1).

4.2.2. Monitoring overview

Monitoring within two High Park Fire watersheds, Skin and Hill Gulch (15 and 14 km^2, respectively; Figure 4.1), began in 2012 with eight rain gauges and 29 hillslope (< 3 ha) sediment fences to capture sediment eroded from hillslopes. In 2014, two additional hillslope sediment fences were established within the headwaters of Skin Gulch. These fences along with two existing sediment fences in the headwaters of Hill Gulch, were instrumented to collect runoff and suspended sediment in addition to the sediment typically captured with sediment fences (Figure 4.1 and 4.2; c.f., chapter 3). Hillslope areas ranged from 0.1-2.8 ha ($\bar{x}$ = 0.5 ha) with average slope of 5-33° and elevations from 1780-2670 m.

A nested watershed design (catchment areas = 0.6-15.1 km^2; Table 4.1) was established within Skin and Hill Gulches between 2014 and 2015. In 2014, the outlets of Skin and Hill Gulch (SO and HO) were instrumented to monitor stream stage, turbidity, and suspended sediment. Three additional sites per watershed (0.6-3.9 km^2) were also instrumented to monitor stage (Figure 4.1; Table 4.1). In 2015, two additional sites per watershed (1.2-10.0 km^2) were added to monitor stream stage, turbidity, and suspended sediment (Figure 4.1; Table 4.1); installation was completed near the time of highest runoff for the year (June 23, 2015). Sites with turbidity monitoring are hereafter referred to as “primary sites” with all other in-stream sites referred to as “secondary sites”.

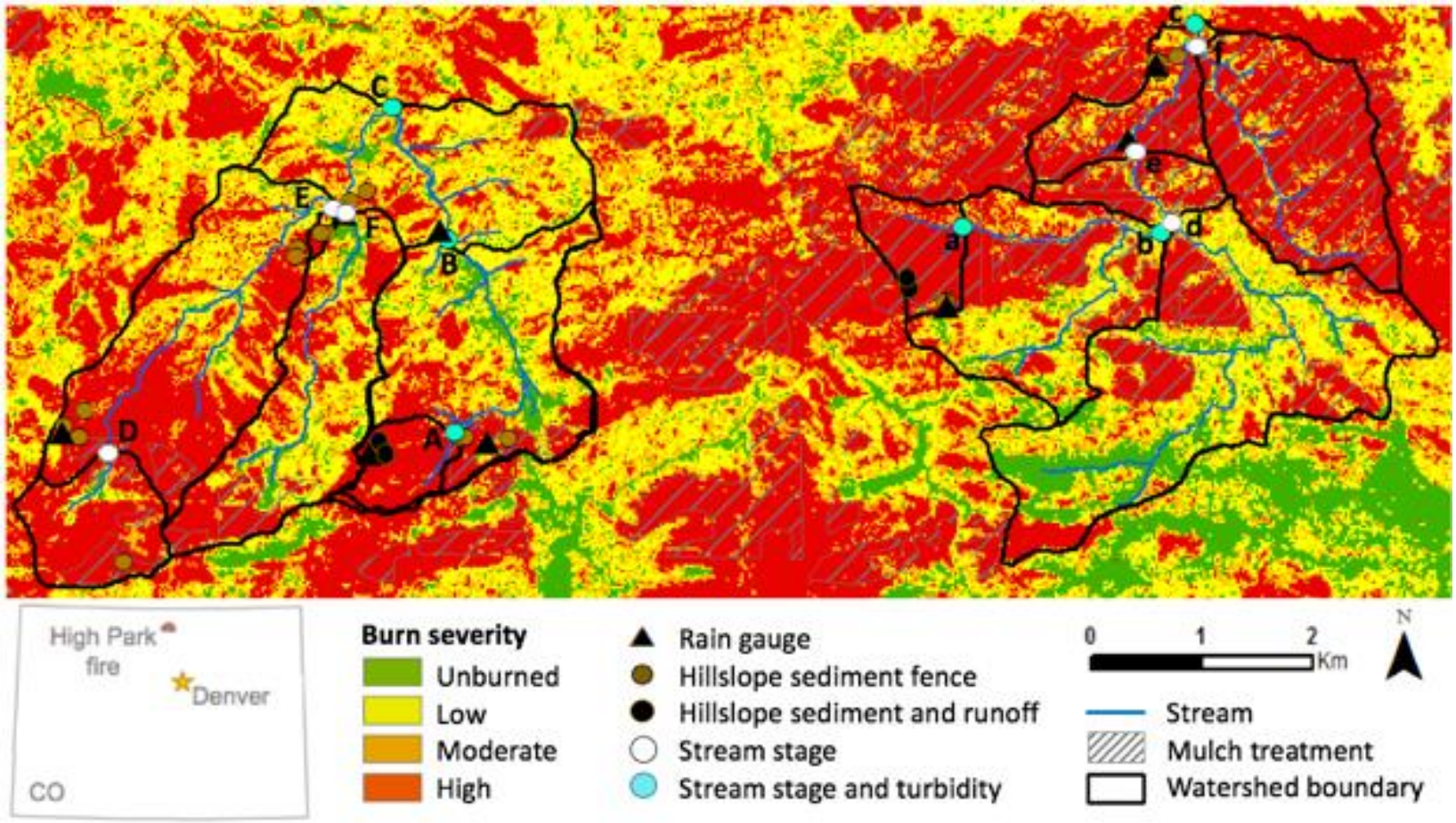

Figure 4.1. Locations of Skin Gulch (west) and Hill Gulch (east) in the 2012 High Park Fire showing burn severity (Stone 2015), streams, monitoring equipment (rain gauges, hillslope sediment and/or runoff collectors, stream stage and/or turbidity), areas targeted to receive mulch treatments, and boundaries of watersheds and sub-watersheds. Stream sites are listed in Table 4.1.

Table 4.1. Characteristics of in-stream monitoring sites within Skin (S-) and Hill Gulch (H-) including drainage area (ha), elevation (m), watershed and channel slope (mean; °), maximum compound topographic index (CTI), unconfined channel (%) and mulch (%). Site names reference locations within the larger watersheds from headwaters to outlets: upper (-U), intermediate (-I), and outlet (-O); site numbers (i.e., -1 to -4) differentiate between sites with similar locations; aliases correspond to those in Figure 4.1. Primary sites within Skin (and Hill) Gulch are A-C (a-c).

Site (alias)	Area (km^2)	Elevation range (m)	Watershed slope (°)	Channel slope (°)	CTI	Unconfined channel (%)	Mulch (%)[1]
SU1 (A)	0.6	2430-2490	11	8	14	50	3
SI1 (B)	3.9	2180-2490	12	6	11	52	0
SO (C)	15.1	1890-2680	23	5	25	61	9
SU2 (D)	1.2	2450-2680	11	5	21	100	26
SI2 (E)	5.2	1980-2590	24	6	23	26	4
SI3 (F)	2.8	1970-2640	20	8	23	40	13
HU (a)	0.8	2050-2380	22	6	21	0	77
HI1 (b)	3.6	1870-2390	24	5	24	31	39
HO (c)	14.1	1740-2220	28	4	25	63	5
HI2 (d)	5.7	1860-2380	22	4	25	85	19
HI3 (e)	10.0	1820-2390	23	4	25	66	30
HI4 (f)	2.9	1750-2230	24	6	24	27	90

[1] percentage based on GIS polygons of the areas targeted to receive mulch treatments.

4.2.3. Precipitation

This paper focuses on rain events during the 2015 growing season (June 1 - Oct 1). Rainfall (P) was continuously monitored with Rainwise tipping bucket rain gauges (resolution of 0.25 mm) at three locations in Hill Gulch and five locations within Skin Gulch (Figure 4.1). Rainfall data were processed using the USDA Rainfall Intensity Summarization Tool (ARS, 2013); storms were separated by at least 6 h with <1 mm of rain (Renard et al. 1997), and the following were calculated for each storm: depth (P; mm), duration (h), maximum intensity (mm h^{-1}) over 5-, 15-, 30-, and 60-minute intervals (MI_5, MI_{15}, MI_{30} and MI_{60}) and 30-minute erosivity (EI_{30}), where EI_{30} is the product of event rainfall kinetic energy and intensity (MJ mm ha^{-1} h^{-1}; Brown and Foster 1987). The depth of rainfall (mm) exceeding MI_5 thresholds from 10 to 20 mm h^{-1} was also calculated in increments of 5 mm h^{-1} (P>I; where I is the MI_5 threshold;

c.f., Kampf et al. 2016). Each of these rainfall event metrics were then interpolated across each catchment using inverse distance squared methods, and the mean value of each rainfall metric was determined for each drainage area using zonal statistics in ArcGIS 10.3.1 (ESRI 2013).

Site visits were conducted within 1-19 days following rainfall events with one hour depths $\geq$10 mm at any of five telemetered rain gauges surrounding Skin and Hill Gulch (https://co.water.usgs.gov/infodata/COPrecip/index.html). This threshold for site visits was determined based on prior research on rainfall intensities required to produce runoff and sediment delivery (Wilson et al. 2018; chapter 2). For sites with continuous stage monitoring, increases in runoff or streamflow and turbidity ("site-event") were linked to coincident rainfall events. For hillslopes without continuous runoff monitoring, the rainfall event with the highest EI_{30} between site visits was assumed to have caused the runoff and erosion production event ("site-event") (Benavides-Solario and MacDonald 2005; Wilson et al. 2018; chapter 2).

To help determine the primary hydrologic flow paths affecting site responses, the daily antecedent precipitation index (I_a) was computed for each rain gauge during the sampling season as:

$$I_a = I_o k + I \quad (4.1)$$

where I_o was the initial value of I_a (mm), k was the recession factor set to 0.9, and I was the rainfall (mm) for a given day (Dingman 2002). Differences in I_a were determined between (1) site-events; and (2) watersheds by site-event using t-tests with a significance level of 0.05.

4.2.4. Hillslope surface cover

Surface cover was systematically quantified for each hillslope in June ("spring") and Aug. ("fall") using transects of at least 100 points per site. For each point, ground and canopy cover were each classified as bare soil, bedrock, live vegetation, litter, rock (> 1 cm diameter),

wood (> 1 cm diameter), tree, straw mulch, or wood mulch. As defined here, canopy cover was observed as the first surface a raindrop would encounter from < 1 m above the ground surface, and ground cover was observed at the ground surface.

4.2.5. Hillslope runoff and erosion

Most (27) of the 31 monitored hillslopes within Skin and Hill Gulch were only instrumented to capture the sediment that was transported by overland flow and trapped behind a sediment fence during a rain storm (Figure 4.2). The mass of this sediment was measured and recorded in the field to the closest 0.5 kg using a hanging scale, and a representative sample was collected and transported to the lab for analysis of gravimetric water content (ASTM D2974-13 Test Method A; ASTM 2013b). Water content was used to adjust the field-wet mass of sediment to a dry mass, which was then normalized by contributing area and reported as Mg ha^{-1}.

For the four headwater hillslopes with added instrumentation, runoff and suspended sediment were measured in addition to sediment captured behind the fence. Runoff was routed from each sediment fence through a 90° v-notch weir into a series of three 250 L barrels. Barrels were numbered sequentially starting with the farthest upslope (barrel 1) (Figure 4.2). Barrels 1 and 2 were fitted with flow splitters (cf. Bonilla et al. 2006; Figure 4.2): flow was split into 15 directions, and 1/15 of the flow was transferred to subsequent barrels. The precision of these devices depends on how well they stay level (Bonilla et al. 2006); observations of barrel level changes were made during site visits. A time lapse camera was installed upslope of each weir to photograph stage height (h) above the weir at 1-min intervals; h was determined from the staff gauge installed adjacent to weir (Figure 4.2). Discharge (Q) was calculated as follows (c.f., Haan et al. 1994; Cone 1916):

$$Q = 4.89 * 10^{-8}\, h^{2.48} \tag{4.2}$$

where Q is in $m^3 s^{-1}$, and h is the height of the water above the weir (mm) as measured at the staff gauge. Peak Q (L s^{-1}) was calculated for each event with runoff collection by multiplying Q from equation 4.2 by 1000. The volume of Q was calculated by multiplying Q (L s^{-1}) by the duration of the event (s); Q volume was divided by contributing area to calculate Q depth in mm; runoff ratios (Q/P) were calculated from the runoff in mm divided by the rainfall in mm.

Hillslope suspended sediment was the sediment transported with runoff into the barrels (Figure 4.2). To determine the hillslope suspended sediment load, collected runoff was stirred, and a 500-mL depth-integrated sample was collected. The suspended sediment concentration (SSC; mg L^{-1}) of each sample was determined through wet sieving and filtration (ASTM D3977-97 Test Method C; ASTM, 2013a). The suspended sediment yield (Mg ha^{-1}) was then determined by multiplying the average barrel SSC (mg L^{-1}) by Q (L) from equation 4.2, and normalizing by contributing area. For hillslopes with runoff collection, the total sediment yield (Mg ha^{-1}) was then calculated as the sum of the sediment yield behind the fence plus the suspended sediment yield for each site-event. The total sediment yield was then used to calculate sediment fence catch efficiency, i.e., the ratio of sediment captured behind the fence to the total yield (chapter 3).

Figure 4.2. Hillslope runoff and erosion monitoring: (a) sediment fence in the foreground captures sediment (SED), and a 90° V-notch weir routes runoff (Q) and suspended load (SL) into a series of three collection barrels; (b) side view of the Q and SL collection system with sample collection barrels labeled sequentially as B1-B3. Note the staff gauge in panel a, which was used alongside a time lapse camera (upslope, not pictured) to determine the height of water above the weir at 1-min intervals for use in equation 4.2.

4.2.6. Streamflow and suspended sediment

Stage height (*h*) was continuously monitored at all 12 in-stream sites using either capacitance rods (TruTrack WT-HR 1000mm Auckland, NZ) or pressure transducers (Model PDCR 1230 Druck) and data loggers (CR100 or CR10X; Campbell Scientific Inc., Logan, UT). Stage height was recorded in intervals of 1-5 minutes, except at the watershed outlets where data were recorded every 10 minutes. At the six primary monitoring sites a time lapse camera was also installed to photograph *h* on a staff gauge at 1-minute intervals. Rating curves were developed to relate streamflow to *h* using the sudden-salt injection method (Kilpatrick and Cobb 1985) at all sites except for the watershed outlets, where the velocity-area method (Nolan and Shields, 2000) was employed. If stream stage at any site exceeded the manual observations by more than 10% during any event, Manning's equation was used to estimate the rating curve for high flows. To do this, the equation was configured using surveyed channel geometry and reach slope, and the roughness coefficient was calibrated to obtain the best fit to observed streamflow. This approximation assumes that the roughness coefficient is constant, whereas this value actually changes with discharge. However, in most cases the approach led to good reconstruction of observed rating curve patterns (Figure C1). Baseflow was determined using the graphical method; i.e., starting at the initial rise of hydrograph a line was drawn with a slope of 0.009 L s^{-1} km^{-2} min^{-1} until the falling limb of the hydrograph was intercepted; this slope is equivalent to 0.05 ft^3 s^{-1} mi^{-2} hr^{-1} used in previous studies (Hewlett and Hibbert 1967). The following streamflow (Q) metrics were calculated: (1) area-normalized peak Q (L s^{-1} km^{-2}); (2) Q depth (mm); and (3) runoff ratio.

Turbidity (NTU) was monitored at the three primary monitoring sites within each watershed using DTS-12 sensors (FTS Inc., Victoria, B.C.) and data loggers (CR1000, CR100 or

CR10x; Campbell Scientific Inc., Logan, UT). Turbidity was recorded every minute, except at the watershed outlets, where data were recorded every 10 minutes. Turbidity was related to suspended sediment concentrations (SSC) using concurrently collected NTU and suspended sediment samples. Suspended sediment samples were collected using depth-integrated and siphon samples (c.f., Mackay and Taylor 2012) at all primary monitoring sites and automated ISCO samples at the watershed outlets. Depth-integrated samples were collected during site visits with a US DH-48 depth-integrating sampler (Federal Interagency Sedimentation Project; https://water.usgs.gov/fisp/products/4101002.html). Siphon samples were collected during higher discharge using siphon samplers that consisted of four 250 mL bottles vertically staggered by 5 cm within two side-by-side 20 cm PVC pipes (c.f., Mackay and Taylor 2012). ISCO samples were collected at turbidity thresholds (Lewis and Eads, 2009): once a turbidity threshold was reached (typically 10 FNU), the automated sampler was activated and collected 300 mL samples at 30-min intervals; sampling continued until measurements dropped below the threshold, or all of the sample bottles were filled. Suspended sediment samples were separated into mineral and organic components using ASTM D2974-13 Test Method C (ASTM, 2013a) as well as fine (<53 μm) and coarse (>53 μm) fractions using ASTM D3977-97 Test Method C (ASTM, 2013b).

In-stream suspended sediment yields (SSY) in Mg ha^{-1} were calculated for each site-event as:

$$SSY = \frac{\sum_i^n (SSC_i \times Q_i)}{A} \quad (4.3)$$

where SSC_i is the suspended sediment concentration (mg L^{-1}) and Q_i is the volume of streamflow (L) for the sample interval, and A is the area of the drainage basin (ha). Suspended sediment was also converted to g s^{-1} to create comparable units to hydrographs (L s^{-1}) by multiplying the SSC in mg L^{-1} by streamflow in L s^{-1} and dividing by 1000.

Hysteresis analysis and sediment delivery ratios were analyzed for each event at primary monitoring sites to help indicate the possible sources of sediment. For hysteresis analysis, SSC was plotted as a function of streamflow during rising and falling limbs of each event hydrograph. SSC vs. Q is often hysteretic, and the direction of the loop from rising to falling limb can be used to infer sources of sediment (Williams 1989): clockwise loops indicate remobilization of in-stream sources (limited hillslope contribution) while counter-clockwise loops indicate the predominance of hillslope inputs (Williams 1989; Beel et al. 2011; Duvert et al. 2011; Lloyd et al. 2016). Secondary hysteresis patterns can also be observed with multiple sources of sediment. Sediment delivery ratios (SDR) were calculated for each primary monitoring site as the sediment yield at a catchment (Mg ha^{-1}) divided by: (1) the sediment yield at each hillslope within the catchment (Mg ha^{-1}; Walling 1983); and (2) the sediment delivered to the upstream catchment (Mg ha^{-1}). SDR values were multiplied by 100 to give values as percentages; higher SDRs indicate more hillslope (or upstream) sediment was delivered to a catchment outlet.

4.2.7. In-stream surveys and pebble counts

In-stream cross section surveys and categorical pebble counts were conducted at primary monitoring sites before and after rain storms. Surveys were conducted using a Cygnus 2LS Total Station, a handheld Trimble Nomad datalogger and a prism attached to an adjustable wading rod (accuracy of $\leq$ 5 mm). Five channel cross-sections were established per site. During surveys, a measuring tape was stretched and leveled between the stakes, and approximately 100 points per site were surveyed at fixed intervals (i.e., 0.25 m within the channel and 0.5 m outside of the channel) with additional points collected as needed to characterize the stream channel (e.g., stream left/right, thalweg, sandbars, boulders). Cross section profiles collected before and after a rainfall event were compared to determine changes caused by the event. First the area of each

cross section was determined using linear interpolation between survey points with the *approx* function in R Version 3.4.3 (R Core Team 2017). Next differences between pre- and post-event cross sectional areas were computed to determine areas of incision and deposition. Normalized net and absolute change were also calculated by dividing in-stream changes (m^2) by catchment area (m^2).

Categorical pebble counts were conducted for approximately 100-points per site along random-walk transects (c.f., Wolman 1954) and for points concurrently located with survey cross-section points. Incident points were recorded as either sand (< 2mm), gravel (2-64 mm), cobble (64-256 mm), or boulder (>256 mm). The percent of each particle size category was compared before and after events to determine if coarsening or fining of the stream channel occurred.

4.2.8. Ephemeral catchments and scour chains

For each primary monitoring site: (a) two flow indicator devices were placed in the main axis of topographically convergent zero-order catchments (0.001-0.1 km^2), and (b) two to three scour chains (c.f. Nawa et al. 1993; 9-36 cm in length) were placed coincident with surveyed cross-sections. Flow indicators consisted of chalk-covered dowels placed in capped 10 cm PVC pipes; each PVC was buried in the channel with approximately 25 cm of PVC above the ground surface. Three holes (<2 cm diameter) were drilled into the exposed upstream side of each PVC pipe to allow streamflow to enter. Flow occurrence was determined as either “yes” or “no” by, respectively, the absence or presence of chalk on a dowel. Scour chains with lengths ranging from 9-36 cm ($\bar{x}$ = 18; s = 9) were attached to a bolt, vertically oriented, and buried completely in the stream bed. The depth of sediment removed or deposited at each scour chain was noted during subsequent site visits.

4.2.9. Geographic analyses

To examine how rainfall and drainage area attributes relate to the runoff and sediment responses, watershed-scale metrics were computed in ArcGIS 10.3.1 (ESRI 2013). Catchment boundaries and channel networks were delineated with 0.75 m LiDAR imagery (FEMA 2013). Catchment outlets were set to monitoring site locations so that catchment boundaries included all upslope contributing area. Channel networks were derived from a flow accumulation grid with a minimum drainage area for channel initiation of 0.23 km^2, as this matched field observations (c.f. Martin 2018). As slope can be used to assess potential for sediment delivery or storage (Cavalli et al. 2013; Moody and Martin 2001a; Brogan et al. 2019), upland (hillslope or watershed) and channel slope (degrees) were calculated: (i) upland slope was summarized over each drainage area and reported as the average; and (ii) channel slope was extracted at 10 m intervals and the total slope was computed as the average over all 10 m increments. Because the percent of a catchment that burned at high severity can be used to indicate potential hydrologic connectivity (Ortíz-Rodrígez et al. 2019), the area of each catchment that burned at high severity was calculated at 25 m resolution (Stone 2015). Because surface cover provided by mulch treatments may decrease connectivity due to increased opportunities for interception and storage of incident rainfall, runoff and overland flow, the percent of each catchment targeted to receive mulch treatments (%) was also calculated (Table 4.1).

Confined channel reaches, i.e., those with limited floodplains, promote longitudinal (upstream-downstream) connectivity of runoff and sediment but may inhibit lateral (hillslope-channel) connectivity. The Valley Confinement Algorithm (VCA; Nagel et al. 2014) was used to calculate the length and percent by length of unconfined stream channel within each monitored watershed. Due to processing time, the 0.75 m resolution LiDAR (FEMA 2013) was scaled up to

2 m. The VCA was calibrated qualitatively until the unconfined areas matched our visual observations of channel confinement. We also computed the compound topographic index (CTI; Moore et al. 1991), which links watershed and drainage network attributes to account for topographic curvature and the convergence of upslope contributing areas for any point within a watershed. CTI was calculated as:

$$CTI = Ln\left(\frac{a}{\tan ß}\right) \quad (4.4)$$

where *a* is the upslope contributing area for each pixel (m^2) from the flow accumulation grid, and ß is the slope (radians). The maximum CTI value was calculated for the area contributing to each monitoring site.

Pearson's correlation coefficients (r) or Spearman's ρ (hillslopes only) between the following were analyzed across all monitoring sites for which the data were available:

- *Rainfall event metrics:* duration (h), depth (mm), intensity (i.e., $MI_{5\text{-}60}$; mm h^{-1}), erosivity (EI_{30}; MJ mm ha^{-1} h^{-1}), P>10-20 (mm) and antecedent rainfall (mm);
- *Site attributes:* area (ha), cover counts (hillslopes only), watershed and channel slope (degrees), unconfined channel (%), high severity burn (%), and CTI (max);
- *Response variables*: runoff depth (Q; mm), runoff ratio (Q/P), area-normalized peak Q (L s^{-1} km^{-2}), sediment yield (Mg ha^{-1}), SDR (%), and normalized channel incision and deposition.

Each variable was assessed to determine whether it was normally distributed, and data were transformed to natural logarithms to normalize distributions when needed. For hillslopes,

Spearman's ρ was used instead of r because many response variables had values of 0, which limited utility of Pearson correlation analysis. Our significance level for all analyses was 0.05.

4.3. Results

4.3.1. Precipitation

The number of rainfall events and total rainfall (mm) in June-October 2015 were similar in Skin Gulch and Hill Gulch: Hill Gulch had on average 36 storms totaling 160 mm, and Skin Gulch had 41 storms totaling 140 mm. However, most rain events did not occur simultaneously in both watersheds, and only two rain storms, one on July 8th and another on August 16th, generated a response in streamflow within both Hill and Skin Gulch. Antecedent precipitation was significantly different during these events but was similar between the two watersheds, averaging 49 mm across all gauges on July 8th and 29 mm on Aug. 16th.

4.3.2. Hillslope surface cover

There were no significant seasonal differences (i.e., spring vs. fall) in canopy or ground cover counts; however, cover counts (i.e., canopy vs. ground) and mulch as a percent of canopy cover were significantly different in spring and fall (ANOVA; $p < 0.05$). Canopy and ground cover were averaged across seasons, and ranged from 70-92% ($\bar{x}$ = 82) and 36-81% ($\bar{x}$ = 58), respectively. Mulch accounted for 0-34% ($\bar{x}$ =4) of ground cover averaged across seasons, and was 0-51% ($\bar{x}$ = 6) of canopy cover in spring and 0-14% ($\bar{x}$ = 1) in fall.

4.3.3. In-stream rating curves

For each of the twelve in-stream sites, the maximum stage height (*h*) observed during rain events ranged from 0.1-1.2 m, whereas *h* during manual discharge measurements ranged from 0.1-0.6 m. During one rainfall event, event *h* was over 10% greater than manual *h* for the three primary monitoring sites in Hill Gulch. For these sites, Manning's equation and pre-event

channel geometry determined from cross section surveys were used alongside event *h* measurements to develop stage-discharge rating curves. For all rating curves the fit (r^2) between observed *h* and discharge measurements ranged from 0.72-0.99 ($\bar{x}$ =0.94; *s* = 0.08 m; Table C1; Figure C1).

Turbidity ranged from <1-1400 NTU ($\bar{x}$ = 90; *s* = 230) with total suspended sediment of <1-630,000 g L^{-1} ($\bar{x}$ = 9400; *s* = 63,000; Figure C2). The relationship between NTU and SSC across both watersheds and all particle types and fractions was moderately to highly correlated (r^2 = 0.74). Separating coarse and fine as well as mineral and organic matter fractions slightly increased the correlations (r^2 = 0.31 to 0.82), particularly for fine particles (r^2 = 0.81 to 0.82). Separating the watersheds resulted in better performance, so rating curves were developed for each watershed. For Skin Gulch, NTU ranged from <1-1200 ($\bar{x}$ = 57; *s* = 120) with total SSC of <1-1300 mg L^{-1} ($\bar{x}$ = 86; *s* = 160); the best rating curve fit was between NTU and fine organic matter (r^2 = 0.95; n = 158). However, as organic matter only represented an average of 30% of the total suspended sediment in Skin Gulch, the relationship between NTU and total SSC was used for the rating curve (r^2 = 0.86; n =170; Table C1; Figure C2). Hill Gulch NTU ranged from <1-1400 ($\bar{x}$ = 120; *s* = 300) with total SSC of 1-630,000 mg L^{-1} ($\bar{x}$ = 18,000; σ = 88,000). High SSC samples were collected with siphon samplers during one event; the ISCO sampling hose was temporarily plugged with debris on the rising limb of the hydrograph. Due to these high SSC, two rating curves were developed to relate NTU to SSC in Hill Gulch: (i) a "high" scenario that includes all samples; and (ii) a "low" scenario that includes only those samples with suspended sediment concentrations <10,000 mg L^{-1} (Figure C2). For these, the relationship between NTU and total fine suspended sediment (organic + mineral) was strongest for both the "low" (r^2 = 0.93; n = 104) and the "high" rating curves (r^2 = 0.84; n = 113); however, as fines

represent only 52-54% of the total suspended sediments, all particle sizes were used to develop the rating curves. These performed nearly as well ("low" $r^2 = 0.90$; "high" $r^2 = 0.78$; Table C1; Figure C2). Due to the two rating curves, subsequent suspended sediment metrics for Hill Gulch were computed with the lower and upper bounds represented by the "low" and "high" rating curves, respectively. The "high" rating curve estimates were better correlated to watershed attributes and other production metrics in most instances, so we focus on those results. For relationships using the "low" rating curve please see Table C4.

The remainder of results focus on the two rainfall events that produced a response in streamflow in both watersheds. The results for these events are presented separately to document and compare the effects of rain storm characteristics on response variables from hillslope-through nested watershed scale.

4.3.4. The first rainfall event: long duration, low intensity

The first rainfall event that caused responses in both watersheds was on July 8th, 2015 (Figure 4.3). This event had 16-25 mm ($\bar{x}$ = 21 mm) of rainfall over 7-14 hours ($\bar{x}$ = 11 h). Rainfall was recorded at most rain gauges during the preceding 6-9 days, and the rainfall on July 8th represented <1-56% ($\bar{x}$ = 34%) of the total rainfall over that time period. The return interval of this rainfall event, estimated from two nearby NOAA Atlas stations (Site IDs 05-6925 and 05-3007) across all rainfall metrics, was <1 year (Perica et al. 2013). The storm return interval increased to 2 years for rainfall depths over 4- to 10-day depths (48-72 mm) across rain gauges in Skin Gulch and at mid- and high-elevation gauges within Hill Gulch (Figure 4.1). Antecedent precipitation (I_a) across our range gauge network ranged from 20-64 mm ($\bar{x}$ = 49 mm).

This low intensity rainfall event led to limited overland flow. Hillslope runoff was not captured at any of the four instrumented sediment and runoff collection sites, but sediment was

captured at eight sediment fences in Skin (0.001-0.05 Mg ha^{-1}; $\bar{x}$ = 0.01) and two in Hill Gulch (0.01-0.02 Mg ha^{-1}; $\bar{x}$ = 0.01; Table 4.3; Figure 4.4). In contrast to the hillslopes, all streamflow monitoring sites responded to this event, but the runoff response was small. Area-normalized runoff (Q; mm) at in-stream monitoring sites was similar within Skin (0.01-0.2 mm; $\bar{x}$ = 0.2) and Hill Gulch (0.04-0.4 mm; $\bar{x}$ = 0.2), corresponding to runoff ratios of 0.0002-0.01 ($\bar{x}$ = 0.01) and 0.002-0.02 (μ $\bar{x}$ = 0.01), respectively (Table 4.2). Area-normalized peak streamflow (L s^{-1} km^{-2}) was also similar across both watersheds ranging from 8-21 L s^{-1} km^{-2} ($\bar{x}$ = 14) in Skin and from 7-31 L s^{-1} km^{-2} ($\bar{x}$ = 19) in Hill Gulch (Figure 4.3). In-stream sediment was more varied between Skin and Hill Gulch with sediment yields of 0.0001-0.0002 Mg ha^{-1} ($\bar{x}$ = 0.0002) in Skin and 0.001-0.003 Mg ha^{-1} ($\bar{x}$ = 0.002) in Hill (Table 4.2).

Correlation analysis indicates that rainfall intensity and watershed slope were the primary drivers of runoff and sediment yield (Table C3). The quantity of rainfall exceeding MI_5 of 10 mm hr^{-1} (P>10; mm) was positively correlated with Q, Q/P and SY for this event (Figure 4.5); however, across all sites P>10 (mm) was only 2-4 mm for this event. Q and Q/P were slightly more correlated with watershed slope, and slightly less correlated with maximum CTI. In-stream sediment yields were most correlated to P>10 and slightly less correlated to rainfall erosivity and all Q metrics (Figure 4.6; Table C3). Site responses were likely due to a combination of infiltration excess overland flow, saturation excess overland flow, and seepage erosion from the soil-bedrock interface (Kampf et al. 2016); although antecedent rainfall was not correlated to any production metrics, site response may not have occurred without it.

The timing of instream sediment transport relative to streamflow can indicate whether sediment more likely came from stream or hillslope sources. The hysteretic SSC vs. Q patterns during this event were clockwise, indicating the predominance of in-stream sources of sediment

(Williams 1989; Figure 4.3). This is consistent with the limited hillslope runoff and erosion recorded for the event. Secondary hysteresis patterns were also evident at most sites, which may indicate both in-stream sources and hillslopes (Figure 4.3); however, sediment delivery ratios from hillslopes to streams were low (<1-30%) for both Skin and Hill Gulch, indicating that > 70% of the sediment produced at hillslopes was not delivered to the catchments (Table 4.3). Sediment delivery ratios from upstream to downstream catchments were higher, but decreased downstream with SDRs of 100-200% in Skin and 50-70% in Hill Gulch (Table 4.3). We were unable to calculate SDR for catchments with no observed hillslope erosion or for catchments without upstream monitoring (i.e., headwater sites, "A" and "a"). SDR increased with most rainfall (MI_{30}, MI_{60}, erosivity and P>10) and runoff metrics (Q depth, runoff ratios) and with the percent of a catchment that burned at high severity (Table C3; Figure 4.5).

Because sediment during this event mainly originated from in-stream sources, surveyed cross-sections indicate the predominance of stream incision with net changes at a site of -0.33-0.05 m^2 ($\bar{x}$ = -0.11; Table C5; Figure 4.8; Figure C3-C5, C9). The number of sites with incision throughout Skin and Hill Gulch was similar (67%), but the sum of incision (m^2) and absolute change (m^2) across all cross-sections within Skin were only about half of those observed in Hill Gulch (Table C5). Normalized net change in cross sections increased with all Q metrics (Q, Q/P and normalized peak Q) while normalized absolute change increased with MI_5 and the percent of a catchment that burned at high severity (Table C3; Figure 4.5).

Table 4.2. Rainfall depth (P; mm), intensity (MI_{60}; mm hr^{-1}), and in-stream runoff (Q; mm), runoff ratio (Q/P), and peak streamflow (Peak Q; L s^{-1} km^{-2}) by site for events on July 8th and Aug. 16th (in parentheses). Site names reference locations within the Skin (S-) and Hill (H-) Gulch from headwaters to outlets: upper (-U), intermediate (-I), and outlet (-O); site numbers (i.e., -1 to -4) differentiate between sites with similar locations; aliases correspond to those in Figure 4.1 and Table 4.1. Primary sites within Skin (and Hill) Gulch are A-C (a-c).

Site (alias)	P (mm)	MI_{60} (mm h^{-1})	Q (mm)	Runoff ratio	Peak Q (L s^{-1} km^{-2})
SU1 (A)	22 (6)	5 (5)	0.01 (0.01)	0.0002 (0.001)	8 (5)
SI1 (B)	19 (11)	5 (12)	0.06 (0.06)	0.003 (0.005)	21 (30)
SO (C)	17 (11)	5 (11)	0.12 (0.02)	0.007 (0.002)	10 (7)
SU2 (D)	21 (6)	6 (6)	0.06 (0.01)	0.003 (0.002)	18 (10)
SI2 (E)	17 (8)	6 (9)	0.09 (0.01)	0.005 (0.002)	11 (6)
SI3 (F)	17 (9)	5 (9)	0.19 (0.05)	0.01 (0.005)	13 (29)
HU (a)	22 (25)	6 (22)	0.36 (3.4)	0.02 (0.1)	29 (1600)
HI1 (b)	21 (23)	6 (21)	0.19 (1.1)	0.009 (0.05)	31 (1000)
HO (c)	20 (21)	7 (19)	0.26 (4.3)	0.01 (0.2)	13 (160)
HI2 (d)	20 (20)	7 (19)	0.15 (0.2)	0.007 (0.01)	21 (30)
HI3 (e)	21 (21)	7 (20)	0.04 (0.05)	0.002 (0.002)	7 (39)
HI4 (f)	19 (19)	7 (19)	0.17 (0.4)	0.009 (0.02)	11 (160)

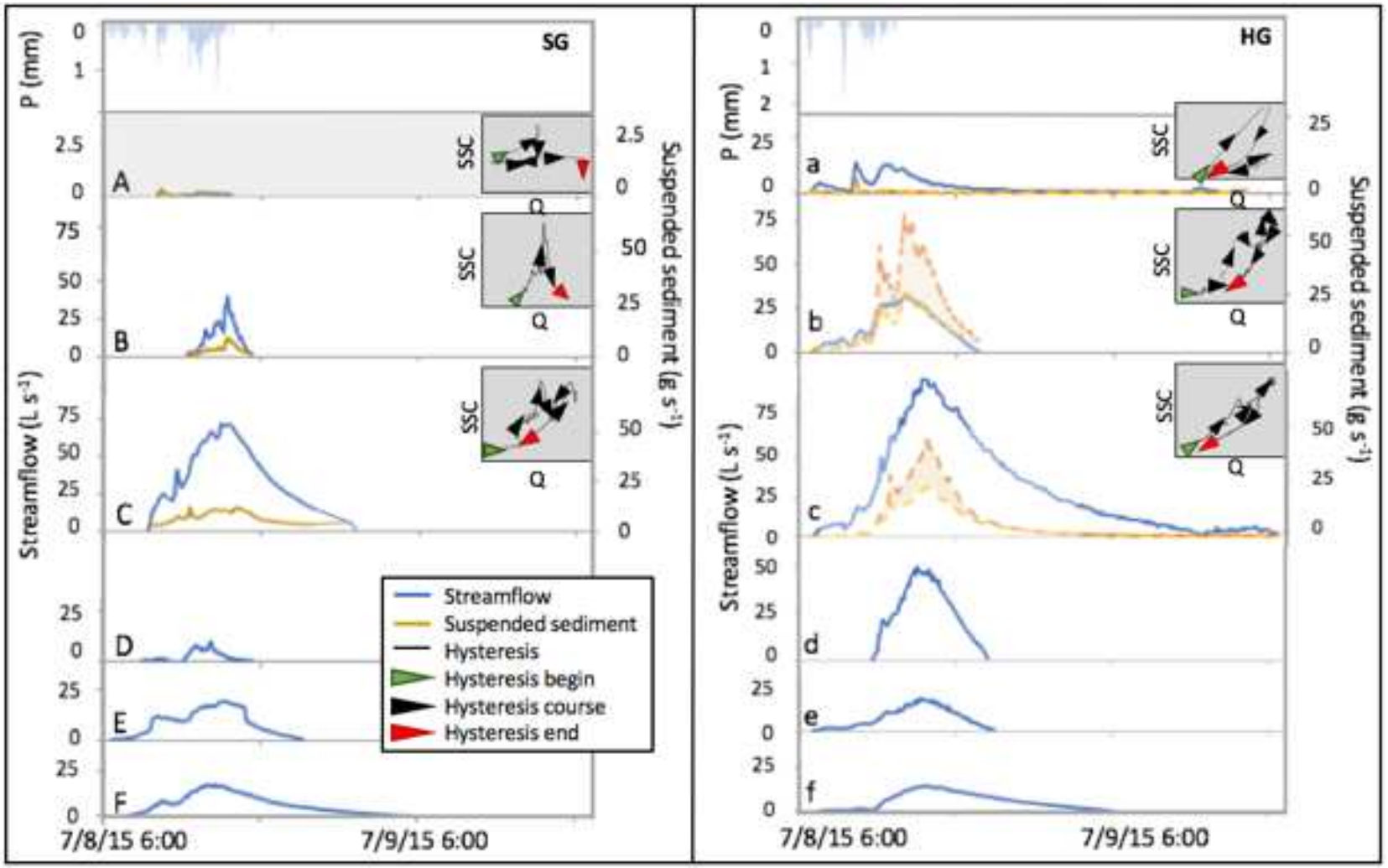

Figure 4.3. July 8th event rainfall (P; mm), streamflow (L s^{-1}), suspended sediment (g s^{-1}) and hysteresis patterns for sites within Skin (SG; left panel) and Hill Gulch (HG; right panel); site aliases correspond to those in Table 4.1 and Figure 4.1. Lower and upper boundaries on HG suspended sediment represent the "low" and "high" rating curve estimates, respectively. Sites without suspended sediment (D-F and d-f) are secondary sites (i.e., only streamflow monitored). Axes limits were held constant if possible; the shaded panel for site "A" indicates deviation from these limits.

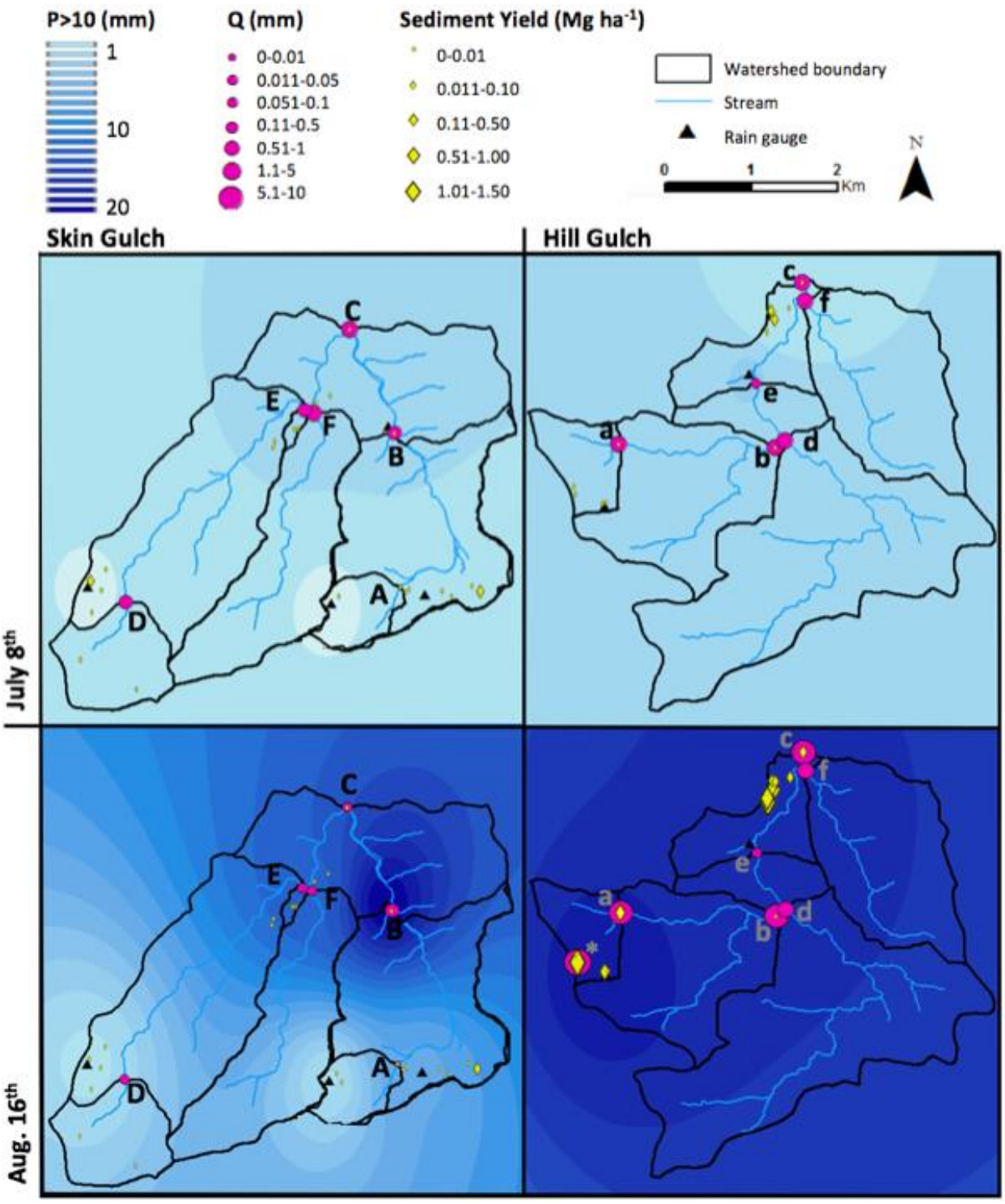

Figure 4.4. Rainfall (P>10; mm), runoff (Q; mm) and sediment yields (Mg ha^{-1}) within Skin (left) and Hill Gulch (right) for rainfall events on July 8th (upper) and Aug. 16th (lower); sediment yields in Hill Gulch calculated from the "high" rating curve; hillslope marked by an "*"; site labels correspond to those in Table 4.1.

Table 4.3. Sediment yields (SY; Mg ha^{-1}) and sediment delivery ratios (SDR; %) by site-event. Hillslope SY reported as the sediment captured behind the fence except for HU3 on Aug. 16th, which represents the total sediment yield. Site names reference locations within Skin (S-) and Hill (H-) Gulch from headwaters to outlets: upper (-U), intermediate (-I), and outlet (-O); site numbers (i.e., -1 to -7) differentiate between sites with similar locations; aliases correspond to those in Table 4.1 and Figure 4.1; "-" indicates data were not available.

		July 8th			Aug. 16th		
Site (alias)	Hillslope	SY (Mg ha^{-1})	Hillslope SDR (%)	In-stream SDR (%)	SY (Mg ha^{-1})	Hillslope SDR (%)	In-stream SDR (%)
SU1 (A)		0.0001			0.00001		
SI1 (B)		0.0002		200	0.001		10,000
	SI1-2	0.009	2				
	SI1-3	0.003	7				
	SI1-5	0.005	4		0.004	25	
	SI1-6	0.02	1		0.08	1	
SO (C)		0.0002		100	0.0001		10
	SI1-2	0.009	2				
	SI1-3	0.003	7				
	SI1-5	0.005	4		0.004	3	
	SI1-6	0.02	1		0.08	0.1	
	SU2-3	0.05	0.4				
	SU2-4	0.006	3				
	SU2-5	0.003	7				
	SU2-6	0.001	20				
HU (a)		0.003	-		0.2		
	HU1				0.006	3000	
	HU2				0.3	70	
	HU3				1.7	10	
	HU4				0.007	3000	
HI1 (b)		0.002		70	0.01		5
	HU1				0.006	200	
	HU2				0.3	3	
	HU3				1.7	1	
	HU4				0.007	100	
HO (c)		0.001		50	0.03		300
	HU1				0.006	500	
	HU2				0.3	10	
	HU3				1.7	2	
	HU4				0.007	400	
	HI4-1	0.02	5		0.4	8	
	HI4-2				0.1	30	
	HI4-3				0.03	100	
	HI4-4	0.01	10		0.06	50	
	HI4-5				0.8	4	
	HI4-6				1	3	
	HI4-7				0.01	300	

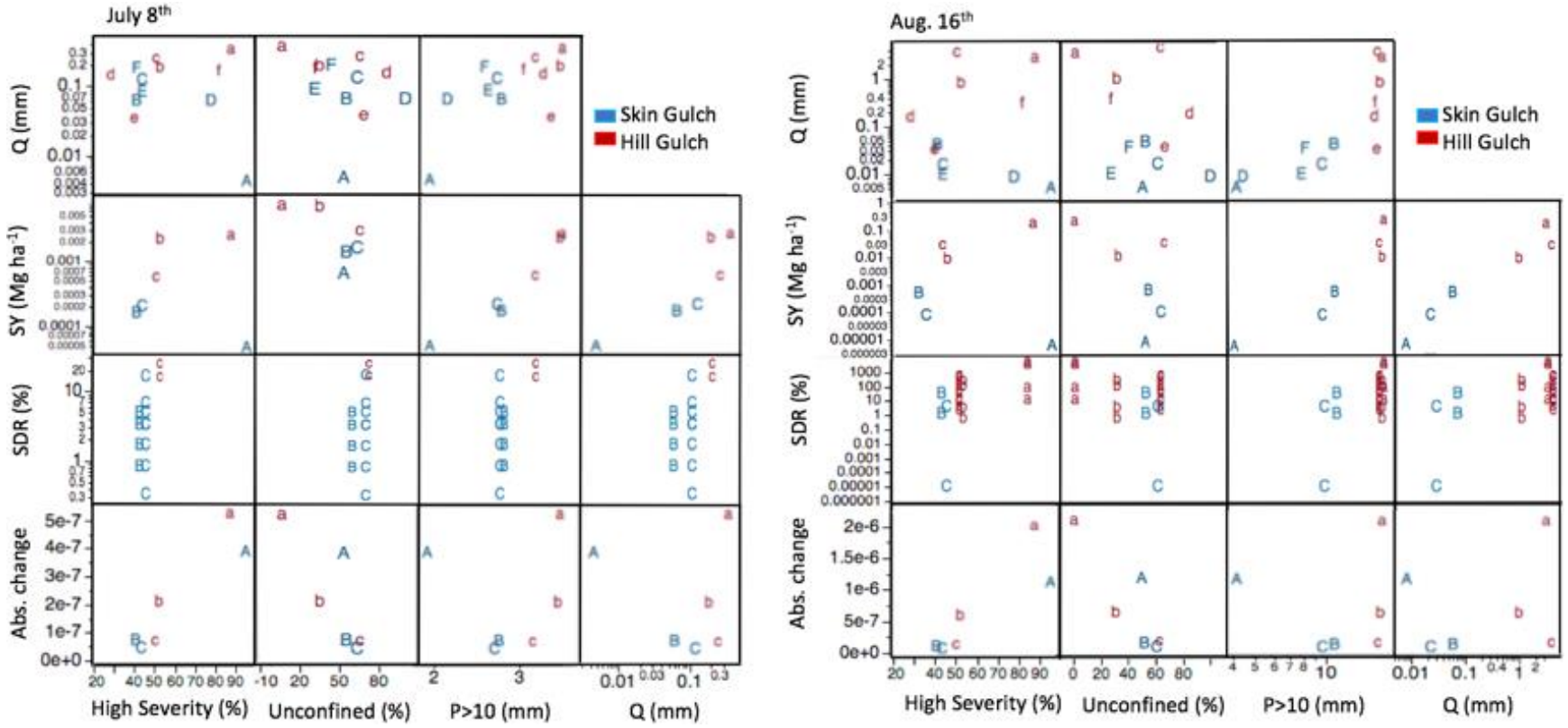

Figure 4.5. High severity (%), unconfined channel length (%), P >10 (mm) vs. runoff (Q; mm), sediment yield (SY; Mg ha^{-1}) sediment delivery ratio (SDR; %) and normalized absolute channel change (Abs. change) for events in Skin and Hill Gulch on July 8th (left) and Aug. 16th (right). The plotted labels correspond to site aliases in Table 4.1 and Figure 4.1.

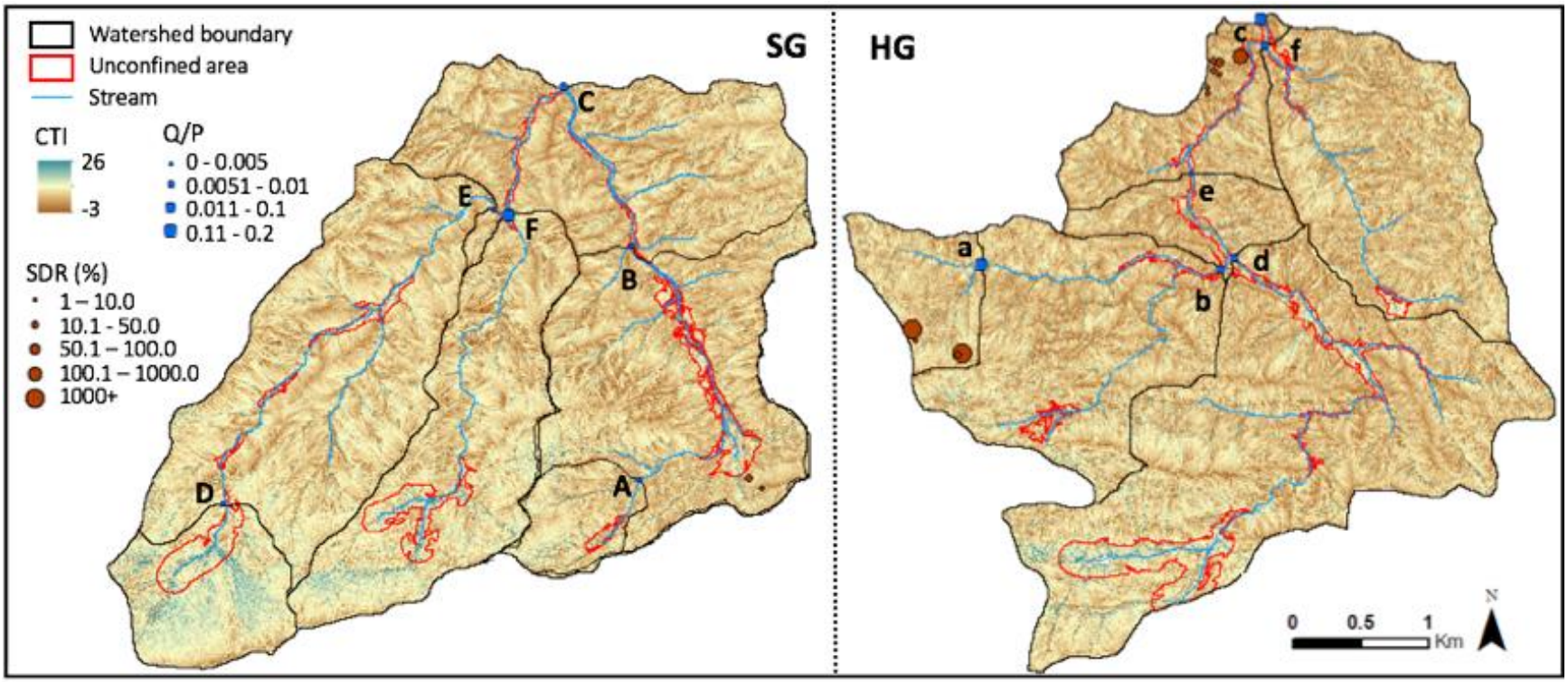

Figure 4.6. Compound Topographic Index and unconfined areas defined using the Valley Confinement Algorithm for Skin (SG; left) and Hill Gulch (HG; right) with watershed boundaries, streams, July 8th runoff ratios (Q/P) for in-stream monitoring sites, and average Aug. 16th sediment delivery ratios (SDR; %) for hillslopes with an observed response. Stream site labels correspond to aliases in Table 4.1 and Figure 4.1.

4.3.5. The second event: high intensity, short duration

The second streamflow event observed in both watersheds had higher peak rainfall intensity and area-normalized peak runoff than observed during the July 8th event, with the highest intensities and runoff in Hill Gulch (Table 4.2; Figure 4.4). This event occurred on August 16th in response to 4-26 mm ($\bar{x}$ = 15 mm) of rainfall that fell during 0.4-2.3 hours ($\bar{x}$ = 1 h; Figure 4.7). The return interval of this storm was between 5-10 years for maximum rainfall intensities over 5- to 15-minutes (i.e., MI_5 and MI_{15}) and <1-5 years for longer time intervals (i.e., MI_{30}, MI_{60} and 0.5-3-hr depths; Perica et al. 2013). In Hill Gulch, MI_5 ranged from 116-128 mm h^{-1} ($\bar{x}$ = 124) with MI_{15} from 69-72 mm h^{-1} ($\bar{x}$ = 71); rainfall intensity in Skin Gulch was slightly lower with MI_5 from 22-149 mm h^{-1} ($\bar{x}$ = 72) and MI_{15} from 14-77 mm h^{-1} ($\bar{x}$ = 38). The greatest rainfall depths and intensities occurred throughout the drainage areas of the Hill Gulch upper (HU; a) and intermediate (HI1; b) primary monitoring sites and near the outlets of the Skin Gulch intermediate (SI1; B) and outlet (SO; C) primary monitoring sites. Antecedent precipitation (I_a) was significantly lower during this event as compared to the July 8th event, and ranged from <1-115 mm ($\bar{x}$ = 29 mm).

Hillslope erosion was collected at two sediment fences within Skin (SY = 0.004-0.08 Mg ha^{-1}; $\bar{x}$ = 0.04) and 11 in Hill Gulch (SY = 0.01-1.3 Mg ha^{-1}; $\bar{x}$ = 0.4; Table 4.3; Figure 4.4). Runoff and suspended sediment were also captured at one site in Hill Gulch where a significant amount of hail was also observed (Supplemental Video). Runoff volume was estimated at 20,000 L (equation 4.2) with area-normalized Q of 6 mm corresponding to a runoff ratio of 0.2. Suspended sediment concentrations were 10,000 mg L^{-1} in barrel 1 and 8,500 mg L^{-1} in barrel 2 ($\bar{x}$ = 9,300 mg L^{-1}). The suspended sediment load was 0.6 Mg ha^{-1} with a total load of 1.7 Mg ha^{-1} corresponding to a catch efficiency of 0.66. However, time lapse photos (Supplemental Video)

reveal runoff and sediment overtopping the sediment fence and therefore bypassing the weir and collection system, which likely led to underestimated Q and suspended sediment and overestimated catch efficiency. Over all hillslopes, SY (Mg ha^{-1}) increased with rainfall intensity (MI_{30-60}; Table C2), decreased with mulch (%) and ground cover (%) (Table C2), and was higher than observed on July 8th.

In-stream runoff and sediment production within Skin Gulch were similar to responses on July 8th (i.e., area-normalized peak Q, SY) or slightly lower (i.e., Q, runoff ratios; Table 4.2; Figure 4.3, 4.7). In contrast, runoff within Hill Gulch was orders of magnitude higher during this event with Q of 0.05-4.3 mm ($\bar{x}$ = 1.6), runoff ratios of 0.002-0.21 ($\bar{x}$ = 0.07; Figure 4.5), and normalized peak Q of 30-1600 L s^{-1} km^{-2} ($\bar{x}$ = 500; Table 4.2). In-stream SY ranged from 0.00001 to 0.001 Mg ha^{-1} in Skin and was much higher in Hill Gulch at 0.01-0.2 Mg ha^{-1} (Figure 4.5). Across all sites, each runoff variable increased with all rainfall metrics (Figure 4.5; Table C3). SY also increased with all P and Q metrics.

Similar to the July 8 event, most hysteretic patterns between SSC and Q were clockwise, indicating in-stream sources of sediment. Exceptions were at two sites: Hill Gulch headwater (HU; a) and Skin Gulch intermediate (SI1; B). These sites had predominantly counterclockwise loops, indicating the prevalence of hillslope inputs. Secondary loops were observed at most sites, indicating sediment was delivered from both in-stream sources and hillslopes (Figure 4.7). Sediment delivery ratios from hillslopes to streams were much lower in Skin (<1-30%) than in Hill Gulch (<1-3,000%; Table 4.3): up to 70% of the hillslope sediment produced within Skin Gulch was not delivered to the catchment outlets, but most hillslope sediment, and in some instances more sediment than was observed at hillslope monitoring sites, was delivered to the catchments in Hill Gulch (Table 4.3). Sediment delivery ratios were higher from upstream to

downstream catchments in Skin Gulch with values of 10-10,000% for the outlet and intermediate Skin Gulch sites ("C" and "B", respectively). The average SDR from hillslopes to streams for Hill Gulch headwater (HU; a), intermediate (HI; b) and outlet (HO; c) were 1,000%, 80%, and 100%, which indicates much greater sediment yields at catchments than hillslopes for the headwater site and watershed outlet. Upstream to downstream sediment delivery ratios in Hill Gulch ranged from 5-300% with the highest value for the watershed outlet ("c"; Table 4.3). Similar to July 8th, SDR increased with site attributes (i.e., the percent of a catchment that burned at high severity), however, SDR on Aug. 16th also decreased with the percent of channel length that was unconfined (Figure 4.6) and increased with area-normalized peak Q (Table C3).

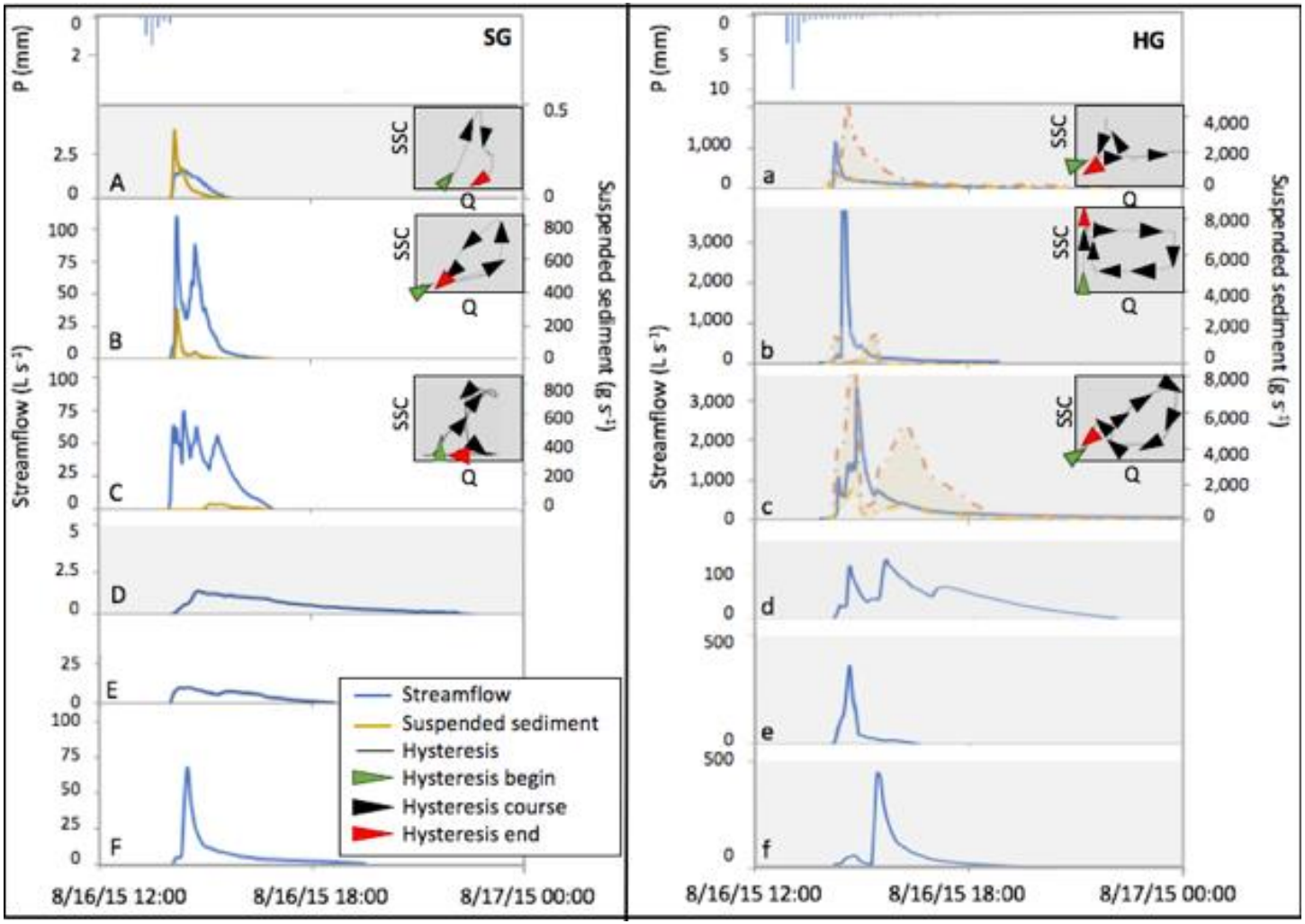

Figure 4.7. Aug. 16th event rainfall (P; mm), streamflow (L s^{-1}), suspended sediment (g s^{-1}) and hysteresis patterns for sites within Skin (SG; left panel) and Hill Gulch (HG; right panel). Site aliases correspond to those in Table 4.1 and Figure 4.1. Lower and upper boundaries on HG suspended sediment represent the "low" and "high" rating curve estimates, respectively. Sites without suspended sediment (D-F and d-f) are secondary sites (i.e., only streamflow monitored). Axes limits were held constant if possible; shaded panels indicate deviations from these limits.

Flow indicators (available for this second event only) showed evidence of flow at five of the six sites within Hill and four of the six sites in Skin Gulch. This is a further indication that some of the in-stream sediment came from hillslopes during this event. The only flow indicator that did not respond in Hill Gulch was one of the headwater sites installed at stream right in an unconsolidated gully. The two flow indicators that did not respond in Skin Gulch were installed at the watershed outlet (SO; C); one of these was installed at stream right just upstream of a culvert that drains the northeastern part of the watershed. Another flow indicator installed at stream left near the Skin Gulch headwater site (SU1; A) may have been exposed to rainfall due to a disconnected PVC cap upon arrival; rainfall may have removed the chalk from the monitoring equipment instead of incident overland flow as intended, thereby indicating a potential false positive for this site-event.

In-stream surveys predominantly reveal deposition during the Aug. 16th event. All cross-sections within Skin had deposition ranging from 0.03-0.4 m^2 ($\bar{x}$ = 0.1; Table C3; Figure 4.8), and most (73%) of the cross-sections in Hill Gulch had deposition (range = 0.1-0.7 m^2; Figure 4.8) with an average of 0.3 m^2, or 300% greater than sites in Skin Gulch for this event (Table C5; Figure C3-C8). Cross-section-specific deposition during this event was on average six times higher than the July 8th event across all sites, four times higher across sites within Skin Gulch, and eight times higher across sites within Hill Gulch (Table C5; Figure C3-C8). Normalized net and absolute change increased with the percent of a catchment that burned at high severity (Figure 4.5).

Scour chains and pebble counts provide evidence of both in-stream scouring and fining during this event. Two of the three Skin Gulch sites were scoured, but the scour chains were either buried or completely removed at all Hill Gulch sites. The sites with scour include: Skin

Gulch outlet (SO; C) with just over 2 cm of scour at the most upstream cross-section (CS5), and Skin Gulch intermediate (SI1; B) with 4.5 cm of scour at the most downstream cross-section (CS1), just over 2 cm just upstream (CS2), and less than 2 cm with gravel deposited at CS4. Analysis of the percent sand, gravel, cobble and boulder from pebble counts reveals fining of the channel substrate at the Skin Gulch Intermediate site (SI1; B), and the Hill Gulch headwater (HU; a) and intermediate sites (HI1; b) (Figure 4.9) with no substantial changes at any other sites.

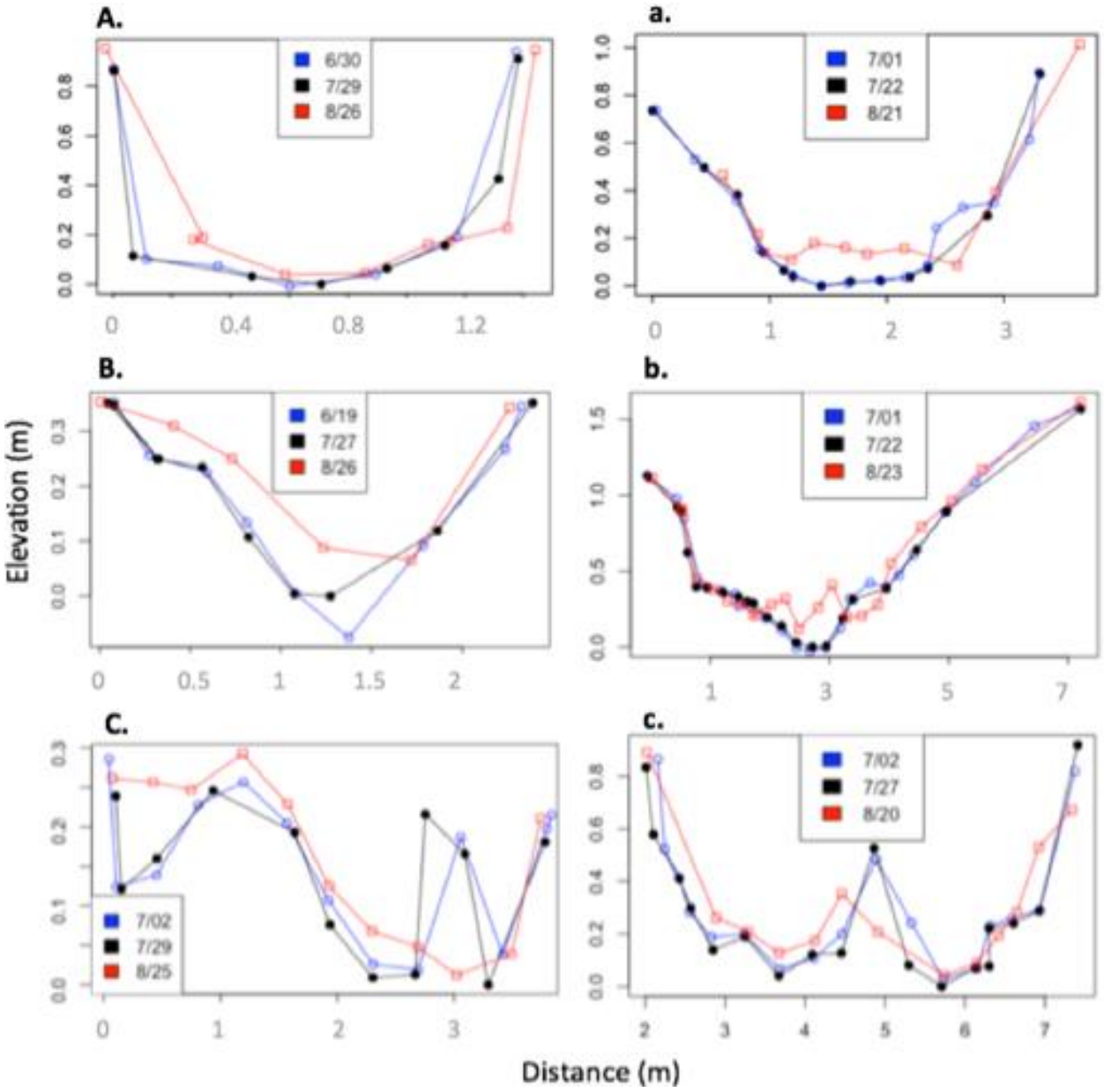

Figure 4.8. In-stream cross-sectional surveys obtained before and after the July 8th and Aug. 16th events for the outlets of each primary monitoring site within Skin (left) and Hill Gulch (right). Labels correspond to site aliases in Table 4.1-4.2: i.e., upper (A,a), intermediate (B,b), and outlet (C,c). Note that the range in elevation shown on the y-axes varies by site. Refer to supplemental figures C2-C10 for full surveys and cross-section photographs.

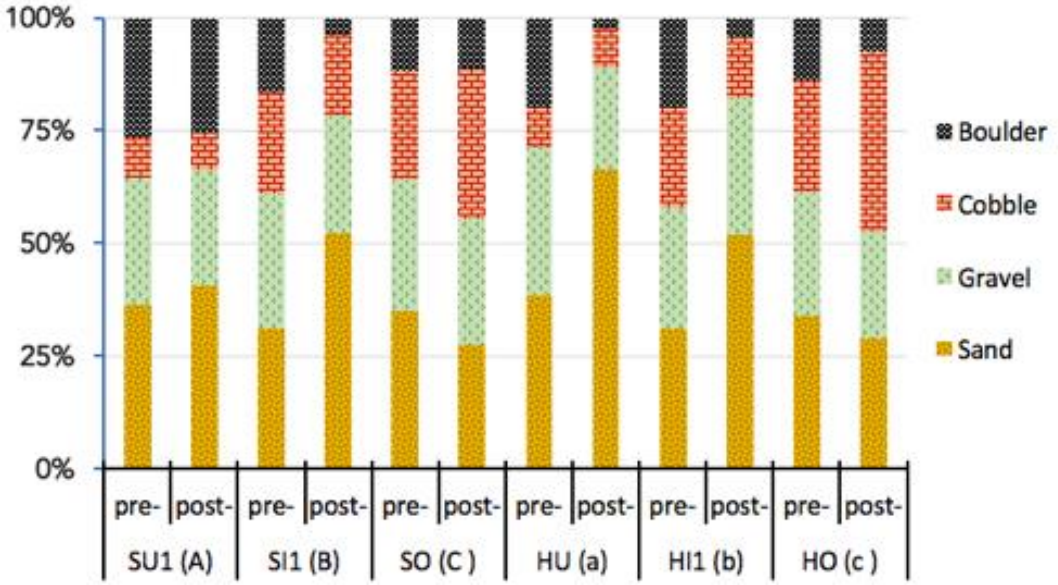

Figure 4.9. Percent sand (< 2 mm), gravel (2-64 mm), cobble (64-256 mm), and boulder (>256 mm) at primary monitoring sites before and after the Aug. 16th event.

4.4. Discussion

4.4.1. Event magnitude comparisons

Peak flows are generally higher post-fire (Moody and Martin 2001a; Hallema et al. 2017; Leibowitz et al. 2019), but this effect decreases over time. Our study took place during the third year post-fire, when peak flow responses had already started to decline. Peak flows at the outlets of Skin and Hill Gulch during the July 8th event were lower than 2-year regional peak flow estimates provided by USGS Streamstats (https://streamstats.usgs.gov/ss/). Flow did exceed the 2-year peak flow estimate of 111 L s^{-1} km^{-2} at the outlet of Hill Gulch during the Aug. 16th event when flow was 280 L s^{-1} km^{-2}, but this is still lower than the 5-year peak flow estimate of 360 L s^{-1} km^{-2}. Across all in-stream sites, peak flows were similar to post-fire streamflow observations within other Colorado Front Range fires. Precipitation and streamflow were available for comparison from the 1996 Buffalo Creek Fire for post-fire year 0-4 (Moody and Martin 2001a) and from the 2000 Bobcat Fire for post-fire year 0-2 (Kunze and Stednick 2006) (Figure 4.10).

For events with similar rainfall intensity (MI_{30}), peak flow during the July 8th event (post-fire year 3) was slightly higher than comparable rainfall events within the Buffalo Creek (post-fire years 1-4) and Bobcat Fire (post-fire year 1) (Figure 4.10). During the Aug. 16th event, peak flow was similar to, or slightly higher than, comparable rainfall events within the Buffalo Creek Fire (post-fire year 1-4). For the sites with the highest Aug. 16th peak flows, magnitudes were comparable to those observed within both the Buffalo Creek and Bobcat Fire during post-fire years 0-2 (Figure 4.10).

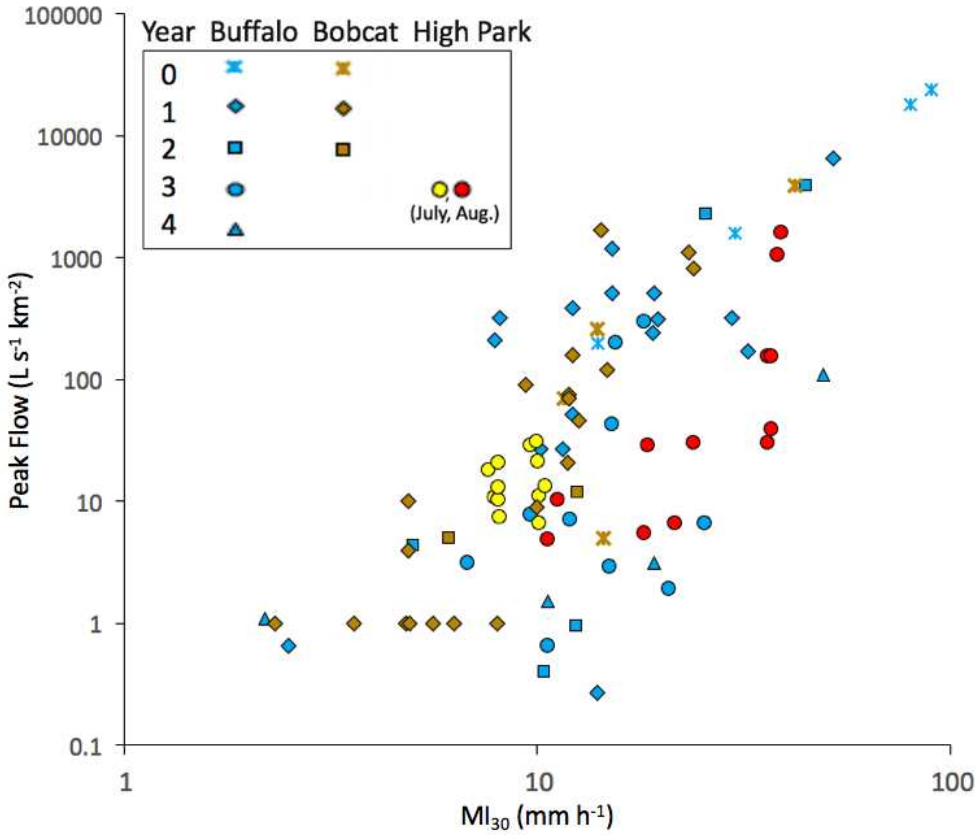

Figure 4.10. Area-normalized peak flow (L s^{-1} km^{-2}) vs. maximum 30-minute rainfall intensity (MI_{30}; mm h^{-1}) by year post-fire (Year) for the Buffalo Creek (Buffalo), Bobcat and High Park Fire. Data include two watersheds each for the Buffalo Creek (26.8 - 122.4 km^2) and Bobcat Fire (2.2-3.9 km^2), and those from Table 4.1 for the High Park Fire.

In contrast to previous research, sediment yields in this study were generally lower at in-stream sites than at hillslopes (Moody and Martin 2009), which may relate to the small size of

the streams and low flow response in post-fire year 3. Maximum in-stream sediment yields during the July 8th and Aug. 16th event were 0.003 and 0.2 Mg ha^{-1}, respectively (Table 4.3) with both observations occurring at the Hill Gulch headwater site (HU; "a"). Sediment yields in the Bobcat Fire (only reported for post-fire year 1) were up to 0.4 and 1 Mg ha^{-1} in Bobcat (2.2 km^2) and Jug Gulch (3.9 km^2), respectively (Kunze and Stednick 2006).

During post-fire year 0-1 of the High Park Fire, Brogan et al. (2017) observed channel changes within Skin Gulch in response to convective (i.e., high intensity) and mesoscale (i.e., long duration) rainfall events. A convective storm occurred just days after the fire was contained, and resulted in estimated peak streamflow of 28,000 L s^{-1} km^{-2} with widespread in-stream deposition in the lower reaches. The mesoscale flood occurred over one week during mid-September 2013 with estimated peak flow of 5,700 L s^{-1} km^{-2} and extensive channel incision and migration (Brogan et al. 2017). Because of vegetation regrowth in the burn area and the relative sizes of storms, these peak flows were orders of magnitude higher than many of those observed for post-fire year 3 (Table 4.2). The high intensity event had high localized connectivity of sediment laterally between hillslopes and channels, and the long duration event had strong longitudinal connectivity of runoff through the channel network.

4.4.2. Connectivity

4.4.2.1. The first event: antecedent precipitation and watershed slope lead to lateral and longitudinal connectivity of runoff

During the July 8th event, the production and connectivity of runoff was likely due to the combined effects of antecedent precipitation and watershed slope. While Q was positively correlated to P>10 (mm), rainfall was below the post-fire year 3 threshold for watershed-scale Q production (i.e., MI_{60} of 7-10 mm h^{-1}; cf., Wilson et al. 2018; chapter 2; Table 4.2), and Q was

slightly more strongly correlated to watershed slope (Table C3). Lateral connectivity of runoff between upslope and/or near-stream areas and stream channels was likely initiated in the days prior to July 8th. Wet antecedent conditions such as these have been shown to produce substantially higher runoff from an unburned semiarid catchment (2.8 km^2) in New Mexico (Schoener and Stone 2019).

Prior studies indicate that connectivity of runoff also increases with slope angle and bare soil (Hopp and McDonnell 2009; Emmanual et al. 2014). The significant and positive relationships between Q, maximum CTI and watershed slope suggests areas with higher CTI and higher slope promoted, respectively, the creation and drainage of flow with low runoff ratios suggesting a combination of minor infiltration excess overland flow at hillslopes along with limited subsurface lateral flow from convergent areas and those adjacent to stream channels. A modeling study suggest that increasing hillslope angle from 6.5-40° improves drainage efficiency of subsurface stormflow (Hopp and McDonnell 2009). Increased subsurface flow is also expected with low post-fire vegetation density: although vegetation was not quantified here, low vegetation density has been shown to decrease evapotranspiration and redistribute incident moisture to the subsurface (Emmanual et al. 2014). As expected from the limited overland flow generation, low sediment delivery ratios from hillslopes to streams were observed (Table 4.3), thereby promoting longitudinal connectivity of runoff and sediment as indicated by incision (Table C5) and higher upstream-downstream SDRs (Table 4.3). Since little to no sediment entered the channel from hillslopes, the stream had high enough sediment transport capacity to incise into stream bed sediments (Table C5; Figure C3-C10). In-stream sources of sediment are supported by the SSC-Q hysteresis patterns (Figure 4.3 and 4.7), and significant increases in normalized absolute cross sectional change with increasing Q (Table C3).

4.4.2.2. The second event: high intensity rainfall promotes lateral connectivity

During the Aug. 16th event, rainfall exceeded post-fire year 3 MI_{60} thresholds of 7.4-10.1 mm h^{-1} for watershed-scale runoff production (Wilson et al. 2018; chapter 2) at all but the two headwater sites in Skin Gulch (i.e., "A" and "D"; Figure 4.1; Table 4.2). Rainfall and burn severity likely controlled the production of runoff and sediment: aside from the percent of a catchment that burned at high severity, neither hillslope nor in-stream production metrics were related to any watershed attributes (Table C3), whereas production uniformly increased with rainfall (Table C2-C3; Figure 4.5).

Although bare soil was not explicitly measured across scales, increased bare soil at the ground surface has been found to reduce post-fire sediment fence catch efficiency (chapter 3) and promote connectivity of runoff and sediment both on hillslopes (Williams et al. 2016) and from hillslopes to channels (Ortíz-Rodrígez et al. 2019). Hillslope cover counts indicate bare soil at the ground surface was higher than at the canopy with values ranging from 19-67% ($\bar{x}$ = 44) and 12-34% ($\bar{x}$ = 19), respectively (ANOVA; $p < 0.05$), indicating the potential for connectivity of runoff and sediment on hillslopes. Consistent with previous research (Moody and Martin 2009), hillslope runoff was higher in Hill Gulch during the Aug. 16th event at 6.1 mm than at any in-stream site (0.05-4.3 mm; $\bar{x}$ = 1.6 mm). Hillslope sediment yields increased with rainfall intensity (Table C2) and were significantly greater than the July 8th event, with higher intensity rainfall likely leading to infiltration excess overland flow and lateral connectivity (hillslope-channel) of sediment.

Lateral connectivity, as indicated by sediment delivery ratios from hillslopes to channels, decreased with increasing unconfined channel length (%), likely because unconfined areas allowed hillslope sediments to be stored in valley bottoms and near channel corridors (Figure

4.5; Table C3). However, 60% of sediment delivery ratios from hillslopes to channels within Hill Gulch were >100% (Table 4.3), indicating sediment yields were higher for in-stream sites than for the associated hillslopes. The upstream to downstream sediment delivery ratio was also >100% at the outlet of Hill Gulch during this event ("c"; Table 4.3). These elevated in-stream sediment yields, which increased with all rainfall metrics and peak flows, may partially be attributed to stream bank erosion (Table C3, C5; Figure C3-C10). In addition, the monitored hillslopes are a small sample of the total hillslopes within a watershed, and not all monitored hillslopes produced an observable response. This indicates greater in-stream sediment production for these comparisons, and highlights the influence perennial flow, and therefore pre-event longitudinal connectivity of runoff, can have on in-stream sediment production.

In contrast, for those in-stream sites with high sediment delivery ratios, longitudinal connectivity of sediment was subsequently reduced, as the sediment delivered to streams was deposited in-stream (Table C3, C5; Figure C3-C10). In-stream sediment deposition (Table C5; Figure C3-C10) and fining (Table 4.9) were greatest at the Hill Gulch headwater (i.e., HU; "a") and intermediate (HI1; "b") sites, and indicate decreased transport capacity. Speculatively, a culvert upstream of HI ("b"), may have ponded water and reduced sediment yields. Decreased transport capacity and supply of fine sediment is supported by suspended sediment concentrations (SSC), which decreased downstream in Hill Gulch, never exceeding the threshold for debris flow (>$1.3x10^6$ mg L^{-1}; Langhans et al. 2017): hillslope SSC decreased from barrel 1 (10,000 mg L^{-1}) to barrel 2 (8,500 mg L^{-1}); siphon sampler SSC decreased from 320,000-630,000 mg L^{-1} at HU to 58,000-390,000 mg L^{-1} at HI1 and 310-170,000 mg L^{-1} at HO. However, deposition of fine sediment was lower at the watershed outlet (HO; Figure 4.9), likely due to supply limitation as smaller tributaries converged before the outlet producing high flow with

high transport capacity, as indicated by increases in the percent cobble and movement of large woody debris (Supplemental Video).

4.4.3. Wildfire effects on connectivity

The effects of high severity wildfire were evident during both the July 8th and Aug. 16th event. Wildfire combusts organic surface cover, subsequently exposing bare soil and altering watershed function: without surface cover to intercept rainfall, soil sealing (Larsen et al. 2009), increased runoff and erosion (Benavides-Solario and MacDonald 2005), and greater connectivity between upslope areas and streams results (Wohl 2013). These effects are evident for both events observed here: increasing the percent of a catchment that burned at high burn severity increased sediment delivery ratios from hillslopes to channels and the normalized absolute channel change observed at in-stream cross sections (Table C3). However, for high intensity short duration events, high severity wildfire may also decrease longitudinal connectivity of sediment through increased deposition within channels (i.e., normalized net change; Table C3) when sediment delivery exceeds in-stream transport capacity (Table C2 and C3, respectively). Although July 8th hillslope sediment yields decreased with the percent mulch observed during cover counts (Table C2), the percent of a catchment targeted to receive mulch treatments was not significantly related to the production of runoff and sediment or downstream effects (Table C2 and C3). To determine the effects of mulch treatments at larger watershed scales, more extensive field observations of cover combined with mulch applications over large fractions of watershed area are likely necessary.

4.5. Conclusions

This research examined connectivity of post-fire runoff and sediment from hillslope through watershed scale during post-fire year 3 of the 2012 High Park Fire. We identified

sources and quantified magnitudes of runoff and sediment during two rain events with varied duration and intensity. The first rainfall event was low intensity and long duration (return interval of $\leq$ 2 years), and it led to low hillslope sediment yields and widespread channel incision because channel transport capacity exceeded hillslope sediment supply. The second rainfall event was high intensity over an average duration of 1 hour (return interval $\leq$ 10 years) leading to infiltration excess overland flow and high sediment yields with greater sediment delivery ratios and in-stream deposition. This led to net aggradation of most channels, but not all because sediment supply relative to transport capacity varied along the channel network. Unconfined reaches of the channel network were likely areas of sediment deposition, reducing delivery of sediment from hillslopes to channels, while tributary junctions increased streamflow and transport capacity, further reducing the amount of sediment deposited at the outlet of Hill Gulch ("c"; Figure 4.1). During both events, the effects of wildfire were evident, as the percent of a catchment that burned at high severity increased sediment delivery ratios from hillslopes to channels and area-normalized absolute channel change. These findings highlight the utility of nested monitoring for quantifying connectivity of runoff and sediment transport in post-fire environments.

CHAPTER 5: CONCLUSIONS

This research demonstrated that post-fire responses and subsequent connectivity of runoff and sediment varied with rainfall, surface cover and spatial scale. Rainfall thresholds for the generation of runoff and sediment delivery increased with added surface cover from mulch treatments and regrowth of vegetation. Hillslope sediment fences modified to collect runoff and suspended sediment improved sediment yield estimates and indicated the type and magnitude of sediment that may be delivered to stream channels. Subsequent nested monitoring within the stream network revealed how rainfall, hillslope runoff and sediment production, and the extent of high burn severity affected connectivity of runoff and sediment both laterally (hillslope-channel) and longitudinally (upstream-downstream). This section highlights the key factors affecting post-fire connectivity of runoff and sediment and presents suggested improvements for future nested monitoring efforts.

The amount of rainfall needed to initiate post-fire responses and connectivity of runoff and sediment across watersheds decreases after wildfire due to interconnected areas of bare soil. The threshold analysis (chapter 2) showed that mulch treatments increased hillslope-scale thresholds during post-fire years 1 and 2 (Table 2.3), with little to no effect during post-fire year 3, when vegetation had regrown enough for soil infiltration capacities to recover. The connectivity analysis (chapter 4) used observations during post-fire year 3 when the watersheds had become less responsive to rainfall. Although the low intensity storm on July 8th was below the associated rainfall threshold identified for production of a watershed scale response in post-fire year 3 (chapter 2), streamflow increased (Figure 4.3) and channels incised (Table C5), thereby highlighting the limitations of rainfall intensity thresholds (chapter 2) as the landscape

recovers from fire. For the July 8th event, higher slopes alongside recovering infiltration capacities likely promoted drainage of antecedent rainfall via subsurface lateral flow from convergent areas and those adjacent to stream channels. Future research could expand on the surface monitoring that was the focus of this project and also include more subsurface soil moisture and groundwater measurements to determine whether or not there is subsurface lateral flow. Monitoring could also include assessment of the properties affecting infiltration capacity (e.g. ground cover, soil structure), as well as the effects of antecedent precipitation on soil moisture and subsurface flow over time after fire across the domains of interest. The threshold analysis could also include responses to mesoscale events as well as the potential for connectivity, both lateral (hillslope-channel) and longituduinal (upstream-downstream), from rain storms with varied duration and intensity as affecting in-stream incision and deposition.

Spatial scale is another important control on post-fire responses because variability in the factors affecting the generation of runoff and sediment increases with spatial scale. For larger areas, multiple types of rainfall-runoff mechanisms may occur in different parts of a watershed. The thresholds identified in chapter two were generally similar across spatial scales, coincide with values from other post-fire basins (24-2200 ha) across the western U.S. (Moody 2002; Moody et al. 2008b; Murphy et al. 2016), and likely represent infiltration overland flow. These thresholds were similar for plots and hillslopes, likely because burn severity and the mechanisms that generate overland flow and downslope connectivity of runoff and sediment are more likely to be uniform at these spatial scales. For watersheds, burn severity, surface cover and rainfall characteristics are more variable and affect the occurrence and extent of connectivity. For example, when higher intensity rainfall produces hillslope erosion that is delivered to streams, such as during the Aug. 16th event of the connectivity analysis (chapter 4), high sediment yields

may lead to in-stream deposition. In contrast, when high antecedent precipitation promotes storage of subsurface water within convergent and riparian zones, low intensity rainfall can also produce streamflow, such as during the July 8th connectivity analysis (chapter 4). This further highlights the importance of understanding the characteristics and sequence of post-fire events as affecting whether runoff and sediment will connect to streams, and whether the streambed will subsequently aggrade or incise. In the absence of lateral connectivity (hillslope-channel) of sediment during the July 8th event, streamflow was more likely to incise the streambed and promote erosion of channel banks. To characterize controls on rainfall-runoff and connectivity across watersheds, future analyses should include continuous measurements of hillslope responses and measurements of rainfall spatial variability. Spatial patterns of rainfall interpolated across the domain of interest may be more informative than assignment of the associated gauge with the maximum erosivity, as in the threshold analysis (chapter 2).

Watershed slope, unconfined stream reaches and burn severity were strong controls on post-fire responses and connectivity throughout post-fire recovery. In post-fire year 3, during both the low and high intensity events of the connectivity analysis (chapter 4), the percent of a catchment that burned at high severity increased sediment delivery ratios and area-normalized absolute channel change. The importance of burn severity is likely tied to the creation of interconnected areas of bare soil that promoted connectivity. Additional watershed characteristics should also be considered in future analyses of connectivity. For example, results of the connectivity analysis (chapter 4) indicate that hillslope sediment was stored in valley bottoms before reaching active channels. Although topographic analyses such as the valley confinement algorithm are steady-state and verifiable with a field campaign, ground cover varies seasonally and with time since burn, and it is difficult to quantify remotely. Future monitoring

should continue to measure ground cover at nested hillslopes with additional sampling points to characterize ground cover across the monitored watersheds and inform remote sensing classifications. These measurements would be particularly useful to evaluate the amount and persistence of mulch cover as well as for connecting watershed responses more directly to ground cover changes.

While this research has shown that post-fire response can vary with spatial scale, time since burn, and the characteristics of previous post-fire storms, determining effects on connectivity across larger spatial scales during post-fire recovery periods remains a monitoring challenge. In chapter 3, commonly used and low-cost sediment fences were found to underestimate sediment yields, but these are still useful for determining which types of storms produced low or high erosion, particularly with continuous monitoring (e.g., time lapse cameras). Other low cost measurements such as ephemeral catchment monitoring devices (Chapter 4) or crest gauges can also be highly informative for identifying connectivity of surface flow paths during a given time period. To further determine the timing or frequency of connections, slightly more expensive, but still low cost HOBO sensors and data loggers can be deployed (Bhamjee et al. 2016). Siphon samplers are another low-cost method that can be used as an alternative to event-based automated samplers (e.g., ISCOs) for determining relationships between suspended sediment and NTU alongside baseline automated and depth-integrated sampling (Figure C2). However, during storms with higher return intervals, such as the one on Aug. 16th ($\leq$ 10 year storm), concurrent measurements from siphon samplers and ISCOs could improve understanding of- and confidence in- siphon sample SSC during high flows (Figure C2). Although the timing of in-stream sediment transport relative to streamflow (i.e., SSC-Q hysteresis) can indicate likely sediment sources, monitoring at nested hillslopes and watersheds can improve understanding of

sources as well as effects of rainfall and surface cover on lateral, and subsequently, longitudinal connectivity. Hillslopes should be nested within watersheds that include representative reaches or at tributary junctions to further understand the factors affecting in-stream sediment storage and transport capacity. Additional modifications to hillslope sediment fences, such as increasing storage capacity and weir dimensions, could be implemented to limit the amount of runoff and suspended sediment that may bypass the weir and overtop the sediment fence. Geomorphic surveys or methods to remotely analyze channel change should continue to be paired with nested hillslopes and watershed monitoring to further determine areas of in-stream incision and deposition.

Consideration of post-fire production, connectivity and recovery in areas with different climates and soils than those presented here should also be included in future analyses along with potential effects of pre-fire mitigation techniques (e.g., thinning and burning). Ultimately, these improvements to future post-fire nested monitoring and research should allow us to better predict the potential of of post-fire effects on water supplies across the western U.S. to target pre- and post-fire management to the areas most likely to negatively affect water supplies.

REFERENCES

Arkle, RS and DS Pilliod. 2010. Prescribed fires as ecological surrogates for wildfires: a stream and riparian perspective. Forest Ecology and Management (259): 893-903.

ARS (Agriculture Research Service). 2013. Rainfall Intensity Summarization Tool (RIST) (Version 3.89) [computer software]. United States Department of Agriculture. Retrieved from http://www.ars.usda.gov/Research/docs.htm?docid=3251.

ASTM Standard D3977-97. 2013a. Standard test methods for determining sediment concentration in water samples. ASTM International, West Conshohocken, PA, 2013, www.astm.org.

ASTM Standard D2974-13. 2013b. Standard test methods for moisture, ash, and organic matter of peat and other organic soils. ASTM International, West Conshohocken, PA, 2013, www.astm.org.

Beel, C.R., Orwin, J.F., and P.G. Holland. 2011. Controls on slope-to-channel fine sediment connectivity in a largely ice-free valley, Hoophorn Stream, Southern Alps, New Zealand. Earth Surface Processes and Landforms 36: 981-994.

Benavides-Solorio JD and LH MacDonald. 2001. Post-fire runoff and erosion from simulated rainfall on small plots, Colorado Front Range. Hydrological Processes 15: 2931–2952.

Benavides-Solorio JD and LH MacDonald. 2005. Measurement and prediction of post-fire erosion at the hillslope scale, Colorado Front Range. International Journal of Wildland Fire 14: 1-18.

Bhamjee, R, Lindsay, JB and J Cockburn. 2016. Monitoring ephemeral headwater streams: a paired sensor approach. Hydrol. Process. (30): 888-898.

Bonilla, CA, Kroll, DG, Norman, JM, Yoder, DC, Molling, CC, Miller, PS, Panuska, JC, Topel, JB, Wakeman, PL, and KG Karthikeyan. 2006. Instrumentation for measuring runoff, sediment and chemical losses from agricultural fields. J. Environ. Qual. 35:216-223.

Braddock WA, Nutalaya P, Gawarecki SJ, and GC Curtin. 1970. Geologic map of the Drake Quadrangle, Larimer County, Colorado. US Department of Interior Geological Survey May GQ-829. USDI Geological Survey, Washington, DC.

Brogan, DJ, Nelson, PA and LH MacDonald. 2019. Spatial and temporal patterns of sediment storage and erosion following a wildfire and extreme flood. Earth surf. Dynam (7): 563-590.

Brogan DJ, Nelson PA and LH MacDonald. 2017. Reconstructing extreme post-wildfire floods: a comparison of convective and mesoscale events. Earth Surfaces Processes and Landforms 42: 2505-2522.

Brown, LC and GR Foster, 1987. Storm erosivity using idealized intensity distributions. Trans. ASAE 30 (2), 379–386.

Burned Area Emergency Response (BAER). 2012. High Park fire burned area emergency response report. Colorado Dept. of Transportation, Larimer County, NRCS, and USDA. 35 p.

Cammeraat LH. 2002. A review of two strongly contrasting geomorphological systems within the context of scale. Earth Surf. Process. Landforms 27, 1201–1222.

Cammeraat LH. 2004. Scale dependent thresholds in hydrological and erosion response of a semi-arid catchment in southeast Spain. Agriculture, Ecosystems and Env. 104: 317-332.

Cavalli, M., Trevisani, S., Comiti, F., and L. Marchi. 2013. Geomorphometric assessment of spatial sediment connectivity in small Alpine catchments. Geomorphology 188: 31-41.

Cawson, JG, Sheridan GJ, Smith, HG and PNJ Lane. 2013. Effects of fire severity and burn patchiness on hillslope-scale surface runoff, erosion and hydrologic connectivity in a prescribed burn. Forest Ecology and Management (310): 219-233.

Cawson, JG, Nyman, P, Smith, HG, Lane, PNJ and GJ Sheridan. 2016. How soil temperatures during prescribed burning affect soil water repellency, infiltration and erosion. Geoderma (278): 12-22.

Cone, VM. Flow through weir notches with thin edges and full contractions. Journal of Agricultural Research, 5 (23): 1051-1113.

DeLong, SB, Youberg, AM, Delong, WM and BP Murphy. 2018. Post-wildfire landscape and erosional processes from repeat terrestrial lidar in a steep headwater catchment, Chiricahua Mountains, Arizona, USA. Geomorphology (300): 13-30.

Dingman SL. 2002. Physical Hydrology, 2nd ed., Prentice-Hall, Inc.

Duvert, C, Gratiot, N, Anguiano-Valencia, R, Némery, J, Mendoza, ME, Carlón-Allende, T, Prat, C and M Esteves. 2011. Baseflow control on sediment flux connectivity: insights from a nested catchment study in Central Mexico. Catena (87): 129-140.

Ebel BA and DA Martin. 2017. Meta-analysis of field-saturated hydraulic conductivity recovery following wildland fire: applications for hydrologic model parameterization and resilience assessment. Hydrological Processes 31: 3682-3696.

Edwards, TK and GD Glysson. 1988. Field Methods for Measurement of Fluvial Sediment. US Geological Survey Open-File Report 86-531.

Elliot WJ. 2004. WEPP internet interfaces for forest erosion prediction. Journal of the American Water Resources Association, 40(2), 299–309. https://doi.org/10.1111/j.1752-1688.2004.tb01030.x

Emelko, MB, Silins, U, Bladon, KD and M Stone. 2011. Implications of land disturbance on drinking water treatability in a changing climate: demonstrating the need for "source water supply and protection" strategies. Water Res. 45(2): 461-472.

Emmanual, RE, Hazen, AG, McGlynn, BL and KG Jensco. 2014. Vegetation and topographic influences on the connectivity of shallow groundwater between hillslopes and streams. Ecohydrology (7): 887-895.

ESRI, 2013. ArcGIS Desktop: Release 10.3. Environmental Systems Research Institute, Redlands, CA.

Ferriera, AJD, Coelho, COA, Ritsema, CJ, Boulet, AK and JJ Keizer. 2008. Soil and water degradation processes in burned areas: lessons learned from a nested approach. Catena (74): 273-285.

Gee, GW and D Orr. 2002. Particle-size analysis. In Methods of Soil Analysis Part 4, Dane, JH and GC Topp (eds.), Soil Science Society of America. Madison, WI, p. 255-293.

Haan, CT, Barfield, BJ and JC Hayes. 1994. Design hydrology and sedimentology for small catchments. San Diego, CA: Academic Press, Inc.

Hohner AK, Cawley K, Oropeza J, Summers RS and FL Rosario-Ortiz. 2016. Drinking water treatment response following a Colorado wildfire. Water Research 105: 187-198.

Hopp L and JJ McDonnell. 2009. Connectivity at the hillslope scale: identifying interactions between storm sitze, bedrock permeability, slope angle and soil depth. Journal of Hydrology (376): 378-391.

Inbar M, Tamir M and L Wittenberg. 1998. Runoff and erosion processes after a forest fire in Mount Carmel, a Mediterranean area. Geomorphology 24: 17-33.

James, CE and B Krumland. 2018. Immediate post-forest fire salvage logging, soil erosion, and sediment delivery. For. Sci. 64(3): 246-267.

JMP®, Version 12.0.1. SAS Institute Inc., Cary, NC, 1989-2007.

Johansen, MP, Hakonson, TE and DD Breshears. 2001. Post-fire runoff and erosion from rainfall simulation: contrasting forests with shrublands and grasslands. Hydrol. Process. 15, 2953-2965.

Jones, JI, Murphy, JF, Collins, AL, Sear, DA, Naden, PS and PD Armitage. 2012. The impact of fine sediment on macroinvertebrates. River Research and Applications (28): 1055-1071.

Kampf SK, Brogan DJ, Schmeer S, MacDonald LH and PA Nelson. 2016. How do geomorphic effects of rainfall vary with storm type and spatial scale in a post-fire landscape? Geomorphology 273: 39-51.

Kampf, SK and MA Lefsky. 2015. Transition of dominant peak flow source from snowmelt to rainfall along the Colorado Front Range: Historical patterns, trends, and lessons from the 2013 Colorado Front Range floods. Water Resour. Res., 52, doi:10.1002/ 2015WR017784.

Kampf, SK, Gannon, B, Wilson, C, Saavedra, F, Miller, ME, Heldmyer, A, Livneh, B, Nelson, P, Schmeer, S and L MacDonald. In review. Selecting erosion models for land management: example application to post-fire erosion on the Colorado Front Range. Environmental Management.

Kilpatrick, FA, and Cobb, ED, 1985, Measurement of discharge using tracers: U.S. Geological Survey Techniques of Water-Resources Investigations, book 3, chap. A16, 52 p.

Kutiel P, Lavee H, Segev M and Y Benyamini. 1995. The effect of fire-induced heterogeneity on rainfall-runoff-erosion relationships in an eastern Mediterranean ecosystem, Israel. Catena (25): 77-87.

Kunze MD and JD Stednick. 2006. Streamflow and suspended sediment yield following the 2000 Bobcat fire, Colorado. Hydrological Processes 20: 1661–1681.

Larsen, IJ, MacDonald, LH, Brown, E, Rough, D, Welsh, MJ, Pietraszek, JH, Libohova, Z, Benavides-Solario, JD, and K Schaffrath. 2009. Causes of post-fire runoff and erosion: water repellency, cover, or soil sealing? Soil Sci. Soc. Am. J. 73: 1393-1407.

Leibowitz, SG, Wigington Jr, PJ, Schofield, KA, Alexander, LC, Vanderhoof, MK, and HE Golden. 2018. Connectivity of streams and wetlands to downstream waters: an integrated systems framework. J Am Water Resour Assoc. 54(2): 298-322.

Lewis, J and R Eads. 2009, Implementation guide for turbidity threshold sampling: principles, procedures, and analysis, *Gen. Tech. Rep. PSW-GTR-212*, United States Department of Agriculture, Forest Service, Pacific Southwest Research Station, Albany, CA.

Lexartza-Artza, I., and J. Wainwright. 2009. Hydrological connectivity: Linking concepts with practical implications. Catena 79: 146-152.

Litschert SE, Brown TC and DM Theobald. 2012. Historic and future extent of wildfires in the Southern Rockies Ecoregion, USA. Forest Ecology and Management, 269: 124-133.

Martin, C. 2018. Spatial and temporal variability in channel surface flow across an elevation gradient on the Colorado Front Range. M.S. Thesis, Colorado State University.

Martin DA. 2016. At the nexus of fire, water and society. Phil. Trans. R. Soc. B. 371: 20150172. http://dx.doi.org/10.1098/rst.2015.0172.

Miller ME, MacDonald LH, Robichaud PR and WJ Elliot. 2011. Predicting post-fire hillslope erosion in forest lands of the western United States. International Journal of Wildland Fire, 20, 982-999.

Moody JA and DA Martin. 2001a. Initial hydrologic and geomorphic response following a wildfire in the Colorado Front Range. Earth Surf. Process. Landforms 26: 1049-1070.

Moody, JA and DA Martin. 2001b. Post-fire, rainfall intensity-peak discharge relations for three mountainous watersheds in the western USA. Hydrol. Process. 15, 2981-2993.

Moody J. 2002. An analytical method for predicting post-wildfire peak discharges. U.S. Geological Survey Scientific Investigations Report 2011-5236, 36 p.

Moody JA, Martin, DA and SH Cannon. 2008a. Post-wildfire erosion response in two geologic terrains in the western USA. Geomorphology (95): 103-118.

Moody JA, Martin DA, Haire SL and DA Kinner. 2008b. Linking runoff response to burn severity after a wildfire. Hydrol. Process. 22: 2063-2074.

Moody JA and DA Martin. 2009. Synthesis of sediment yields after wildland fire in different rainfall regimes in the western United States. Int. J. Wildland Fire (18): 96-115.

Moody JA, Shakesby RA, Robichaud PR, Cannon SH and DA Martin. 2013. Current research issues related to post-wildfire runoff and erosion processes. Earth-Science Reviews 122: 10-37.

Moore, ID, Grayson, RB and AR Larson. 1991. Digital terrain modelling: A review of hydrological, geomorphological, and biological applications. Hydrological Processes (5): 3-30.

Moreno-de las Heras, M, Nicolau, JM, and L Merino-Martin. 2010. Plot-scale effects on runoff and erosion along a slope degradation gradient. Water Resources Research, 46, W04503, doi: 10.1029/2009WR007875.

Murphy SF, Writer JH, McCleskey RB and DA Martin. 2016. The role of precipitation type, intensity, and spatial distribution in source water quality after wildfire. Environ. Res. Lett. 10 08400.

Murphy, SF, McCleskey, RB, Martin, DA, Writer, JH and BA Ebel. 2018. Fire, Flood and Drought: Extreme Climate Events Alter Flow Paths and Stream Chemistry. Journal of Geophysical Research: Biogeosciences (123): 2513-2526. 2513–2526. https://doi.org/10.1029/2017JG004349.

Nagel, DE, Buffington, JM, Parkes, SL, Wenger, S, and JR Goode. 2014. A landscape scale valley confinement algorithm: Delineating unconfined valley bottoms for geomorphic, aquatic, and riparian applications. Gen. Tech. Rep. RMRS- GTR-321. Fort Collins, CO: U.S. Department of Agriculture, Forest Service, Rocky Mountain Research Station. 42 p.

Nawa, RK and CA Frissell. 1994. Measuring scour and fill of gravel streambeds with scour chains and sliding-bead monitors. North American Journal of Fisheries Society (13): 634-639.

Nolan, KM and RR Shields. 2000. Measurement of stream discharge by wading, U.S. Geol. Surv. Water Resources Investigation Report 00-4036, [On CD-ROM].

Noske, PJ, Nyman, P, Lane, PNJ, and GJ Sheridan. 2016. Effects of aridity in controlling the magnitude of runoff and erosion after wildfire. Water Resources Research, 52, 4338-4357, doi: 10.1002/2015WR017611.

Nyman P, Sheridan GJ, and PN Lane. 2013. Hydro-geomorphic response models for burned areas and their applications in land management. Progress in Physical Geography 37: 787-812.

Olsen, WH. 2016. Effects of wildfire and post-fire salvage logging on rill networks and sediment delivery in California forests. MS thesis, Michigan Technological University. Houghton, MI 149 pp.

Osborn HB, Lane LJ and Hundley JF. 1972. Optimum gaging of thunderstorm rainfall in southeastern Arizona. Water Resources Research 8(1): 259–265.

Osborn HB and EM Laursen. 1973. Thunderstorm runoff in southeastern Arizona. Journal of the Hydraulics Division 99(HY7): 1129-1145.

Ortíz-Rodríquez, AJ, Muñoz-Robles, C and L Borselli. 2019. Changes in connectivity and hydrological efficiency following wildland fires in Sierra Madre Oriental, Mexico. Science of the Total Environment (655): 112-128.

Pannkuk, CD and PR Robichaud. 2003. Effectiveness of needle cast at reducing erosion after forest fires. Water Resources Research, 39 (12), 1333, doi: 10.1029/2003WR002318, 2003.

Parsons, A, Robichaud PR, Lewis, SA, Napper, C and JT Clark. 2010. Field Guide for mapping post-fire soil burn severity. Gen. Tech. Rep. RMRS-GTR-243. Fort Collins, CO: U.S. Department of Agriculture, Forest Service, Rocky Mountain Research Station. 49 p.

Parsons, AJ, Brazier, RE, Wainwright, J, and M Powell. 2006. Scale relationships in hillslope runoff and erosion. Earth Surface Processes and Landforms 31: 1384-1393.

Perica S, Martin D, Pavlovic S, Roy I, St. Laurent M, Trypaluk C, Unruh D, Yekta M and G Bonnin. 2013. NOAA Atlas 14 Volume 8 Version 2, Precipitation-Frequency Atlas of the United States, Midwestern States. NOAA, National Weather Service, Silver Spring, MD.

Pietraszek, JH. 2006. Controls on post-fire erosion at the hillslope scale, Colorado Front Range. MS thesis, Colorado State University.

Pringle, CM. 2001. Hydrologic connectivity and the management of biological reserves: a global perspective. Ecological Applications: 11(4): 981-998.

PRISM Climate Group, Oregon State University. 2017. http://www.prism.oregonstate.edu/normals/. (accessed 5 July 2017).

Prosser, IP and L Williams. 1998. The effect of wildfire on runoff and erosion in native Eucalyptus forest. Hydrol. Process. 12: 251-265.

R Core Team. 2017. R: A language and environment for statistical computing. R Foundation for Statistical Computing, Vienna, Austria. URL http://www.R-project.org/.

Renard, KG, Foster, GR, Weesies, GA, McCool, DK, and DC Yoder, 1997. Predicting soil erosion by water: a guide to conservation planning with the Revised Universal Soil Loss Equation (RUSLE). USDA Agricultural Handbook No. 703 404 pp.

Robichaud, PR, McCool DK, Pannkuk, CD, Brown, RE and PW Mutch. 2001. Trap efficiency of silt fences used in hillslope erosion studies. Soil Erosion Research for the 21st Century, Proc. Int. Symp. January 2001, Honolulu, HI, USA. Pp. 541-543.

Robichaud, PR and RE Brown. 2002. Silt fences: An economical technique for measuring hillslope soil erosion. USDA Forest Service General Technical Report RMRS-STR-94.

Robichaud PR, Elliot WJ, Pierson FB, Hall DE, and CA Moffet. 2007. Predicting postfire erosion and mitigation effectiveness with a web-based probabilistic erosion model. Catena, 71, 229–241.

Robichaud PR, Wagenbrenner JW, Brown RE, Wohlgemuth PM, and JL Beyers. 2008. Evaluating the effectiveness of contour-felled log erosion barriers as a post-fire runoff and erosion mitigation treatment in the western United States. International Journal of Wildland Fire, 17(2), 255–273. https://doi.org/10.1071/Wf07032.

Robichaud, PR, Jordan, P, Lewis, SA, Wagenbrenner, JW, Ashmun, LE, and RE Brown. 2013a. Post-fire mulching for runoff and erosion mitigation Part I: Effectiveness at reducing hillslope erosion rates. Catena 105: 75-92.

Robichaud, PR, Wagenbrenner, JW, Lewis, SA, Ashmun, LE, Brown, RE, and PM Wohlgemuth. 2013b. Post-fire mulching for runoff and erosion mitigation Part II: Effectiveness in reducing runoff and sediment yields from small catchments. Catena 105: 93-111.

Robichaud, PR, Storrar, KA and JW Wagenbrenner. 2019. Effectiveness of straw bale check dams at reducing post-fire sediment yields from steep ephemeral channels. Science of the Total Environment (676): 721-731.

Rough D. 2007. Effectiveness of rehabilitation treatments in reducing post-fire erosion after the Hayman and Schoonover Fires, Colorado Front Range. MS thesis, Colorado State University.

Ryan, SE, Dwire, KA and MK Dixon. 2011. Impacts of wildfire on runoff and sediment loads at Little Granite Creek, western Wyoming. Geomorphology (129): 113-130.

Schmeer, SR. 2014. Post-fire erosion response and recovery, High Park fire, Colorado. MS thesis, Colorado State University.

Schmeer SR, Kampf SK, MacDonald LH, Hewitt J and C Wilson. 2018. Empirical models of annual post-fire erosion on mulched and unmulched hillslopes. Catena (163): 276-287.

Schoener G, and MC Stone. 2019. Impact of antecedent soil moisture on runoff from a semiarid catchment. Journal of Hydrology (569): 627-636.

Shi, ZH, Fang, NF, Wu, FZ, Wang, L, Yue, BJ and GL Wu. 2012. Soil erosion processes and sediment sorting associated with transport mechanisms on steep slopes. Journal of Hydrology. 454-455: 123-130.

Sivapalan, M. Jothityangkoon C and M Menabde. 2002. Linearity and nonlinearity of basin response as a function of scale: discussion of alternative definitions. Water Resources Research 38(2), 1012. doi: 10.1029/2001WR000482.

Smith, HG, Sheridan, GJ, Lane, PNJ, Nyman, P, and S Haydon. 2011. Wildfire effects on water quality in forest catchments: A review with implications for water supply. Journal of Hydrology 396: 170-192.

Soil Survey Staff, Natural Resource Conservation Service, United States Department of Agriculture. Soil Survey Geographic (SSURGO) Database for Colorado. Available online. Accessed 7/15/19.

Stone, B., 2015. Mapping burn severity, pine beetle infestation, and their interactions at the High Park Fire. M.S. Thesis, Colorado State University.

Sutherland, RA. 1991. Selective erosion and sediment source identification, Baringo District, Kenya. Annals of Geomorphology (35): 293-304.

USDA-FSA_APFO Aerial Photography Field Office, 2013. NAIP Digital Georectified Image. Salt Lake City, UT.

Veblen TT, Kitzberger T and J Donnegan. 2000. Climatic and human influences on fire regimes in Ponderosa Pine forests in the Colorado Front Range. Ecological Applications, 10(4): 1178-1195.

Viera AJ and JM Garrett. 2005. Understanding interobserver agreement: the kappa statistic. Family Medicine 37 (5): 360-363.

Wagenbrenner, JW, MacDonald, LH, and D Rough. 2006. Effectiveness of three post-fire rehabilitation treatments in the Colorado Front Range. Hydrol. Process 20: 2989-3006.

Wagenbrenner, JW and PR Robichaud. 2014. Post-fire bedload sediment delivery across spatial scales in the interior western US. Earth Surface Proc. & Landforms. 39 (2014): 865-876.

Wagenbrenner, JW, MacDonald, LH, Coates, RN, Robichaud, PR and RE Brown. 2015. Effects of post-fire salvage logging and a skid trail treatment on ground cover, soils, and sediment production in the interior western United States. Forest Ecology and Mgt. 335, 176–193

Wainwright, J, Parsons, AJ, and AD Abrahams. 2000. Plot-scale studies of vegetation, overland flow and erosion interactions: case studies from Arizona and New Mexico. Hydrol. Process (14): 2921-2943.

Wainwright, J, Turnbull, L, Ibrahim, TG, Lexartza-Artza, I, Thornton, SF and RE Brazier. 2011. Linking environmental régimes, space and time: Interpretations of structural and functional connectivity. Geomorphology (126): 387-404.

Walling, DE. 1983. The Sediment Delivery Problem. Journal of Hydrology (65): 209-237.

Wan, Y and SA El-Swaify. 1998. Characterizing interrill sediment size by partitioning splash and wash processes. Soil Sci. Soc. Am. J. 62: 430-437.

Westerling AL, Hidalgo HG, Cayan DR and TW Sweetnam. 2006. Warming and earlier spring increase U.S. forest wildfire activity. Science 313: 940-943.

Wilson, CR, Kampf, SK, Wagenbrenner, JW and LH MacDonald. 2018. Rainfall thresholds for post-fire runoff and sediment delivery from plot to watershed scale. Forest Ecology and Management (430): 346-356.

Williams, CJ, Pierson, FB, Robichaud, PR, Al-Hamdan, OZ, Boll, J and EK Strand. 2016. Structural and functional connectivity as a driver of hillslope erosion following disturbance. International Journal of Wildland Fire (25): 306-321.

Williams GP. 1989. Sediment concentration versus water discharge during single hydrologic events in rivers. J. Hydrol. 111: 89-101.

Wohl E and DN Scott. 2017. Transience of channel head locations following disturbance. Earth Surf. Procss. Landforms 42: 1132-1139.

Wolman, M.G. 1954. A method of sampling coarse river-bed material. Transactions, American Geophysical Union 35:6.

Woods, SW and VN Balfour. 2010. The effects of soil texture and ash thickness on the post-fire hydrological response from ash-covered soils. Journal of Hydrology 393: 274-286.

Yanosek, KA, Foltz, RB and JH Dooley. 2006. Performance assessment of wood strand erosion control materials among varying slopes, soil textures, and cover amounts. Journal of Soil and Water Conservation 61(2): 45-51.

Yochum, SE, Comiti, F, Wohl, E, David, GCL and L Mao. 2014. Photographic guidance for selecting flow resistance coefficients in high-gradient channels. Gen. Tech. Rep. RMRS-GTR-323. Fort Collins, CO: U.S. Department of Agriculture, Forest Service, Rocky Mountain Research Station. 91 p.

APPENDIX A: Supplemental material for Chapter 2

Table A1. Percent of summer rain storms that resulted in false positives (FP; %) or false negatives (FN; %) for plots, hillslopes, and watersheds by year post-fire, fire and mulch status (Y/N). Blank cells indicate no data.

	Spatial scale:		Plot		Hillslope		Watershed	
Year	Fire	Mulch	FP (%)	FN (%)	FP (%)	FN (%)	FP (%)	FN (%)
0	BC	N	0	10	4	8	9	5
		Y	0	50	0	11		
	HM	N			0	4		
		Y			0	3		
	HP	N			6	5		
		Y			3	0		
1	BC	N	0	5	3	11	20	4
		Y	4	8	1	7		
	HM	N	0	1	3	12		
		Y	0	0	4	6		
	HP	N			10	1		
		Y			3	4		
2	BC	N	0	4	1	6	4	7
		Y	0	7	0	6		
	HM	N	4	1	0	5		
		Y	4	1	5	2		
	HP	N			2	7	0	3
		Y			1	7		
3	BC	N	0	2	0	2		
		Y	0	0	0	0		
	HM	N	0	0	0	0		
		Y	0	0	4	0		
	HP	N			0	3	1	5
		Y			2	3		
4	HM	N	6	1	0	3		
		Y	7	1	0	3		
	HP	N					7	2

Table A2. Tukey's HSD p-values for significant effects in Table 2.4. Bold text indicates $p \leq 0.05$.

Model	Effect	Comparison	p-value
Hillslope	Year	0-1	0.78
		0-2	0.68
		0-3	0.16
		0-4	**0.01**
		1-2	1.00
		1-3	0.71
		1-4	**0.05**
		2-3	0.81
		2-4	0.06
		3-4	0.23
All Spatial scales	Year	0-1	0.82
		0-2	0.55
		0-3	**0.01**
		0-4	0.05
		1-2	0.99
		1-3	0.10
		1-4	0.22
		2-3	0.22
		2-4	0.37
		3-4	1.00
All Spatial scales	Spatial scale	hillslope-plot	**0.02**
		hillslope-watershed	**0.04**
		plot-watershed	0.86
Year*Spatial scale	Spatial scale	hillslope-plot	**0.01**
		hillslope-watershed	**0.01**
		plot-watershed	0.72

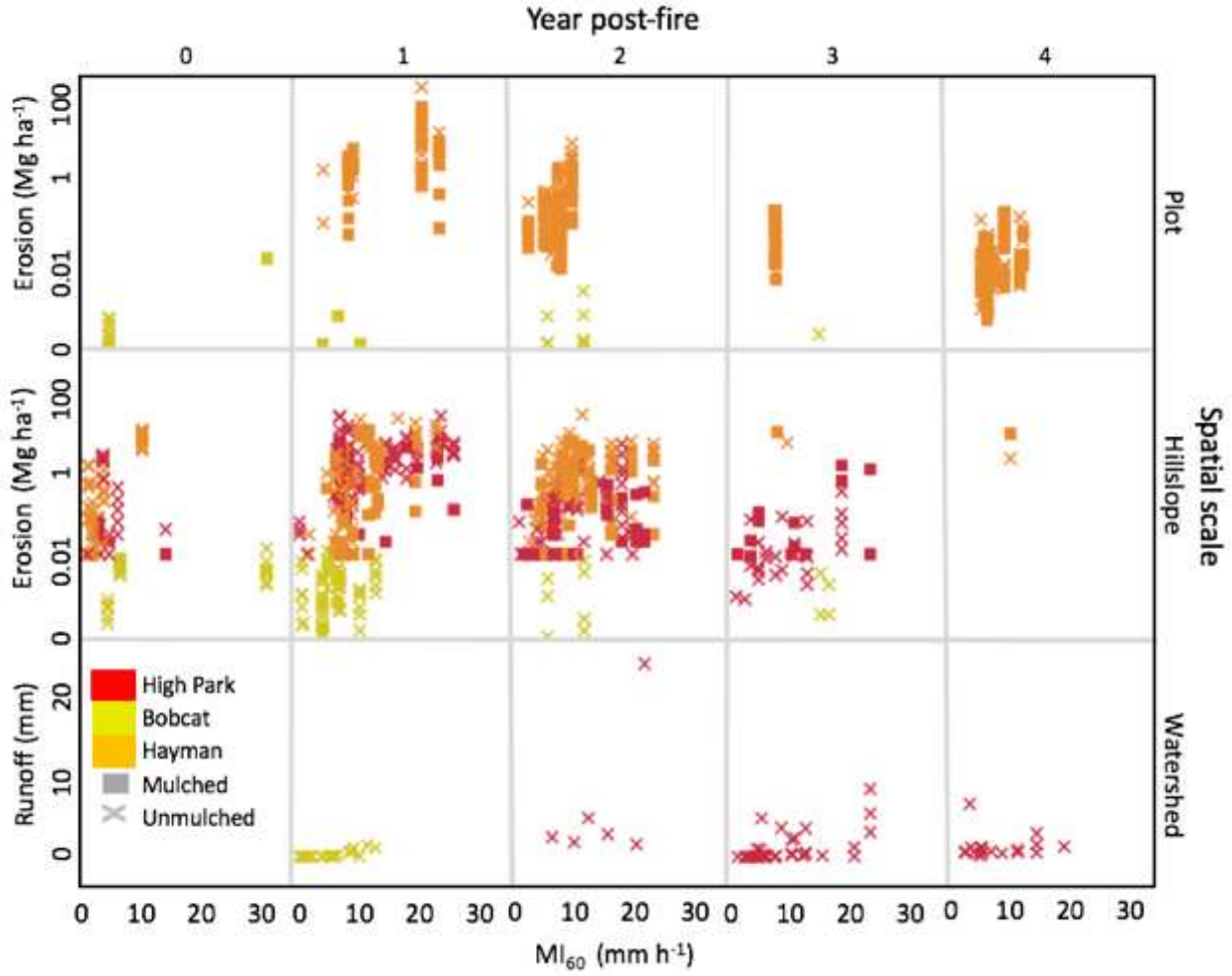

Figure A1. Sediment delivery (Mg ha^{-1}) and runoff (mm) vs. MI_{60} by spatial scale and year post-fire. Note the log-scale for sediment delivery. Runoff (mm) for watersheds in post-fire year 0 was not available.

APPENDIX B: Supplemental material for Chapter 3

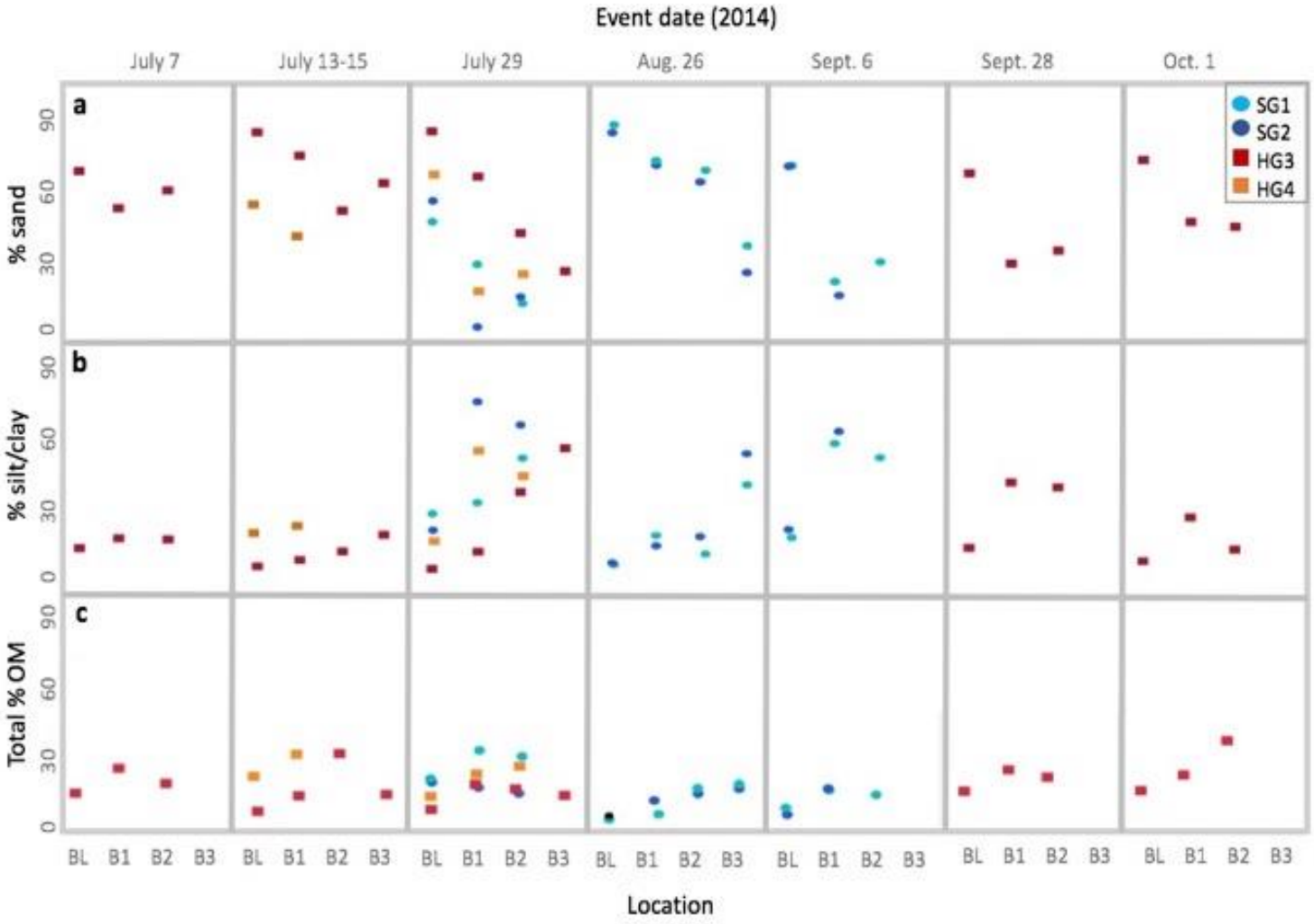

Figure B1**.** Particle size class fractions for bedload (BL), barrel 1 (B1), barrel 2 (B2), and barrel 3 (B3) for all sites for the 2014 events. Sand is > 53 μm, silt/clay is ≤ 53 μm, and total organic matter (OM) is > 53 μm + ≤ 53 μm.

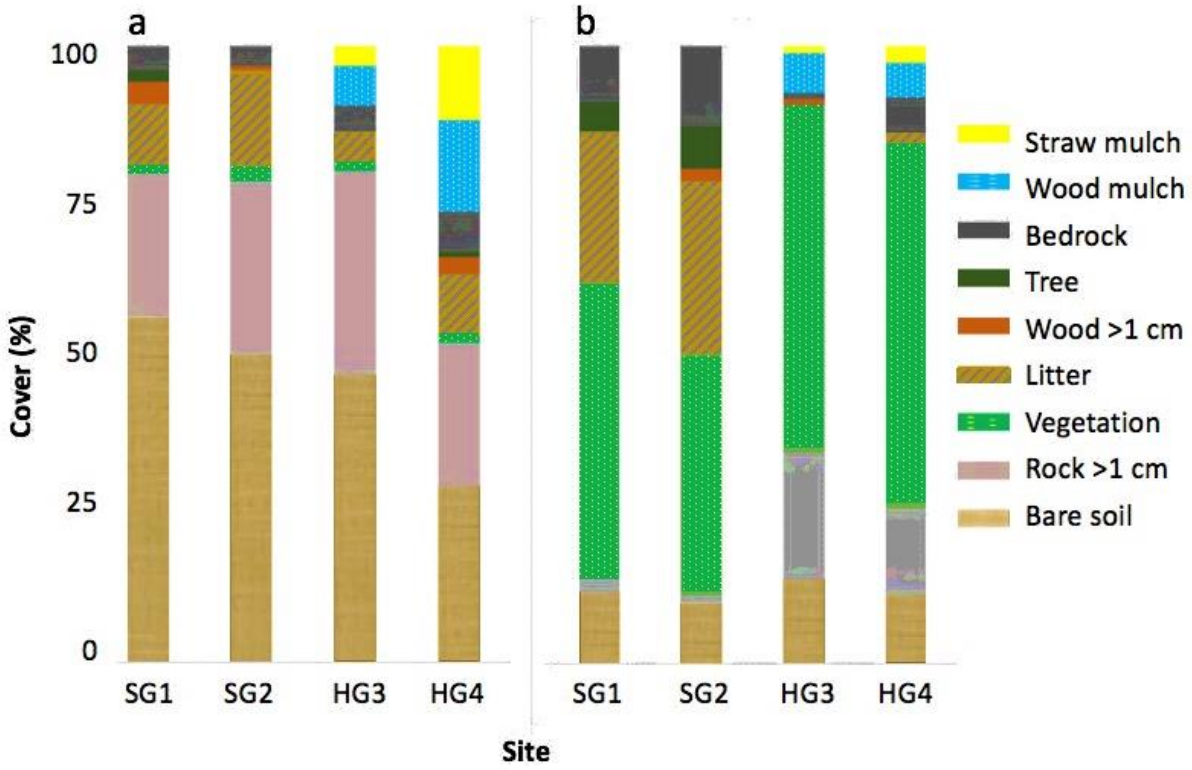

Figure B2. August 2014 surface cover measurements for Skin Gulch (SG1 and SG2) and Hill Gulch (HG3 and HG4) at the (a) ground surface and (b) canopy.

APPENDIX C: Supplemental material for Chapter 4

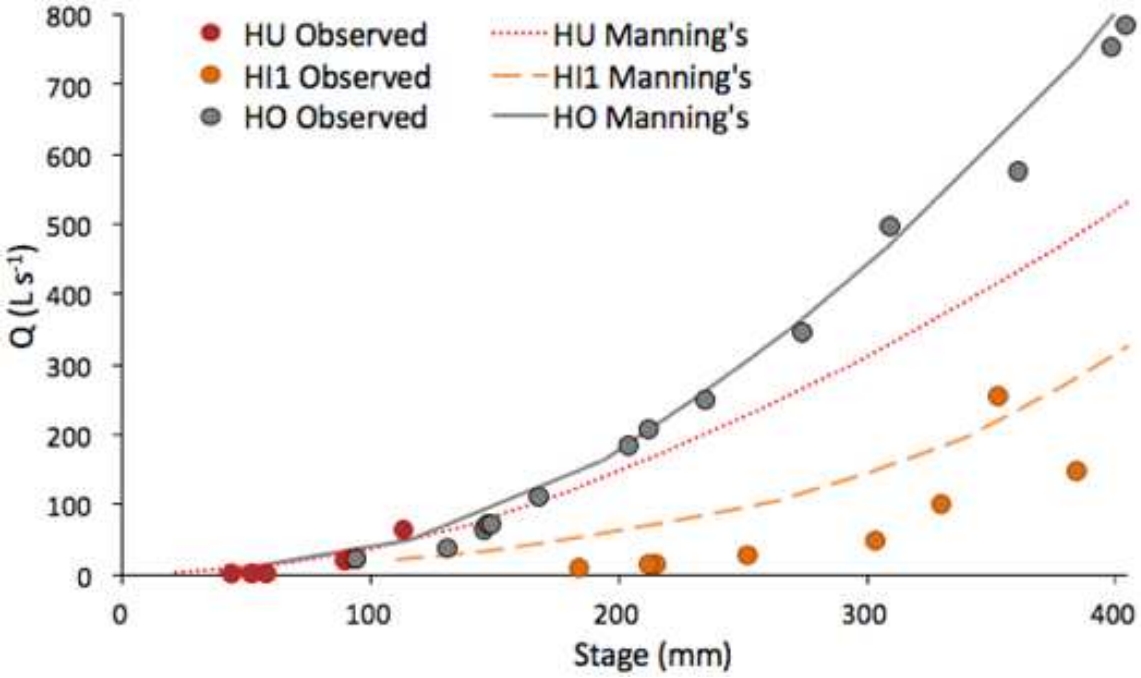

Figure C1. Observed and Manning's discharge (Q; L s^{-1}) over the range of observed stage heights. Note that for HI1, where the curve fit is not strong, Manning's n was adjusted from 0.01-1, and the best fit was for n = 0.5; this is within the range of roughness values estimated for other streams in the Southern Rocky Mountains of Colorado (Yochum et al. 2014).

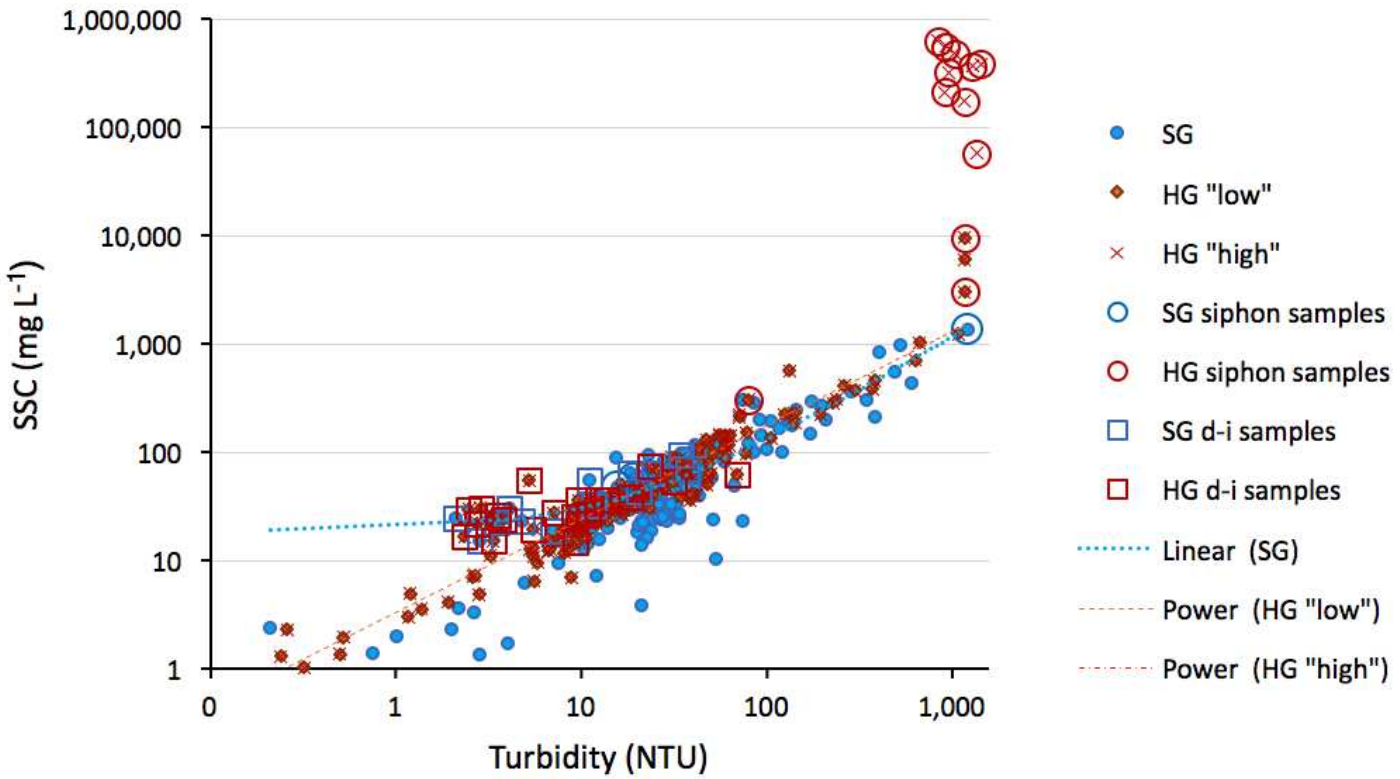

Figure C2. SSC-NTU rating curves for Skin Gulch (SG) and Hill Gulch (HG) "low" and "high" scenarios. Samples collected with automated ISCO samplers unless otherwise noted as siphon samples or depth-integrated samples ("d-i"). Note that no curve fit matched the highest values from the siphon sampler.

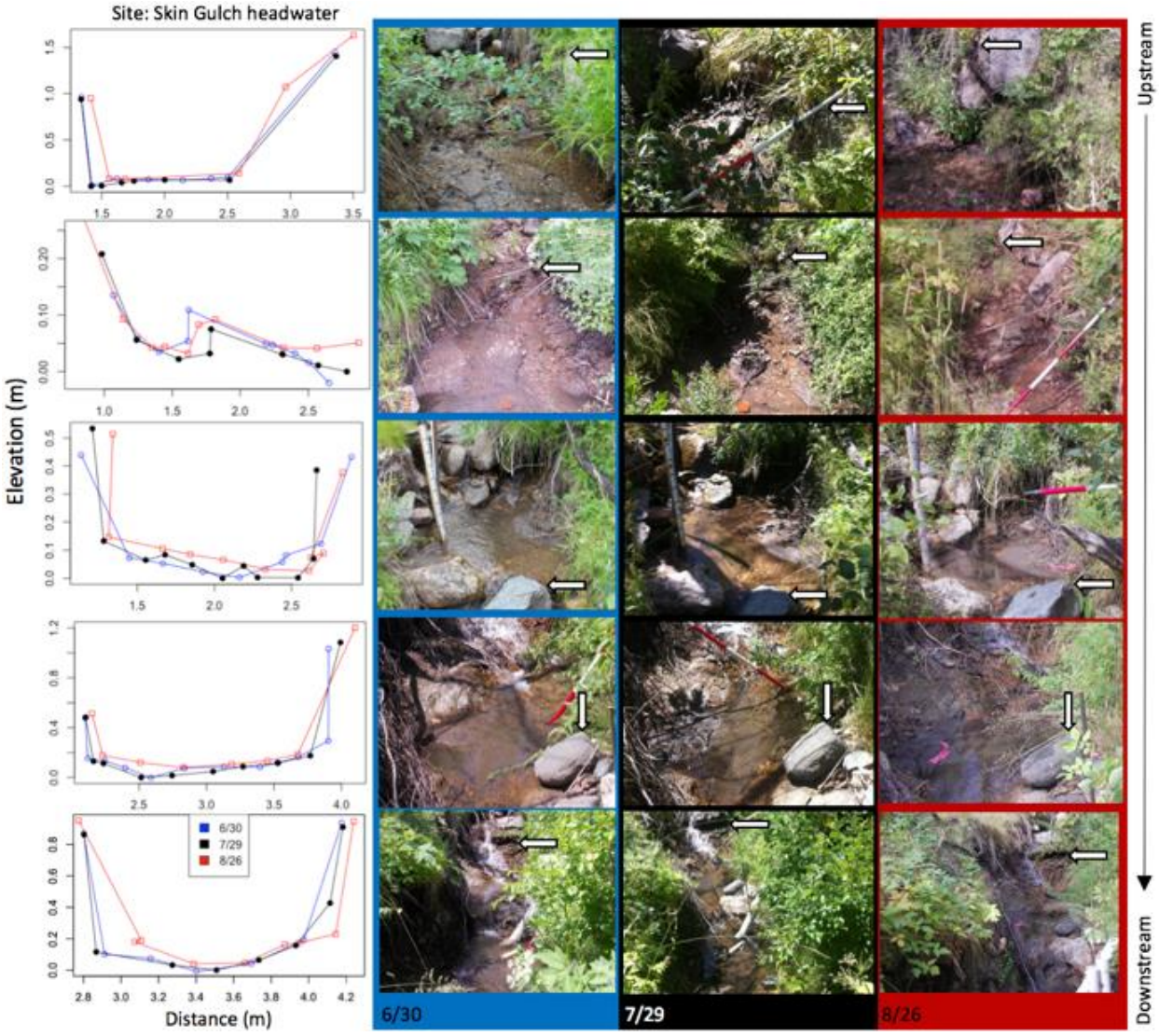

Figure C3. In-stream cross-sectional surveys and photographs for Skin Gulch headwater (SU; site alias from Table 4.1 and Figure 4.1 is "A") pre- and post-events on July 8th and Aug. 16th; cross-sections are numbered from one to five from downstream to upstream. Arrows reference the same location within each image to allow comparisons between survey dates.

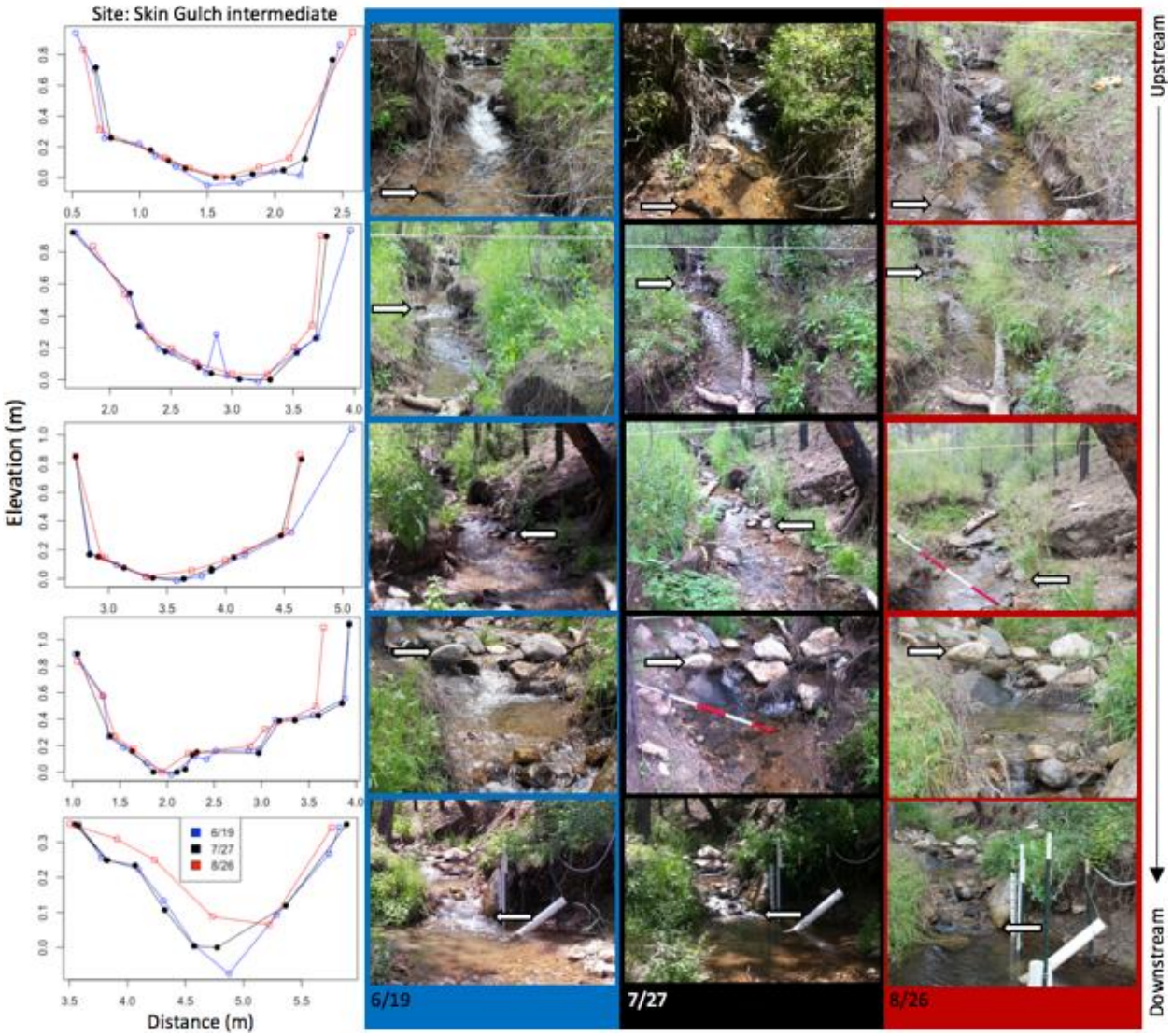

Figure C4. In-stream cross-sectional surveys and photographs for Skin Gulch intermediate (SI; site alias from Table 4.1 and Figure 4.1 is "B") pre- and post-events on July 8th and Aug. 16th; cross-sections are numbered from one to five from downstream to upstream. Arrows reference the same location within each image to allow comparisons between survey dates.

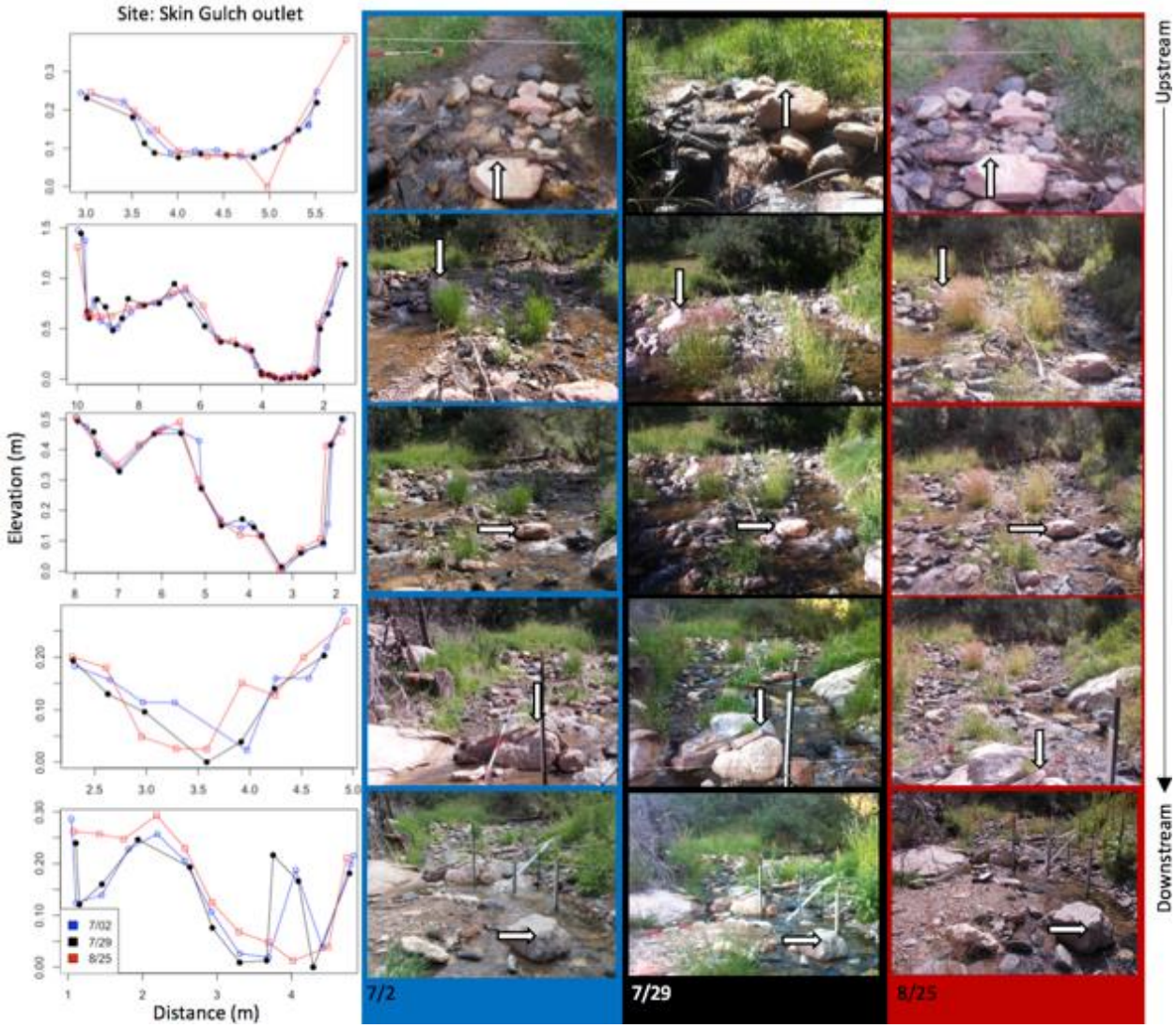

Figure C5. In-stream cross-sectional surveys and photographs for Skin Gulch outlet (SO; site alias from Table 4.1 and Figure 4.1 is "C") pre- and post-events on July 8th and Aug. 16th; cross-sections are numbered from one to five from downstream to upstream. Arrows reference the same location within each image to allow comparisons between survey dates.

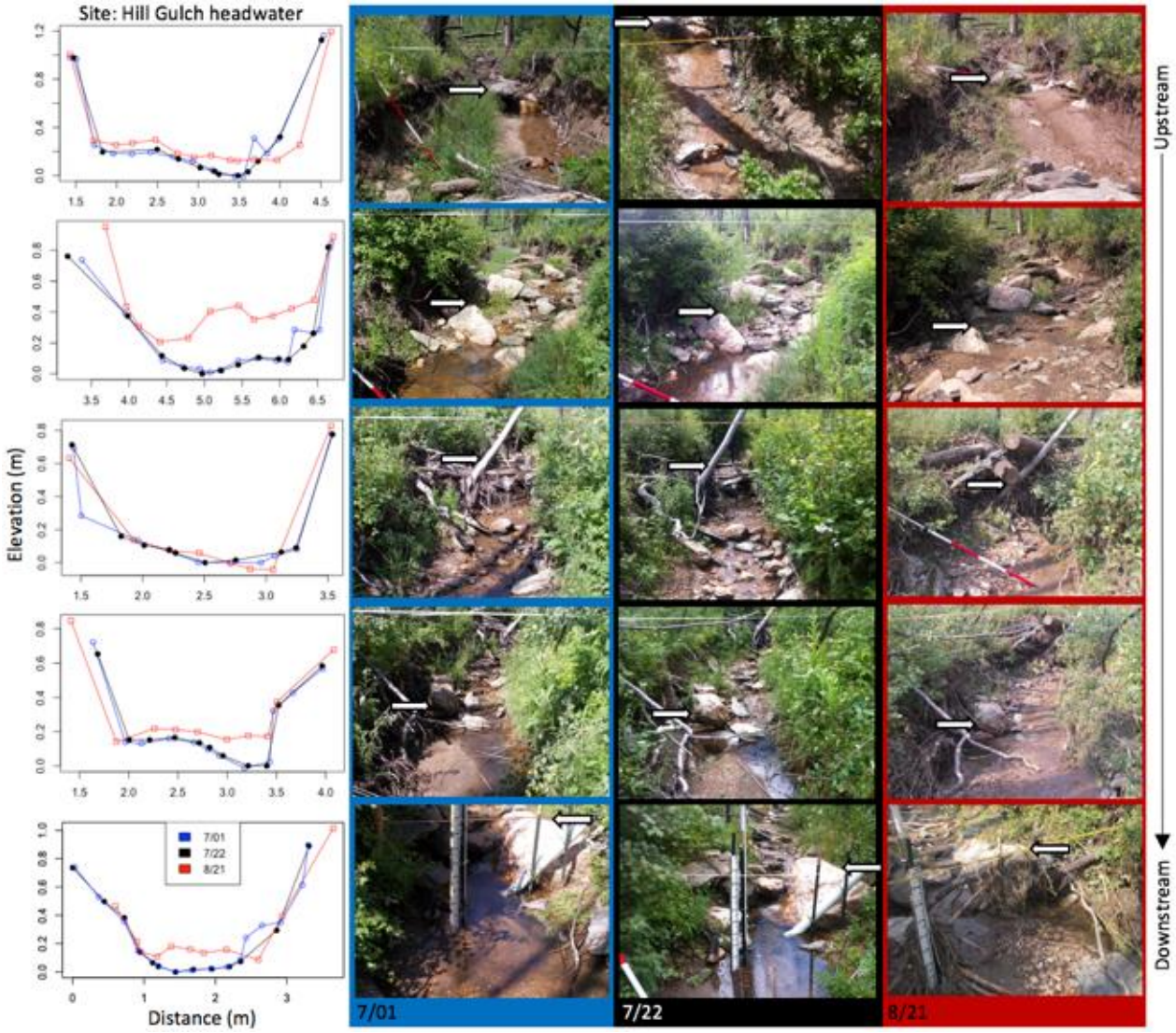

Figure C6. In-stream cross-sectional surveys and photographs for Hill Gulch headwater (HU; site alias from Table 4.1 and Figure 4.1 is "a") pre- and post-events on July 8th and Aug. 16th; cross-sections are numbered from one to five from downstream to upstream. Arrows reference the same location within each image to allow comparisons between survey dates.

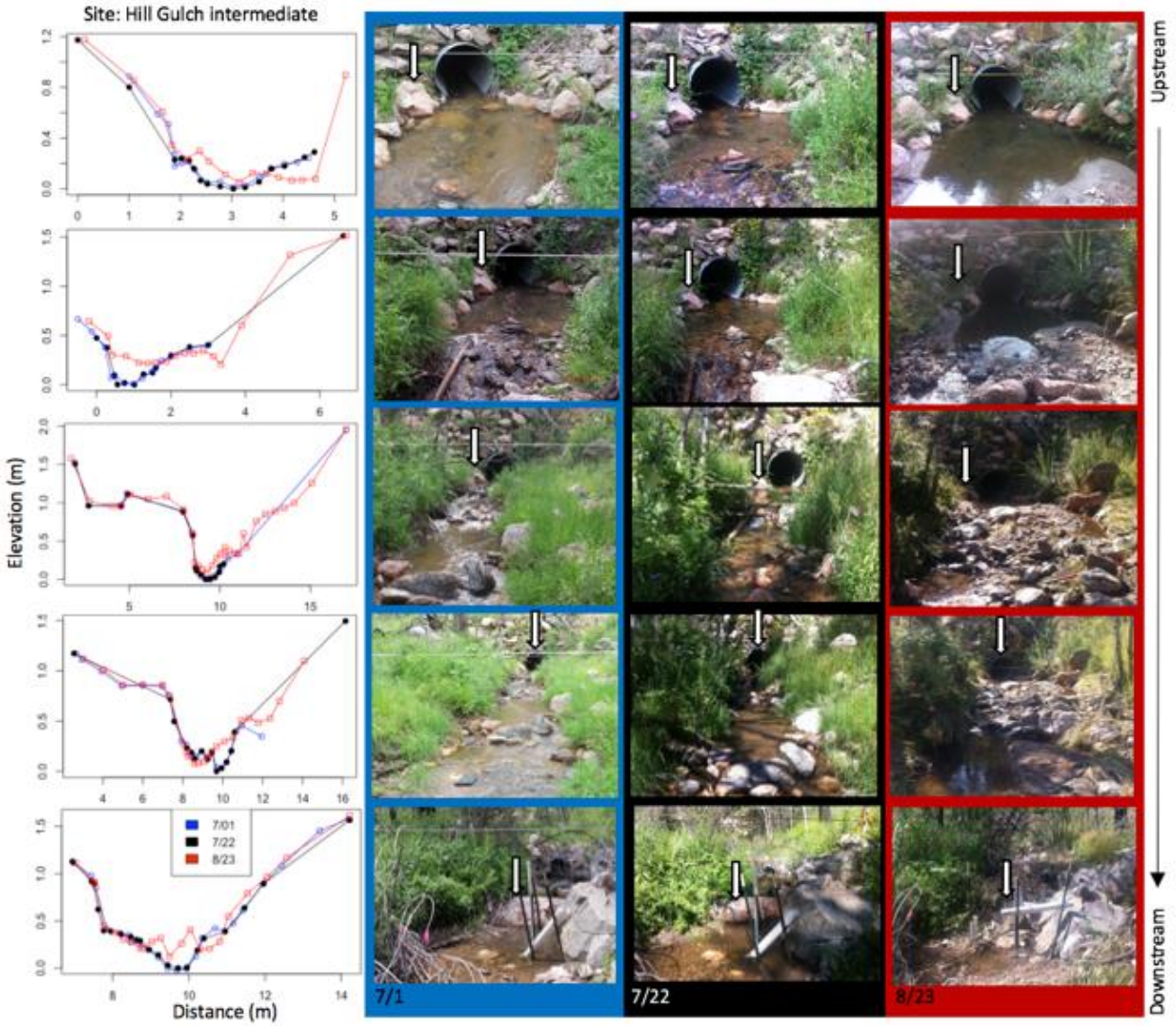

Figure C7. In-stream cross-sectional surveys and photographs for Hill Gulch intermediate (HI; site alias from Table 4.1 and Figure 4.1 is "b") pre- and post-events on July 8th and Aug. 16th; cross-sections are numbered from one to five from downstream to upstream. Arrows reference the same location within each image to allow comparisons between survey dates.

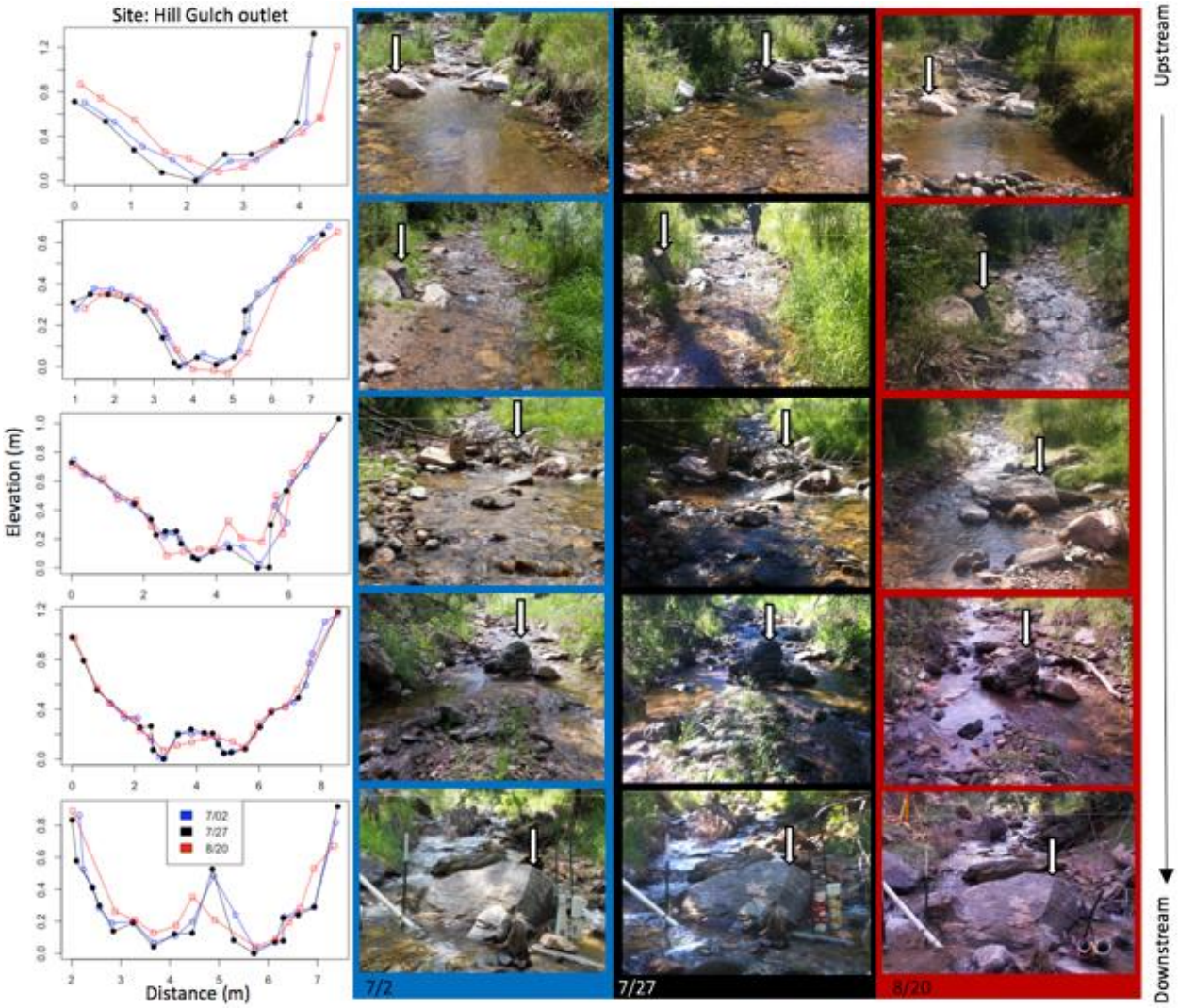

Figure C8. In-stream cross-sectional surveys and photographs for Hill Gulch outlet (HO; site alias from Table 4.1 and Figure 4.1 is "c") pre- and post-events on July 8th and Aug. 16th; cross-sections are numbered from one to five from downstream to upstream. Arrows reference the same location within each image to allow comparisons between survey dates.

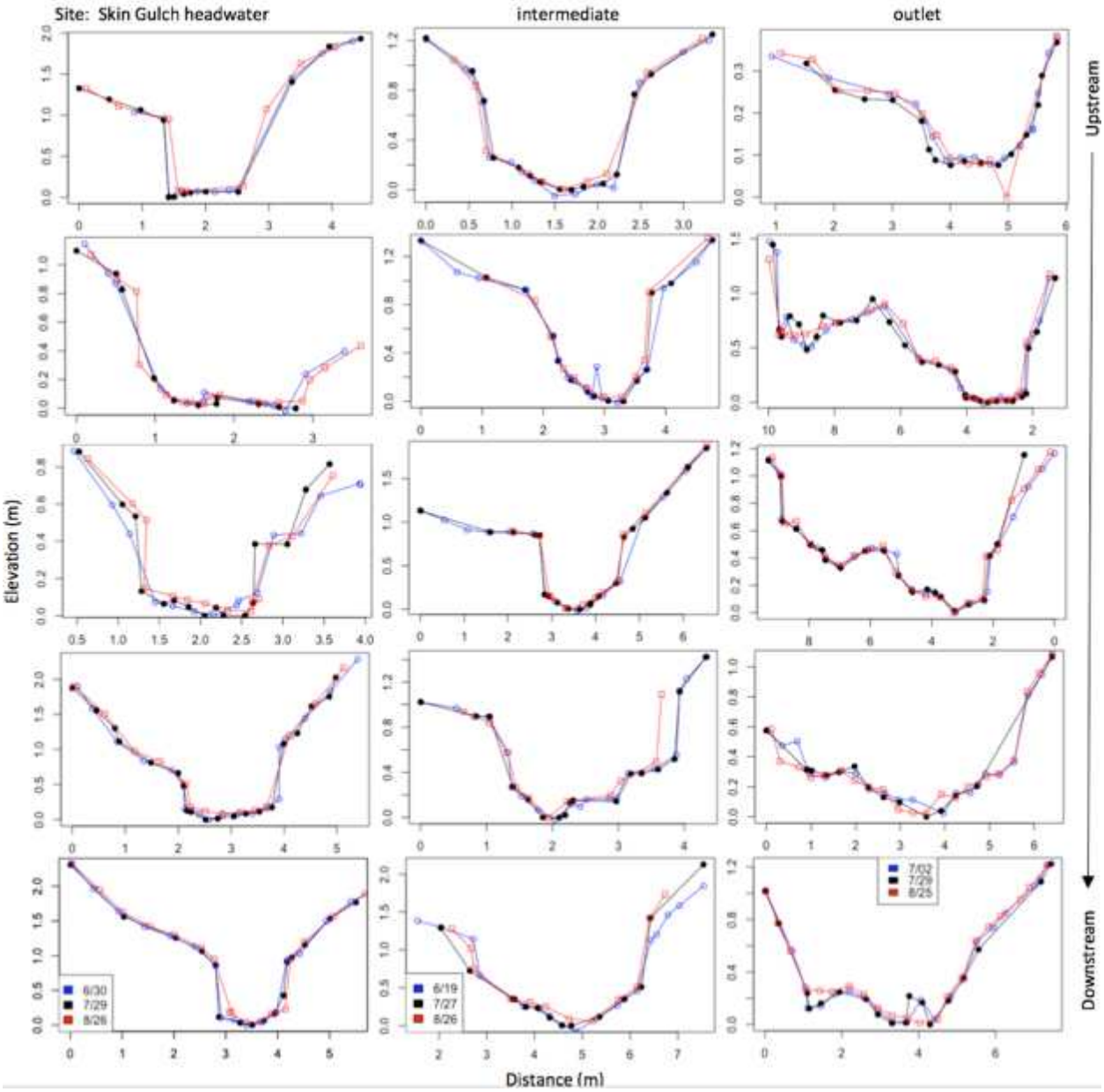

Figure C9. Full cross-sectional surveys for all Skin Gulch sites pre- and post-events on July 8th and Aug. 16th; cross-sections are numbered from one to five from downstream to upstream.

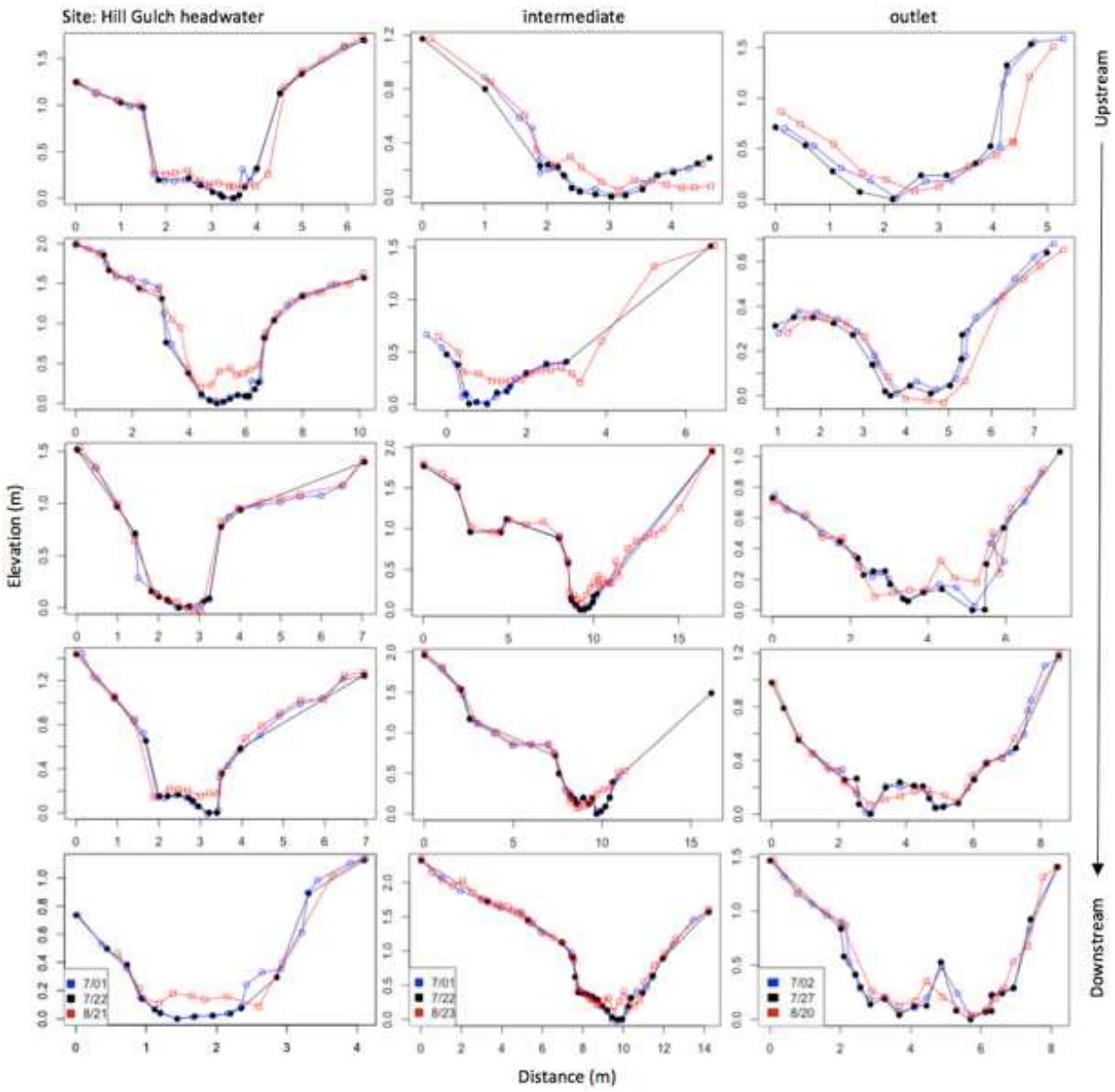

Figure C10. Full cross-sectional surveys for all Hill Gulch sites pre- and post-events on July 8th and Aug. 16th; cross-sections are numbered from one to five from downstream to upstream.

Table C1. Rating curves for stage-discharge and NTU-SSC by location. Manning's equation shown for Hill Gulch primary sites (a-c) with roughness (n) and slope (%). Stage-discharge equations estimate streamflow (y; L s^{-1}) using stage height (h; mm); NTU-SSC equations estimate suspended sediment concentration (y; SSC; mg L^{-1}) and using NTU (x). Note that for HI1, Manning's n was adjusted from 0.01-1, and the best fit was for n = 0.5; all Manning's n values are within the range of those estimated for other streams in the Southern Rocky Mountains of Colorado (Yochum et al. 2014). Site aliases correspond to those in Figure 4.1 and Table 4.1-4.2.

Rating curve	Site (alias)	Equation	R^2
Stage-discharge	SU (A)	$y=0.00001h^{2.962}$	0.96
	SI (B)	$y=2E\text{-}40h^{16.443}$	0.83
	SO (C)	$y=10.987e^{0.0164h}$	0.99
	SUS1(D)	$y=0.1268e^{0.0228h}$	0.72
	SLS1 (E)	$y=0.9271e^{0.016h}$	0.93
	SLS2 (F)	$y=1.5455e^{0.0226h}$	0.99
	HU (a)	$y=0.0023h^2+0.4289h-22.752$ (n=0.12; slope=0.07)	0.99
	HI (b)	$y=0.0033h^2-0.7629h+78.977$ (n=0.5; slope=0.08)	0.99
	HO (c)	$y=0.0054h^2-0.149h-2.6129$ (n=0.15; slope=0.05)	0.99
	HUS2 (d)	$y=0.8344e^{0.0108h}$	0.99
	HMS1 (e)	$y=15.484e^{0.0077h}$	0.96
	HLS1 (f)	$y=0.0158e^{0.0235h}$	0.98
NTU-SSC	Skin Gulch	$y=1.1592x+18.944$	0.86
	Hill Gulch - low	$y=3.3087x^{0.8664}$	0.90
	Hill Gulch - high	$y=1.3224x^{1.2699}$	0.78

Table C2. Spearman's ρ (n = 31) for July 8th and Aug. 16th hillslope sediment yields (Mg ha^{-1}) vs. rainfall metrics and site characteristics. Bold and italic font indicates significance at the 0.05 level.

	July 8th	Aug. 16th
P (mm)	-0.21	***-0.43***
P (h)	-0.27	0.11
MI_5 (mm h^{-1})	***-0.40***	***0.74***
MI_{15} (mm h^{-1})	***-0.46***	***0.74***
MI_{30} (mm h^{-1})	***-0.45***	***0.74***
MI_{60} (mm h^{-1})	0.03	***0.74***
Erosivity (MJ mm ha^{-1} h^{-1})	***-0.45***	***0.74***
P>10 (mm)	***-0.51***	***0.74***
P>15 (mm)	-0.32	***0.74***
P>20 (mm)	-0.28	***0.73***
Area (ha)	-0.27	***-0.61***
Slope (°)	-0.22	-0.09
CTI (average)	0.06	***-0.58***
CTI (maximum)	-0.02	***-0.63***
High burn severity (%)	-0.31	-0.02
Areas targeted to receive mulch (%)	0.00	0.08
Canopy cover (%)	-0.20	0.03
Ground cover (%)	-0.09	-0.23
Canopy mulch (Spring; %)	***-0.45***	0.25
Canopy mulch (Fall; %)]	-0.33	0.17
Ground mulch (Seasonal Ave; %)	***-0.45***	0.25

Table C3. July 8th and Aug. 16th Pearson's correlation coefficients between rainfall metrics, watershed and channel attributes, and production metrics with "high" rating curve estimates for Hill Gulch. Bold and italic font indicates significance at the 0.05 level.

	July 8th							Aug. 16th						
	Log [Q]	Log [Q/P]	Log [Peak Q]	Log [SY]	Log [SDR]	Net change	Abs. change	Log [Q]	Log [Q/P]	Log [Peak Q]	Log [SY]	Log [SDR]	Net change	Abs. change
Rainfall metrics														
P (mm)	-0.33	-0.39	0.25	0.20	0.44	-0.43	0.77	***0.89***	***0.79***	***0.85***	***0.96***	0.33	0.04	0.33
Log[P; hrs]	-0.02	0.04	-0.25	-0.36	-0.34	-0.03	-0.32	***0.81***	***0.73***	***0.82***	***0.88***	***0.44***	0.20	0.48
Log[M_5; mm h^{-1}]	-0.18	-0.20	0.19	0.15	***-0.82***	-0.18	***0.83***	***0.80***	***0.69***	***0.73***	***0.91***	0.20	-0.33	-0.02
Log[MI_{15}; mm h^{-1}]	0.19	0.15	0.35	0.72	-0.06	0.20	0.80	***0.81***	***0.70***	***0.75***	***0.93***	0.19	-0.29	0.01
Log[MI_{30}; mm h^{-1}]	0.42	0.38	0.18	0.80	***0.81***	0.33	0.14	***0.83***	***0.72***	***0.77***	***0.94***	0.22	-0.26	0.05
Log[MI_{60}; mm h^{-1}]	0.48	0.45	0.09	0.62	***0.82***	0.37	-0.28	***0.84***	***0.73***	***0.78***	***0.95***	0.28	-0.21	0.10
Log[Erosivity]	0.46	0.45	0.13	***0.85***	***0.55***	0.28	0.36	***0.82***	***0.71***	***0.76***	***0.93***	0.29	-0.27	0.04
Log[P>10; mm]	***0.67***	***0.64***	0.42	***0.97***	***0.79***	0.80	0.04	***0.81***	***0.71***	***0.75***	***0.93***	0.21	-0.30	0.01
Log[P>15; mm]	-0.30	-0.29	0.09	-0.15	***-0.82***	-0.13	0.46	***0.79***	***0.69***	***0.73***	***0.91***	0.17	-0.34	-0.03
Log[P>20; mm]	-0.26	-0.27	0.11	0.12	***-0.75***	-0.30	0.80	***0.77***	***0.67***	***0.71***	***0.89***	0.23	-0.35	-0.04
Watershed attributes														
Log[Area; ha]	0.33	0.36	-0.23	0.04	0.30	0.38	***-0.91***	-0.36	-0.38	-0.10	0.07	***-0.55***	***-0.94***	***-0.85***
Log [WS slope; °][a]	***0.68***	***0.68***	0.03	0.75	0.50	0.56	-0.18	0.54	0.48	0.46	0.71	-0.06	-0.33	-0.07
Log[CTI; max.]	***0.60***	***0.60***	-0.03	0.62	0.33	0.35	-0.13	-0.11	-0.14	0.24	0.50	-0.07	-0.25	-0.05
Burn severity (%)	-0.29	-0.33	-0.02	-0.07	***0.79***	-0.51	***0.92***	0.05	0.04	0.17	-0.07	***0.64***	***0.97***	***0.87***
Log[Mulch; %]	0.35	0.33	0.06	0.66	0.27	0.09	0.52	0.44	0.37	0.44	0.46	0.37	0.40	0.56
Channel attributes														
Log[MS slope; °][b]	-0.42	-0.39	-0.25	-0.53	***-0.78***	-0.63	0.61	-0.45	-0.42	-0.26	-0.60	0.39	0.73	0.51
Log[VCA; %] [c]	-0.17	-0.19	0.03	-0.56	0.44	0.08	-0.43	-0.14	-0.02	-0.30	-0.22	***-0.64***	-0.23	-0.45
Production metrics														
Log[Q; mm]	***1.00***	***1.00***	***0.59***	***0.85***	***0.69***	***0.89***	-0.15	***1.00***	***0.96***	***0.91***	***0.98***	0.19	-0.02	0.25
Log[Runoff ratio]		***1.00***	0.56	***0.83***	***0.62***	***0.90***	-0.19		***1.00***	***0.83***	***0.95***	0.17	-0.09	0.19
Log[Q; L s^{-1} km^{-2}]			***1.00***	***0.85***	0.31	0.71	0.20			***1.00***	***0.93***	***0.56***	0.18	0.45
Log[SY; Mg ha^{-1}]				***1.00***	***0.82***	0.67	0.25				***1.00***	0.39	0.03	0.32
Log[SDR]					***1.00***	-0.52	0.24					***1.00***	0.63	0.63
Net change						***1.00***	0.00						***1.00***	0.00
Absolute change							***1.00***							***1.00***

[a]WS = watershed
[b]MS = mainstem
[c]VCA = Valley Confinement Algorithm used to determine unconfined stream reaches

Table C4. July 8th and Aug. 16th Pearson's correlation coefficients between rainfall metrics, site characteristics, and response variables with "low" rating curve estimates for Hill Gulch. Bold and italic font indicates significance at the 0.05 level.

	July 8th		Aug. 16th	
	Log [SY]	Log [SDR]	Log [SY]	Log [SDR]
P (mm)	-0.06	-0.28	***0.94***	0.34
Log[P; hrs]	-0.22	0.28	***0.86***	***0.43***
Log[M_5; mm h^{-1}]	-0.09	0.16	***0.92***	0.21
Log[MI_{15}; mm h^{-1}]	0.43	-0.23	***0.93***	0.20
Log[MI_{30}; mm h^{-1}]	0.69	-0.17	***0.94***	0.23
Log[MI_{60}; mm h^{-1}]	0.66	-0.13	***0.95***	0.29
Log[Erosivity; MJ mm ha^{-1} h^{-1}]	0.70	0.09	***0.93***	0.30
Log[P>10; mm]	***0.88***	-0.20	***0.93***	0.22
Log[P>15; mm]	-0.20	0.16	***0.92***	0.18
Log[P>20; mm]	-0.07	0.22	***0.90***	0.24
Log[Area; ha]	0.37	0.18	0.08	***-0.53***
Log [Watershed slope; °]	0.74	0.11	0.67	-0.05
Log[CTI; maximum]	0.63	0.17	0.45	-0.06
High burn severity (%)	-0.46	-0.06	-0.10	***0.63***
Log[Mulch; %]	0.46	0.19	0.40	0.36
Log[Mainstem slope; °]	-0.68	0.06	-0.59	0.37
Log[Unconfined channel; %]	-0.59	0.13	-0.18	***-0.62***
Log[Q; mm]	0.79	0.02	***0.95***	0.20
Log[Runoff ratio]	0.78	0.06	***0.93***	0.18
Log[Peak Q; L s^{-1} km^{-2}]	0.57	0.16	0.63	***0.48***
Log[Lag time; mins]	0.57	-0.23	0.10	-0.35
Normalized net change	0.60	-0.10	0.02	***0.62***
Normalized absolute change	-0.17	-0.27	0.31	***0.61***
Log[SY; Mg ha^{-1}]	***1.00***	-0.11	***1.00***	0.40
Log[SDR]		***1.00***		***1.00***

Table C5. In-stream cross-sectional changes including deposition (m^2), erosion (m^2), net and absolute change (m^2) for all primary sites and cross-sections in Skin (S-) and Hill (H-) Gulch pre- and post-events on July 8th and Aug. 16th; cross-sections are numbered from one to five from downstream to upstream, respectively. The "all" CS data for each site represents the sum of changes all cross-sections. Site aliases correspond to those in Figure 4.1 and Table 4.1-4.2.

		July 8th				Aug. 16th			
Site (alias)	CS	Deposition (m^2)	Erosion (m^2)	Net change (m^2)	Absolute change (m^2)	Deposition (m^2)	Erosion (m^2)	Net change (m^2)	Absolute change (m^2)
SU1 (A)	5	0.00	-0.07	-0.07	0.07	0.25	0.00	0.25	0.25
	4	0.00	-0.02	-0.02	0.02	0.03	0.00	0.03	0.03
	3	0.01	-0.03	-0.02	0.04	0.11	0.00	0.11	0.11
	2	0.03	-0.03	0.00	0.06	0.13	-0.01	0.12	0.14
	1	0.00	-0.05	-0.05	0.05	0.13	-0.04	0.09	0.17
	all	0.04	-0.20	-0.16	0.24	0.65	-0.05	0.60	0.70
SI1 (B)	5	0.06	0.00	0.06	0.06	0.06	-0.02	0.04	0.08
	4	0.02	-0.03	-0.01	0.05	0.06	0.00	0.06	0.06
	3	0.05	0.00	0.05	0.05	0.06	-0.01	0.05	0.07
	2	0.02	-0.06	-0.04	0.08	0.14	0.00	0.14	0.14
	1	0.04	-0.01	0.03	0.05	0.13	0.00	0.13	0.13
	all	0.19	-0.10	0.09	0.29	0.45	-0.03	0.42	0.48
SO (C)	5	0.00	-0.03	-0.03	0.03	0.04	-0.02	0.02	0.06
	4	0.18	-0.23	-0.05	0.41	0.41	-0.15	0.26	0.56
	3	0.04	-0.06	-0.02	0.10	0.08	-0.04	0.04	0.12
	2	0.01	-0.06	-0.05	0.07	0.06	-0.02	0.04	0.08
	1	0.04	-0.04	0.00	0.08	0.15	-0.08	0.07	0.23
	all	0.27	-0.42	-0.15	0.69	0.74	-0.31	0.43	1.05
HU (a)	5	0.04	-0.05	-0.01	0.09	0.15	-0.22	-0.07	0.37
	4	0.04	-0.05	-0.01	0.09	0.68	0.00	0.68	0.68
	3	0.08	-0.01	0.07	0.09	0.08	-0.04	0.04	0.12
	2	0.03	-0.01	0.02	0.04	0.15	-0.06	0.09	0.21
	1	0.04	-0.06	-0.02	0.10	0.16	-0.05	0.11	0.21
	all	0.23	-0.18	0.05	0.41	1.22	-0.37	0.85	1.59
HI1 (b)	5	0.01	-0.04	-0.03	0.05	0.17	-0.11	0.06	0.28
	4	0.00	-0.07	0.07	0.07	0.07	-0.23	-0.16	0.30
	3	0.02	-0.07	-0.05	0.09	0.48	-0.02	0.46	0.50
	2[1]	0.17	-0.11	0.06	0.28	0.32	-0.17	0.15	0.49
	1	0.05	-0.23	-0.18	0.28	0.54	-0.09	0.45	0.63
	all	0.25	-0.52	-0.13	0.77	1.58	-0.62	0.96	2.20
HO (c)	5[2]	0.15	-0.10	0.05	0.25	0.21	-0.25	-0.04	0.46
	4[2]	0.02	-0.14	-0.12	0.16	0.09	-0.23	-0.14	0.32
	3	0.08	-0.14	-0.06	0.22	0.35	-0.16	0.19	0.51
	2	0.07	-0.13	-0.06	0.20	0.21	-0.12	0.09	0.33
	1	0.03	-0.17	-0.14	0.20	0.40	-0.11	0.29	0.51
	all	0.35	-0.68	-0.33	1.03	1.26	-0.87	0.39	2.13

[1] Pre-July 8th event survey (July 1st) limited bankfull height on stream left to 0.5 m;

[2] surveys adjusted 0.2 m vertically for 7/27 surveys due to potential field error in prism height.

C1. Supplemental Discussion

C1.1. Measurement uncertainties

C1.1.1. Rainfall

In a previous analysis of MI_{60} rainfall thresholds, 7.4-10.1 mm h^{-1} was found to produce in-stream runoff during post-fire year 3 (i.e., 2015) of the High Park Fire (Wilson et al. 2018; chapter 2). Although rainfall was consistently below this threshold during the July 8th event and above this threshold for all but two sites during the Aug. 16th event, site responses were observed throughout both watersheds. During the threshold analysis, the rain gauge with the highest erosivity was linked to a site-event, while in this analysis, rainfall was interpolated across all associated rain gauges. Interpolation of rainfall likely decreased the influence of gauges with greater erosivity, and indicates much less rainfall is needed to produce a response. This should be considered for future studies of post-fire watershed-scale runoff response, particularly for sites with greater antecedent rainfall.

C1.1.2. Hillslope runoff and catch efficiency

The addition of time lapse cameras to the ensemble of hillslope monitoring equipment during the 2015 sampling season showed differences between runoff computed from the weir equation and from the barrel water collection. Weir equation results were consistently higher than barrel-estimated runoff, likely because the barrel collection system had some problems with leakage and leveling. Time lapse cameras installed in 2015 provided additional information, such as evidence of runoff overtopping the sediment fence and bypassing the collection system. If the higher weir equation values are accurate, then the catch efficiencies calculated in 2014 (c.f., Wilson et al. in review; chapter 3) were probably over-estimated. In 2014, catch efficiency was estimated from rating curves that related the runoff collected in each barrel to runoff volume,

with additional consideration for flow splitting in subsequent barrels that was strongly dependent on whether the barrels remained level. For 2015, the catch efficiency estimated with the barrel data only would have been 0.92, whereas the catch efficiency we used was computed with the weir data, which produced higher runoff and a lower catch efficiency of 0.66. To provide more accurate estimates of post-fire hillslope production, future monitoring should increase sediment fence and runoff collection capacities to accommodate higher runoff volumes. Additional observations, such as time lapse photos, of rainfall-runoff events would allow researchers to improve confidence in runoff and sediment yield estimates through identification of: (1) rainfall events that resulted in runoff (i.e., refine rainfall thresholds); and (2) potential sampling issues (e.g., overtopping).

C1.1.3. Suspended sediment

During the August 16th event, the siphon samplers collected higher suspended sediment than the ISCO samplers during peak sediment transport, likely because the ISCO at the outlet of Hill Gulch became plugged during the initial rise of the hydrograph. During the July 8 event, however, SSC values were more comparable between sampling methods. At the outlet of Skin Gulch (SO; "C"), the ISCO begin collecting samples about 40 minutes before the stage level rose high enough to collect two siphon samples at the intermediate site (SI; "B"). Although only two siphon samples were collected at SI (B), 14 samples were collected with the ISCO and all samples had comparable SSC (23-57 mg L^{-1}). Although the ISCO inlet was installed at a fixed location near the stream bed, these findings indicate use of low-cost siphon samplers for collecting SSC during runoff events for use in developing rating curves in addition to baseline data collection (e.g., depth-integrated samplers).